TSUNAMIS GENERATED BY SUBMARINE LANDSLIDES IN THE MARMARA SEA

by

Derya Aydın

B.Sc., Geology Engineering, Cumhuriyet University, 2006

Submitted to
the Boğaziçi University
Kandilli Observatory and Earthquake Research Institute
in partial fulfillment of the requirements for the degree of
Master of Science

Graduate Program in Geophysical Engineering
Boğaziçi University
2014

ACKNOWLEDGEMENTS

I would like to express my sincere gratitude to my advisor Prof. Nurcan Meral Özel who was abundantly helpful and offered invaluable assistance, support and guidance throughout my studies.

I would like to thank to Prof. Dr. Ahmet Cevdet Yalçıner for sharing his valuable knowledge, his helpful guidance and supporting me throughout my thesis.

I would like to also thank to Mr. Öcal Necmioğlu for for his helpful guidance and his suggestion.

I thank all the faculty members and staff of the Boğaziçi University, Department of Geophysics, especially my friends.

I would like to thank my family members for their support me with endless love, patience, their understanding and encouragement.

ABSTRACT

In this study, we investigated tsunamis generated by submarine landslides in the Marmara Sea. The area of Ganos, Küçükçekmece, Yenikapı and central portion in Central Basin (CNI) have been selected as a pilot landslide case area in the Marmara Sea and bathymetry data with 150 m resolution has been used. We have benefited from the General Directorate of Mineral Research and Exploration (MTA) landslide map and previous studies to determine possible landslide locations in Marmara Sea. We modelled the generation of the landslide generated tsunamis using TWO-LAYER model and the propagation and coastal amplification of the landslide generated waves are investigated using the tsunami simulation and visualization code NAMI-DANCE. Sediment thicknesses are set as 10 m-50 m for Ganos and CN1, whereas for Küçükçekmece, they are set as 5 m, 10 m and 50 m. In Yenikapı case, thicknesses are 5 m, 10 m, 30 m, 60 m and 120 m. We have assigned the velocity of the slide for the selected landslide points according to the sediment thickness to understand its effect. Our investigations indicated that velocity is reduced from the slide center to the boundary of the sliding (rupture) surface and the velocity increases while the thickness is increased. In addition, it is observed that there is a linear relation between the thickness and the velocity in Yenikapı case. The effects of the tsunami waves may change depending on the velocity of the slide, the thickness of the sediment. Tsunami generated by submarine landslides should be considered as hazardous for the Marmara Sea coasts.

ÖZET

Çalışmada Marmara Denizi'nde denizaltı heyelanları tarafından yaratılan tsunamiler araştırıldı. Marmara-150 m batimetri verileri kullanıldı ve Marmara da heyelan alanı olarak Ganos, Küçükçekmece, Yenikapı ve CN1 noktaları seçildi. Bu noktaların seçiminde MTA heyelan haritası ve önceden yapılan çalışmalardan yararlanıldı. Heyelan etkisi ile oluşan tsunami benzetimleri TWO-LAYER modeli ve NAMI-DANCE kodu ile yapıldı. Ganos ve CN1 noktaları için sediman kalınlıkları 10 m ve 50 m alındı. Küçükçekmece için 5 m,10 m ve 50 m sediman kalınlığı seçildi. Yenikapı için ise sediman kalınlıkları 5 m, 10 m, 30 m, 60 m ve 120 m alındı. Heyelan için TWO-LAYER kodunu kullanarak bu noktalardaki heyelan hızları elde edildi. Buradan çıkan sonuçlar NAMI-DANCE programında kullanarak heyelan etkisi ile oluşan dalgaların ilerlemesi ve kıyıdaki yükselmeleri hesaplanarak tsunami heyelan benzetimi yapıldı. Seçilen heyelan noktaları için hız-zaman ve hız-kalınlık değerlendirmeleri yapıldı. Yapılan çalışmalar hızın kayma merkezinden dışarıya doğru azaldığını gösterdi. Kalınlık artarken hızın da arttığı gözlemlendi. Yenikapı da kalınlık ve hız arasında doğrusal bir ilişki olduğu gözlendi. Tsunami dalgalarının etkisi kayma hızına, sediman kalınlığına bağlı olarak değişebildiği anlaşıldı. Çalışma sonucunda Marmara Denizi'nde denizaltı heyelanları tarafından yaratılan tsunamilerin Marmara kıyıları için tehlike oluşturabileceği görüldü.

TABLE OF CONTENTS

LIST OF FIGURES

LIST OF TABLES

LIST OF SYMBOLS/ABBREVATIONS

Fr	Froud Number
FNPF	Fully nonlinear potential flow
SMF	Submarine Mass Failure
V	Volume
H	Maximum amplitude
h	Still water depth
η	Water surface elevation
M, N	Water discharge
ρ	Density of fluid
NSW	Nonlinear Shallow Water
n	Temporal grid points
i, j	The spatial grid points along x and y directions
$\Delta x, \Delta y, \Delta t$	Spatial grid spacings
CFL	Courant-Friedrichs-Lewys
$D=h+\eta$	Total depth
$\alpha=\rho_1/\rho_2$	Subscripts 1 and 2 symbolize the upper and lower layers respectively
$\beta= h_1/h_2$	Subscripts 1 and 2 symbolize the upper and lower layers respectively
t	Time

1. INTRODUCTION

Tsunami is recognized by the Greek historian Thucydides in 426 BC for the first time in the history (Shuto, 2003). A tsunami is described as a series of ocean waves of extremely long wave length and long period created in a body of water by an impulsive disturbance that displaces the water (Yalçıner *et al*., 2005). Tsunamis are distinguished from wind-driven waves. Periods, wavelengts, and velocities of tsunamis are so much larger than wind-driven waves. Thus, they have different propagation features and shoreline results (Yalçıner *et al*., 2005).

A tsunami can have a period between ten minutes to two hours and a wavelength in excess of 500 km. It is due to their long wave lengths that tsunamis act as shallow-water waves. Since a tsunami has a very large wave length, it will lose little energy as it propagates. Therefore in very deep water, a tsunami will travel at high speeds. In addition, it travels great transoceanic distances with limited loss of energy (Yalçıner *et al*., 2005). For instance, about 6000 meters on the depth, unnoticed tsunami can travel about 890 km/hr, as the equivalent speed of a jet plane. That is to say, tsunami waves can cross oceans in less one day (Yalçıner *et al*., 2005).

Tsunamis can be generated by earthquakes, submarine landslides, submarine volcanic eruptions and atmospheric conditions (Gutenberg, 1939).

Tsunamis are most commonly created by earthquakes in marine and coastal regions. Major tsunamis are generated by large (greater than magnitude 7 on the Richter scale), shallow focus (less than 30 km beneath the surface) earthquakes associated with the movement of oceanic and continental tectonic plates (Bernardi *et al*., 2006).

Earthquakes create tsunamis when the sea floor suddenly deforms and displaces the overlying water from its equilibrium position. Submarine landslides occur frequently during a large earthquake and so it can also generate a tsunami. During a submarine landslide, the equilibrium sea-level is changed by sediment moving along the sea-floor. Gravitational forces then propagate the tsunami given the initial perturbation of the sea-floor. In addition, a violent marine volcanic eruption can also generate an impulsive force

that displaces the water column and induces a tsunami. Above water (subarial) landslides and space born objects can disturb/destroy/damage the water from above the surface. Once the event which initiates the tsunami happens the potential energy that originates from pushing water above mean sea level is then transferred to horizontal propagation of the tsunami wave (kinetic energy) (Yalçıner *et al*., 2005).

In several minutes of the initiation, the initial tsunami is split into a tsunami that goes out to the deep ocean (distant tsunami). Another tsunami is local tsunami that travels towards the nearby coast. The height above mean sea level of these tsunamis is nearly half that the original tsunami. The speed of both tsunamis is proportional to the square root of the water depth. Thus, the deep ocean tsunami is faster than the local tsunami near shore (Yalçıner *et al*., 2005).

Several things occur while the local tsunami travels over the continental slope. The amplitude increases and the wavelength decreases. It leads to steepening of the leading wave a significant control of wave run-up at the coast. Due to the higher propagation speed, the deep ocean tsunami travels much farther than the local tsunami. When the deep ocean tsunami approaches a distant shore, amplification and shortening of the wave will occur (Yalçıner *et al*., 2005).

The tsunami wave travels from the deep-water, the continental slope region to the near shore region. So tsunami run-up occurs. Run-up is defined as; a measurement of the height of the water onshore observed above a referance sea level (Yalçıner *et al*., 2005).

In this thesis, tsunamis generated by submarine landslides are investigated. The aim of this study is to do modelling of submarine landslides induced tsunami in the West Part of the Marmara Sea and North Part of the Marmara Sea. For this purpose, TWO-LAYER codes and NAMI-DANCE programme are used. The models are used possible submarine landslides at offshore of Ganos, offshore of Küçükçekmece, offshore of Yenikapı and CN1 (central portion in Central Basin). The velocity of the submarine landslides is analysed by using TWO-LAYER code. The propagation and coastal amplification of the submarine landslide created tsunami waves in the Marmara Sea are studied. Graphs and maps are produced by using GRAPHER 6 and SURFER 8 programmes of Golden Software Company.

The thesis includes 7 Chapters. Chapter 1 is the introduction part of the thesis. It introduces information about tsunamis, programmes using in the study and aim of the study. Chapter 2 includes landslides and submarine landslides. The features of landslides and submarine landslides are given in this chapter. In Chapter 3, literature survey and historical events about submarine landslides are given. Chapter 4 contains morphological and tectonic features of the Marmara Sea and causes of submarine landslides in the Marmara Sea. Methodology is given in Chapter 5. Chapter 6 gives modeling of underwater landslides in the Marmara Sea at offshore Yenikapı, Ganos, CN1 and Küçükçekmece cases. In Chapter 7, results of the thesis and conclusions are given.

2. LANDSLIDES AND SUBMARINE LANDSLIDES

2.1. Landslides

Landslide is defined as a wide variety of processes that result in the downward and outward movement of slope-forming materials consisting of rock, soil, artificial fill, or a combination of these. When the gravitional forces exceed the strength of material in a slope, landslides occur. Weak geologic materials leads to landslides such as; rapidly deposited fine grained sediments or fractured rocks. They are exposed to strong environmental stresses such as; earthquake, large storm waves and high internal pore pressure (Hampton, 1996).

The various types of landslides can be distinguished by the kinds of material included and the mode of movement. A classification system based on these parameters is indicated in Figure 2.1 (modified from USGS).

TYPE OF MOVEMENT		TYPE OF MATERIAL		
		BEDROCK	ENGINEERING SOILS	
			Predominantly coarse	Predominantly fine
FALLS		Rock fall	Debris fall	Earth fall
TOPPLES		Rock topple	Debris topple	Earth topple
SLIDES	ROTATIONAL	Rock slide	Debris slide	Earth slide
	TRANSLATIONAL			
LATERAL SPREADS		Rock spread	Debris spread	Earth spread
FLOWS		Rock flow (deep creep)	Debris flow (soil creep)	Earth flow
COMPLEX		Combination of two or more principal types of movement		

Figure 2.1. Types of landslides. Abbreviated version of Varnes' classification of slope movements (Varnes, 1978).

Although landslides are primarily associated with mountainous regions, they can also take place in areas of generally low relief. In low-relief areas, landslides take place as

cut and fill failures (roadway and building excavations), river bluff failures, lateral spreading landslides, collapse of mine-waste piles (especially coal), and a wide variety of slope failures associated with quarries and open-pit mines. The most common types of landslides are identified as follows and are indicated in Figure 2.1 (from USGS).

SLIDES: Although many types of mass movements are involved in the general term “landslide,” the more restrictive use of the term refers only to mass movements, where there is a distinct zone of weakness that separates the slide material from more stable underlying material. There are two basic types of slides that are rotational slides and translational slides (from USGS).

Rotational slide: In this type of slide, the surface of rupture is curved concavely upward. Moreover, the slide movement is roughly rotational about an axis that is parallel to the ground surface and transverse across the slide (Figure 2.2A) (from USGS).

Translational slide: In the translational slide, the landslide mass moves along a roughly planar surface with little rotation or backward tilting (Figure 2.2B). A block slide is a translational slide and the moving mass is composed of a single unit or a few closely related units that move downslope as a relatively coherent mass (Figure 2.2C) (from USGS).

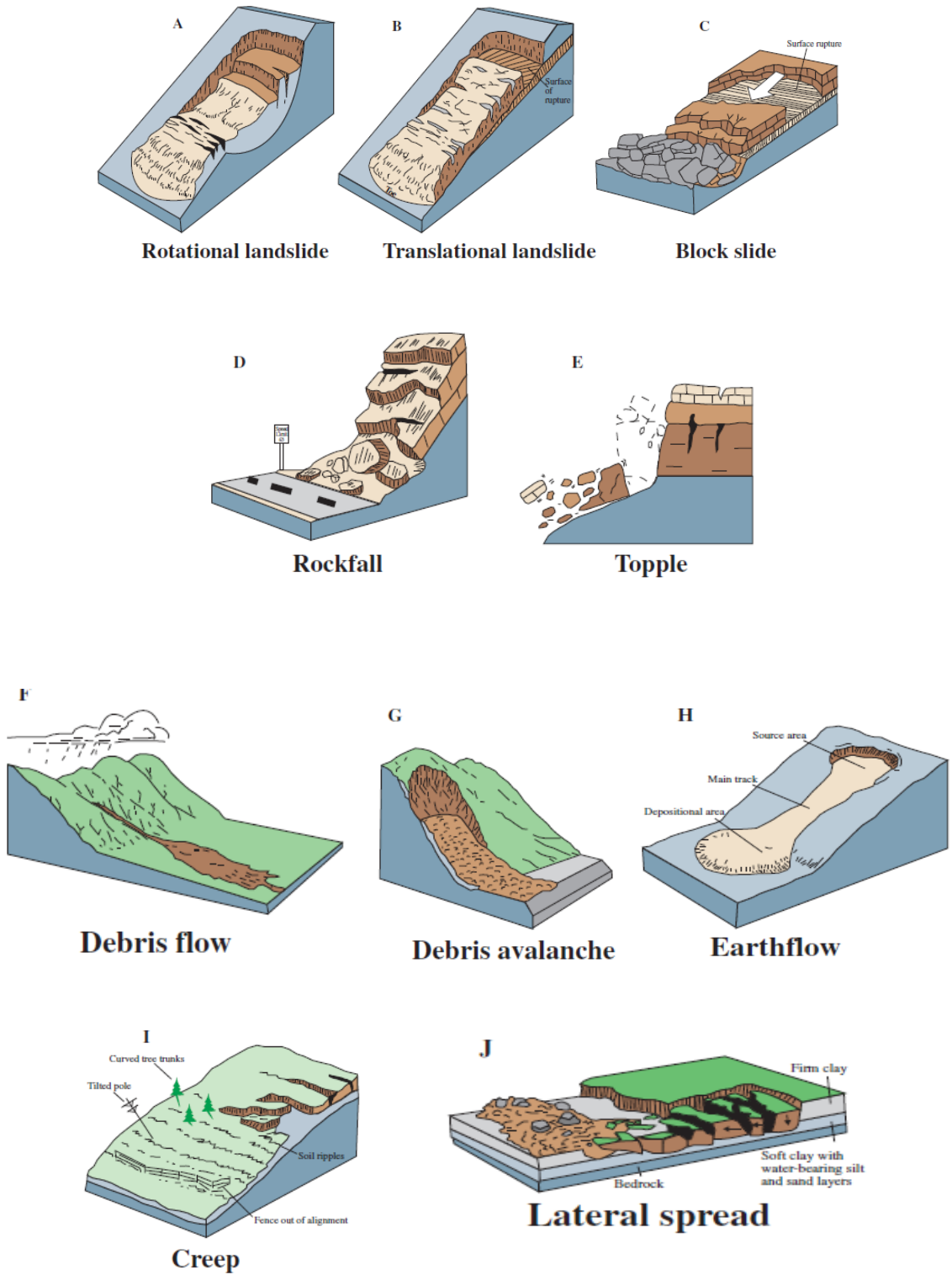

Figure 2.2. These schematics illustrate the major types of landslide movement (from USGS).

FALLS: Falls define as abrupt movements of masses of geologic materials, such as rocks and boulders, that become detached from steep slopes or cliffs (Figure 2.2D). In this type of movements, separation happens along discontinuities such as fractures, joints, and bedding planes, and movement occurs by free-fall, bouncing, and rolling. In addition, falls are strongly affected by gravity, mechanical weathering, and the presence of interstitial water (from USGS).

TOPPLES: Toppling failures are differentiated by some features such as; the forward rotation of a unit or units about some pivotal point, below or low in the unit, under the actions of gravity and forces exerted by adjacent units or by fluids in cracks (Figure 2.2E) (from USGS).

FLOWS: There are five main categories of flows such as debris flow, debris avalanche, earthflow, mudflow, creep that differ from one another in fundamental ways (from USGS).

Debris flow: This kind of flow is a form of rapid mass movement and a combination of loose soil, rock, organic matter, air, and water mobilize as a slurry that flows downslope (Figure 2.2F) (from USGS).

Debris avalanche: Debris avalanche is a variety of very rapid to extremely rapid debris flow (Figure 2.2G) (from USGS).

Earthflow: It is stated that earthflows have a characteristic “hourglass” shape (Figure 2.2H). In the earthflow, the slope material liquefies and runs out, forming a bowl or depression at the head. The flow itself is elongate. Furthermore, it generally occurs in fine-grained materials or clay-bearing rocks on moderate slopes and under saturated conditions and dry flows of granular material are also possible (from USGS).

Mudflow: A mudflow is an earthflow and it consists of material that is wet enough to flow rapidly. In addition, material is composed of at least 50 percent sand-, silt-, and clay-sized particles (from USGS).

Creep: Creep is defined as the imperceptibly slow, steady, downward movement of slope-forming soil or rock. There are generally three types of creep: (1) First type of creep

is seasonal, where movement is within the depth of soil affected by seasonal changes in soil moisture and soil temperature; (2) Another creep is continuous, where shear stress continuously exceeds the strength of the material; and (3) The third type of creep is progressive, where slopes are reaching the point of failure as other types of mass movements. Moreover, creep is showed by curved tree trunks, bent fences or retaining walls, tilted poles or fences, and small soil ripples or ridges (Figure 2.2I) (from USGS).

LATERAL SPREADS: Lateral spreads are distinctive because they generally take place on very gentle slopes or flat terrain (Figure 2.2J). The failure is resulted in liquefaction, the process whereby saturated, loose, cohesionless sediments (generally sands and silts) are transformed from a solid into a liquefied state. Rapid ground motion usually triggers the failure (from USGS).

2.2. Features of Submarine Landslides

Submarine landslides are one of the basic agents that sediments are moved across through the continental slope to the deep ocean (Hampton, 1996).

Landslides have two basic features: One of these features is a rupture surface (sliding surface) and another feature is a displaced mass of sediment or rock (Figure 2.3). The rupture surface is where failure occurred. In addition, downslope movement occurred and more than one such surface may be show in a particular landslide complex. The displaced mass is the material that moved downslope. On the rupture surface, it usually rests partially. However, it might have moved completely beyond it. The rupture surface is vacated by the displaced mass. The upper part of the rupture surface is defined as the main scarp or headwall scarp. Crown cracks can be within marginally stable material upslope from the main scarp. Within the displaced mass, minor scarps can exist itself. The head of the landslide consists of the upslope terminus of the displaced mass. In addition, the toe is the downslope terminus (Hampton, 1996).

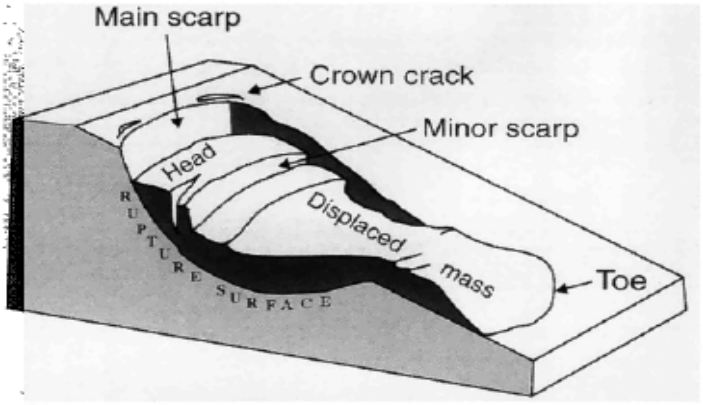

Figure 2.3. Features of submarine landslides; rupture surface (sliding surface) and displaced mass of sediment or rock (Hampton, 1996).

2.3. The Classification, Causes and Characterization of the Submarine Mass Failures

There are some reasons for triggering the failure of the submarine slopes. First reason is over-steepening because of the rapid deposition of the sediments. Another reason is generation of the gas originated by the decomposition of the organic matter. In addition, earthquakes and storm waves are other reasons. They are the main reason of the landslides on the continental slopes (Gutenberg, 1939). There are the materials included in the submarine mass movements and they are quite variable. The types of submarine mass movements are classified in Figure 2.4. This Figure is a altered version of the same classification offered for subaerial mass movements by the International Society for Soil Mechanics and Geotechnical Engineering (ISSMGE) Technical Committee on Landslides (Locat and Lee, 2002; Hayır *et al*., 2008).

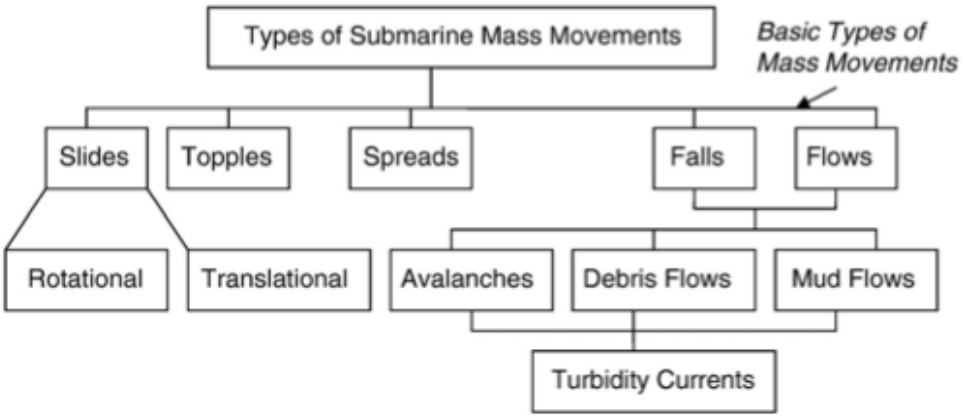

Figure 2.4. Classification of submarine mass movements adapted from subaerial classification proposed by the ISSMGE Technical Committee on Landslides (TC-11) (Hayır *et al*., 2008).

The gravity forces move the failed material. When the moving sediment is similar to a viscous fluid, the process is identified mass flow. A slide is constituted by the translational or rotational movement of fundamentally rigid segments with many discrete slope planes within the moving mass (Trifunac *et al.,* 2002a). Slumps are the slides in which the blocks of the failed material turn along the curved slip surfaces. When the sediment is heterogeneos, debris flow may consist of the end product of the disintegrating slides. Diluted suspension of the sediment grains supported by the fluid turbulence is transported the turbidity currents (Hayır *et al*., 2008).

The submarine landslides occur all depths (less than 2500 m). In addition, most of these initiate at the depths 800 m and 1000 m water depth. Furthermore, many landslides occur at the base of the slope (2.000 to 2.200 m water depth). Similarly, landslides can remove over the entire depth range (Booth *et al.,* 1993). The measured lengths of the landslides vary from 0.3 km to 380 km (the mode of distribution is at 2 km to 4 km). Moreover, the measured widths of the landslides range from 0.2 km to 50 km (the mode is at 1 km to 2 km) (Trifunac *et al.,* 2001). However, most of landslides have an area in the region of 10 km^2. Fifty six percent of landslides have originated at slopes equal or less than 4 degree. Large landslides which are more than 10 km^2 can occur on gentle the slopes ranging from 3 degree to 4 degree (Booth *et al.,* 1993). The debris slides (35%), the slumps (20%), the slab slides (17%) and the block slides (11%) often run into landslides. The

frequency of occurrence of debris flow and thick layer slides is about 8% (Hayır *et al*., 2008).

2.4. Tsunamis Generated by Submarine Landslides

Tsunamis generated by submarine landslides can be classified as long waves as most of the energy transferred from the landslide to the water motion is distributed on waves with typical wavelengths much larger than the characteristic water depth. Tsunami generation from submarine landslides depends primarily on the volume of the slide material and also on other factors such as angle of the slide, water depth, density of the slide material, the speed with which the material moves, duration of the slide, etc (Murty, 2003). According to Harbitz *et al.*,2006, the length of the landslide affects both the wave-length and the surface elevation, while the thickness and the acceleration or deceleration of the landslide as well as the wave speed (which again is determined by the water depth) determine the surface elevation. The maximum tsunami elevation usually correlates with the product of the landslide volume and acceleration divided by the wave speed squared, whilst the elevated water volume correlates with the product of the landslide volume and the Froude number. The Froude number (the ratio between the slide and wave speeds) is the basic parameter identifying the generation of surface waves and the most efficient generation happens near resonance when Fr = 1.0 (Fine *et al.,* 2003). Froud number is defined as:

$$Fr = u / c_0 \tag{2.1}$$

In addition, only a limited part of the potential energy released by the landslide is transferred to wave energy. Tsunamis generated by submarine landslides generally have very large run-up heights close to the source area. However, they have more limited far-field effects than earthquake tsunamis (Harbitz *et al.,* 2006). Furhermore, landslide generated tsunamis are much more localized than seismically generated tsunamis, and they can produce destructive coastal run-up and lead to severe damage to coastal emplacements (Fine *et al.,* 2003).

Wave formation and propagation thanks to submarine landslides are complex phenomena that can be divided into four parts: Landslide dynamics, energy transfer from landslide motion to water motion, wave propagation in open water, and wave run-up along the shores (Harbitz *et al.*, 2006).

Moreover, The total volume of the slide material is expected to be the basic parameter which influences the amplitude of a tsunami generated by a submarine landslide although several other parameters also play important roles (Murty, 2003). These factors, in random order, are the following:

a) Depth at which the slide occurs, or rather, depth of water above slide.
b) Angle of the slide from the horizontal (or vertical) direction.
c) Total distance moved by the slide.
d) Duration of the slide.
e) Density of the slide material.
f) Coherent nature of the slide.
g) Grain size and spectrum.
h) Characteristic speed with which the slide moves.
i) Volume of slide
j) Thickness of the slide material
k) Acceleration

Submarine landslides also alter the shape of the ocean bed, though unlike conventional tsunami the water surface is drawn down by the motion rather than raised up.

This drawing down of the ocean surface, as is demonstrated in the Figure 2.5 creates a void into which water inundates, creating a tsunami wave which propagates towards the shore (Richardson, 2002).

The definition sketch of the landslide generated tsunami parameters are indicated in Figure 2.6.

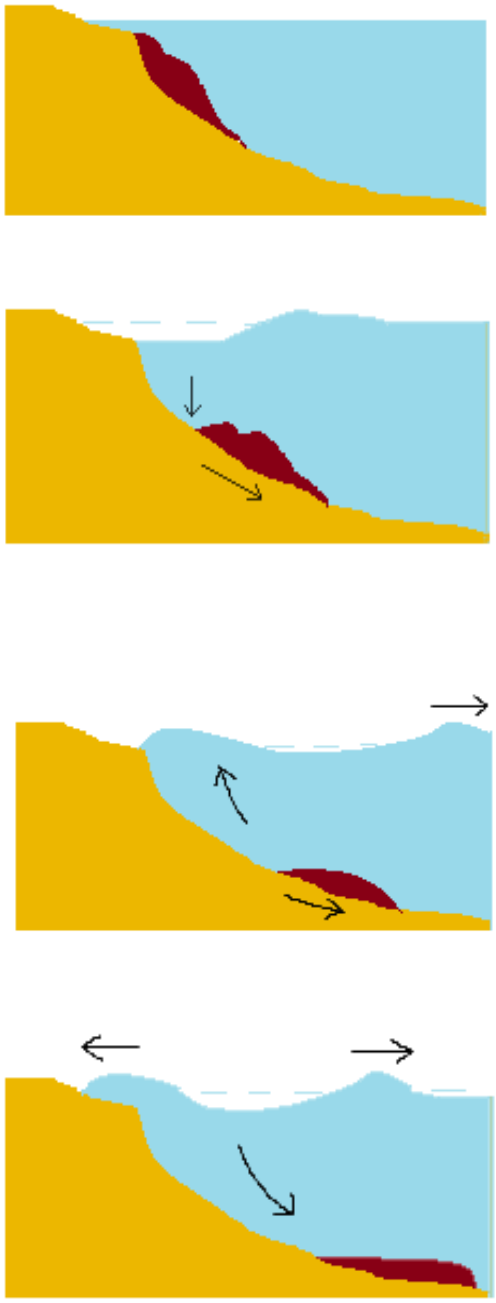

Figure 2.5. Tsunamis: Submarine landslide tsunami generation mechanism (modified from Richardson, 2002).

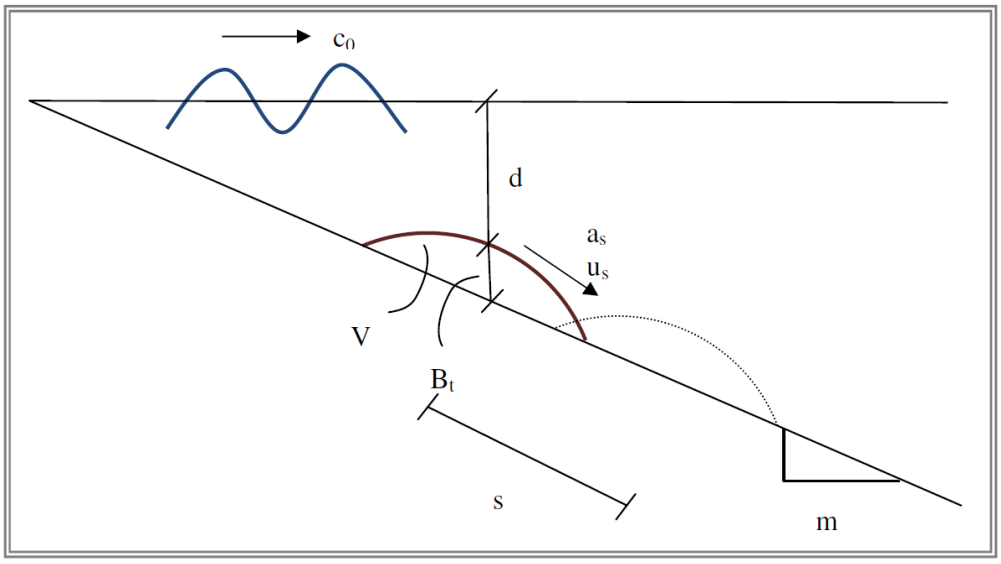

Figure 2.6. Definition sketch, landslide generated tsunami parameters (İnsel, 2009).

c_0 : linear long wave speed, $\sqrt{gh}$

u_s : speed of slide

a_s : acceleration of slide

d : depth of water above the slide

V : volume of the slide

B_t : thickness of the slide

m : slope of the landslide location

s : slide distance

t : time

Considering a block with uniform thickness moving on a horizontal seabed with constant velocity and ignoring dispersion, the demonstrations indicated that the length of the sliding block impacts the wave length, and the thickness, velocity and wave speed (depends on water depth) of the slide impacts surface elevation (İnsel, 2009).

3. LITERATURE SURVEYS AND HISTORICAL EVENTS

3.1. Literature Surveys

Tsunamis have important causes that are earthquakes, submarine landslides, volcanic eruptions and atmospheric conditions. In this thesis, tsunamis in the Marmara Sea generated by submarine landslides are studied. Numerical, analytical and experimental studies have performed about submarine landslides generated tsunamis. There are some studies about submarine landslides generated tsunamis in the world in the literature.

Pelinovsky and Poplavsky (1996) suggested a simple hydrodynamic model to describe/identify the water displacement above a moving slide. The model is based upon linear potential theory for an inviscid fluid with sources modelling the landslide motion. The maximal displacement of sea water will be for large values of the Froude number and an analytical formula for the wave height is attained. The maximal height of the tsunami wave relys only on the geometry of the landslide and on the basin depth. The landslide motion is examined with the mechanical model by Harbitz. Its results are used to compute the Froude number. In addition they are used to exam applicability of the hydrodynamic theory water waves and the mechanical model for a landslide motion. They observed that the estimates of tsunami waves created by the Storegga Slides (Norway) are in good agreement with outcomes of numerical simulations (Pelinovsky and Poplavsky, 1996).

Alpar *et al.,* (2001) investigated the probable underwater failures and modelling of tsunami propagation in the Sea of Marmara. The multibeam data, and the shallow and deep seismic reflection data of various marine surveys are examined to determine the slope failure potential as a possible tsunamigenic source in the Sea of Marmara. In this study, the underwater landslide and slump traces and potential landslide areas in eastern Marmara are indicated. A scenario of tsunami generation related to three landslides at the offshore region of the towns of Çınarcık and Yalova is determined as a study area. In order to define and discuss the propagation and distribution of maximum water surface elevation along the shores, a mathematical model Two-Layer was applied (Alpar *et al*., 2001).

Fine *et al.,* (2003), undertook several numerical experiments to analyze the effect of the subaerial component of slides on surface wave generation and to compare the tsunami generation efficiency of viscous and rigid-body slide models. They obtained that a rigid-body slide generates much higher tsunami waves than a viscous (liquid) slide. The maximum wave height and energy of created surface waves were found to rely on various slide parameters and factors, involving slide volume, density, slope angle and position. They also concluded that the added volume that happens when a subaerial slide enters the water causes a displacement of the sea surface and a significant increase in height of of the leading wave crest. Moreover, the critical parameter determining the occurrence of surface waves is the Froude number. It is defined as the ratio between the slide and wave speeds (Fine *et al*., 2003).

Lynett and Liu (2003) studied submarine landslide generated waves modeled using depth-integrated equations. In their study, they derived a mathematical model in order to define the generation and propagation of water waves by a submarine landslide. This mathematical model consists of depth-integrated continuity equation and a momentum equation, in which the ground movement is a forcing function. In addition, these equations contain full nonlinear, but weakly dispersive impacts and also this model is capable of describing wave propagation from relatively deep water to shallow water. Authors developed a numerical algorithm for the general fully nonlinear model. In the study, tsunamis generated by a prehistoric massive submarine slump off the northern coast of Puerto Rico are modeled as a case study. Finally, the evolution of the created waves and the large runup owing to them is discussed (Lynett and Liu, 2003).

Murty (2003) investigated tsunami wave height dependence on landslide volume. Tsunami generation from submarine landslides relys on the volume of the slide material. In addition, it depends on other factors which involves: angle of the slide, water depth, density of the slide material, duration of the slide, the speed with which the material moves etc. Based on an incomplete data set of volume V of slide versus maximum amplitude H of the resulting tsunami waves, gleaned through available literature, a simple linear regression relationship was improved. Moreover, another partial data set was improved from published literature, on V versus H values, based on numerical models. It was obtained that the agreement between the consequences of the numerical simulations and the observations is rather poor. The purpose of the study is modest and simple; to obtain a relationship

between the volume V of the slide (expressed in millions m^3) and the maximum amplitude H (in meters) of the resulting tsunami waves, based on observational data available in the published literature and to compare relationship with the consequences of some numerical models. The basic argument used in this study is that the slide volume must remain the most important and main parameter. The aim then is to obtain an orde of magnitude relationship between V and H (Murty, 2003).

Okal and Synolakis (2003), in their study, are motivated by recent investigations of the catastrophic tsunami of 17 July 1998 in Papua New Guinea. They display a number of theoretical discussions of the excitability of tsunami waves by both earthquakes sources and underwater landslides or slumps. In the study, they use simple physical models to evaluate and compare the orders of magnitude of the energy created into a tsunami wave by seismic dislocations and underwater slumps. They conclude that the two sources can create tsunamis of comparable total energy. But, the slumping source leads to a low-frequency deficiency in the far field because it is displayed to be fundamentally dipolar in nature (Okal and Synolakis, 2003).

Grilli and Watts (2005) studied tsunami generation by submarine mass failure. In this study, using a two-dimensional (2D) fully nonlinear potential flow (FNPF) model, numerical simulations are performed for tsunami generation by two types of submarine mass failure (SMF): underwater slides and slumps. According to Grilli and Watts, slides is defined as thin, translational failures travelling over long distances and slumps is defined as thick, rotational failures occurring with minimal displacement. In each case, the SMF center of motion is stated as a function of geometric, hydrodynamic, and material parameters, following a simple wavemaker formalism. In addition, it is prescribed as a boundary condition in the FNPF model. Tsunami amplitudes and runup are found from computed free surface elevations. Model consequences are experimentally validated for a rigid 2D slide. Using the two-dimensional (2D) tsunami generation model, sensitivity studies are performed to estimate the impacts of SMF shape, deformation, type and initial submergence depth on the generated tsunami amplitude and runup. A strong SMF deformation during motion is displayed to significantly enhance tsunami generation, especially in the far-field. Typical slumps are displayed to generate smaller tsunamis than corresponding slides. Both tsunami amplitude and runup are displayed to rely strongly on initial SMF submergence depth. For the selected SMF idealized geometry, this dependence

is simply stated by power laws. In conclusion, they indicate that for rigid slides of Gaussian shape, both near and far field tsunami amplitudes increase if shape spreading decreases. Moreover, they indicate that , for slides, a reasonable rate of deformation during motion has little impact on near field tsunami features, but more significantly influences far field features. But, an extreme rate of deformation, significantly influences both near and far field tsunami features. Finally, the impact of initial submergence depth is examined for a rigid slide, and a detailed analysis of tsunami amplitude and run-up is made (Grilli and Watts, 2005).

Minoura *et al.*, (2005) in their study, examined the tsunami generated by a possible submarine slide. They have discovered a tsunamigenic sediment layer in fluvio-alluvial sequences on the north coast of the Marmara Sea. The layer is composed of unsorted silty coarse sand containing terrestrial molluscs and charcoal fragments. They suggest that a tsunami occurred in the Sea of Marmara in the middle of 11 the century and invaded the fluvial plains. In this study, they wanted to relate the development of a landward-tapering sand layer to the seawater flooding. The tsunami run-up resulted in the catastrophic invasion of seawater and they conclude that a submarine landslide slide probably triggered by th loss of slope stability, generated the tsunami. In this paper, the results proposed that the coastal zones of the Marmara Sea have been subjected to erosion and regress on a large scale during the active intervals of the North Anatolian Fault movement.

Harbitz *et al.*, (2006) studied mechanisms of tsunami generation by submarine landslides. The features of tsunami generated by a submarine landslide are primarily determined by the volume, the maximum velocity, the initial acceleration, and the possible retrogressive behaviour of the landslide. Submarine landslides are often clearly sub-critical (Froude number $<<1$), and so it is stated that that the maximum tsunami elevation generally correlates with the product of the landslide volume and acceleration divided by the wave speed squared. Examples of numerical simulations indicate that only a limited part of the potential energy (0.1-15 %) released by the landslide is transferred to wave energy. In addition, it is stated that frequency dispersion is of little importance for waves created by large and sub-critical submarine landslides. Finally, tsunamis created by submarine landslides often have very large run-up heights close to the source area, but have more limited far-field effects than earthquake tsunamis. Authors exemplified these

aspects via simulations of the Holocene Storegga Slide, the 1998 Papua New Guinea, and the 2004 Indian Ocean tsunamis (Harbitz *et al*., 2006).

Masson *et al.,* (2006) summarize current knowledge of such landslides and the problems of assessing their hazard potential in their study. The hazards related to submarine landslides contain destruction of seabed infrastructure, collapse of coastal areas into the sea and landslide-generated tsunamis. The key factors affecting landslide occurrence are elevated pore pressures (leading to decreased frictional resistance to sliding) and specific weak layers within stratified sequences. Elevated pore pressures can originate from normal depositional processes or from transient processes. They are earthquake shaking; historical evidence offers that the majority of large submarine landslides are triggered by earthquakes. Due to their tsunamigenic potential, ocean-island flank collapses and rockslides in fjords have been determined as the most dangerous of all landslide related hazards. In the study, the Storrega slide and Canary Islands slides are exemplified (Masson *et al*., 2006).

Hayır *et al.,* (2008) studied the tsunamis originating from a submarine mass failure such as slides and slumps induced by earthquakes or other environmental effects, which is settled at the bottom of the north eastern Sea of Marmara. They developed one hybrid method as the solution method. The main purpose of this solution method is to combine an analytical solution presenting near-field tsunami amplitudes above the submarine mass failure with a numerical solution displaying the tsunami amplitudes in the coastal regions. One common linear boundary between analytical and numerical solution domains is determined for this purpose in the study. With the help of one simple kinematics source model, Movements of Submarine Mass Failures (SMF) are modeled. In addition, the amplitudes of the tsunamis are determined by using the analytical method. The solutions are determined in the numerical region using TELEMAC-2D software system. The generation, propagation and coastal amplifications of the tsunamis are exemplified at some certain points and regions (Hayır *et al*., 2008).

Lopez-Venegas (2008) studied submarine landslide as the source for the October 11, 1918 Mona Passage tsunami in this paper. The October 11, 1918 ML 7.5 earthquake occurred in the Mona Passage between Hispaniola and Puerto Rico. It generated a local tsunami that claimed approximately 100 lives along the western coast of Puerto Rico. Now the area affected by this tsunami is substantially more populated. A fresh submarine

landslide is indicated by newly acquired high-resolution bathymetry and seismic reflection lines in the Mona Passage. The landslide area is about 76 km^2 and possibly displaced a total volume of 10 km^3. Furthermore, the landslide's headscarp is at a water depth of 1200 m, with the debris flow extending to a water depth of 4200 m. The authors modeled the tsunami as created by a landslide with a duration of 325 s (corresponding to an average speed of ~27 m/s) and with the observed dimensions and location by using the extended, weakly non-linear hydrodynamic equations implemented in the program COULWAVE. In addition, computed marigrams indicated a leading depression wave followed by a maximum positive amplitude in agreement with the reported polarity, relative amplitudes, and arrival times. Their results propose this newly-identified landslide, which was likely triggered by the 1918 earthquake , was the main reason of the October 11, 1918 tsunami and not the earthquake itself. Finally, results from this study should be useful to help discern poorly constrained tsunami sources in other case studies (Lopez-Venegas, 2008).

İnsel (2009), in her thesis, studied mechanism an modeling of tsunamis generated by landslides. In the study, landslide parameters affecting the surface wave characteristics are investigated. The generation of the submarine landslide generate tsunamis are investigated by using TWO-LAYER model. This model solves nonlinear long wave equations simultaneously within two interfacing layers with necessary boundary conditions at the sea bed, interface and water surface. One of the probable landslides at offshore Yalova in the Sea of Marmara is selected as a study area. The density and the thickness of the slide material are examined. Furthermore, a sensitivity analysis is performed to determine the level of their effects on the evolution and amplitude of the tsunami source. Finally, the propagation and coastal amplification of the landslide generated waves are studied using the tsunami simulation and visualization code NAMI-DANCE (İnsel, 2009).

3.2. Historical Events

There are several tsunami events induced by landslides in history. In this part, some information about some of the tsunamis generated by landslides is given.

The Storegga Slide (7000 BC)

The Storegga slide which is one of the largest pre-historical submarine landslides occurred ca. 7000BC in the Northern Sea at the edge of the continental shelf of Norway. The estimated volume of mass flow was 1,700 km^3. The tsunami hit a large part of the Scottish coast. Wave height was 6-8 meters (Gusiakov, 2003)**.**

Mona Passage (1918, October 11)

An earthquake magnitude of ML 7.5 occurred in the Mona Passage between Hispaniola and Puerto Rico and a local tsunami was generated by this earthquake. The high-resolution bathymetry and seismic reflection lines in the Mona Passage indicate a submarine landslide 15 km northwest of Rincon in northwestern Puerto Rico. The landslide area is nearly 76 km^2 and a total volume of 10 km^3 (Lopez-Venegas, 2008).

The Grand Banks, Newfoundland (1929, November 18)

A magnitude M=7.2 earthquake took place at the southern edge of the Grand Banks, about 280 km south of Newfoundland. A large submarine slope failure (200 km^3) was triggered by the earthquake. The landslide was turned into a turbidity current carrying mud and sand and its speeds ranged from 60 – 100 km/ h. The tsunami generated by this failure is the most catastrophic tsunami in Canadian history (Fine *et al*., 2004). In addition analyses of the 1929 Grand Banks tsunami show that it was created by the large submarine slope failure rather than the earthquake itself (Murty, 1977). Amplitudes of tsunami waves were 3 m and 8 m (Fine *et al*., 2004).

Unimak Island (Aleutian Islands, 1946, April 1)

The Unimak (eastern Aleutians) earthquake of April 1, 1946 caused a large tsunami (Mt=9.3) with 42 m runup at Unimak Island. The narrow beam of large waves in the far field and the rapid variation in near-source run-up could not be defined by only eartquake/seismic source. The writers believe that the slow rupture, the tsunami directivity, the rapid variation in near-source wave heights, the period of the waves, and the strong T-phase generation, together offer an earthquake-triggered landslide rather than a purely tectonic source (Fryer *et al*., 2004).

Amorgos Island, Greece (1956, July 9)

The earthquake of 1956 July 09 with magnitude 7.8 was the largest one to strike/(hit) Greece in the 20th century, near Amorgos Island in the southcentral Aegean Sea. It produced a local tsunami affecting the shores of the Cyclades and Dodecanese Islands, Crete and the Turkish coast of Asia Minor. The run-up had values of 30, 20 and 10 m reported on the southern coast of Amorgos, on Astypalaia and Folegandros, respectively. The highest reported in the 20th century over the whole Mediterranean Basin caused to suggest a submarine landslide (or a series of landslides) as the source of the tsunami, based upon the excessive amplitude and general heterogeneity of run-up in the epicentral area (Okal *et al*., 2009).

Lituya Bay, Alaska (1958, July 9)

On July 10, 1958 the magnitude 7.8 earthquake occurred in the south-eastern Alaska. Among the best-known examples of the extreme water splash in the recent history is a well-documented 525 meter run-up in the Lituya Bay (Alaska) induced by a massive landslide took place after the earthquake. Another cases of the extreme run-up heights in the same bay are the 1936 and 1853 events. The maximum run-up heights of these events are 150 and 120 meters, respectively (Gusiakov, 2003).

Alaska (1964, Mar 28)

The Great Alaska Earthquake of 1964 (Mw = 9.2) took place in North America and led to major damage to all of the coastal communicities especially Seward and Valdez in southcentral Alaska. In addition, it caused 43 deaths in these communicaties. Most of the damage and deaths were resulted from tsunamis that took place immediately after the

earthquake. In addition, they were most probably induced by local submarine landslides. According to the investigations; landslide deposits near Seward typically take the form of a series of large and small blocks lying directly off the front of the town, eventhough there are indications of sandy and muddy debris flows occurring off river deltas. Near Valdez, landslide morphologies contain at least three forms. These forms are a field of large blocks (up to 40 m high), an intricate series of gullies, channels, and talus near the fjord-head delta and a broad debris lobe that apparently flowed half-way down the fjord and stopped. The 1964 landslide tsunamis may have been composites originating from a number of landslide events (Lee *et al*., 2006).

Kitimat Inlet (1975, April 17)

On April 27th, 1975, A large tsunami was generated in the Kitimat Inlet in the Douglas Channel system on the West Coast of Canada due to a submarine landslide (Murty, 2003).

In history, there are several landslides in the Kitimat Inlet on the West Coast of British Columbia. They occurred during the period 1952 to 1968 and in 1971. On October 17, 1974, following a submarine landslide, amplitude of water wave was 2.8 m. On April 27, 1975, following a major slide, water waves with varies to 8.2 m were created. In addition, major slides occur in other parts of British Columbia such as in Howe Sound, in 1995 (Murty, 2003).

Flores Island, Indonesia (1982, December)

In December 1982, an earthquake of magnitude MS=5.6 occurred at the eastern tip of Flores Island. It created landslides and reportedly resulted with the tsunami (Brune *et al*., 2010).

Flores Island, Indonesia (1992 – December 12)

An earthquake of magnitude Mw 7.8 occurred in December 1992 at the northern coast of the Flores island, Indonesia. The wave height was 26 m. The village of Riangroko was destroyed by the waves and claimed 122 lives possibly resulted from a nearby underwater landslide (Synolakis *et al*., 2003).

İzmit (1999, August 17th)

At the Kocaeli 1999 Earthquake; subsidence, masses of coastal landslides and the sea water inundation were happened at Kavaklı, Değirmendere, Halıdere, Ulaşlı and Karamürsel. Masses of coastal landslides at Değirmendere led to about 20 m deepening (Altınok *et al*., 2000). The wave height was 2.5 m and also maximum run-up was 4 m in Gölcük (Yalçıner *et al*., 2005).

Along the southern coast between Değirmendere and Güzelyalı, run-up heights of 0.8 m in Halıdere and other areas maximum 2.5 m proceeded up to 6 km east of Gölcük and 10 km west of Güzelyalı (Yalçıner *et al*., 2001).

1998, July 17- Aitape, Papua New Guinea

On the evening of Friday July 17, 1998, a magnitude Ms 7.1 Earthquake took place near the northwest coast of Papua New Guinea 850 km northwest of Port Moresby, the capitol of Papua New Guinea (PNG). The earthquake was followed by the catastrophic tsunami (Yalçıner *et al*., 2001) and PNG tsunami damaged villages with the loss of over 2200 lives (Tappin *et al*., 2008). In addition, a landslide occurred near Sissano lagoon, west of Aitape (Brune *et al*., 2010). Recent investigations show that slump width is 4.2 km, the slump length is 4.5 km and the slump thickness 0.75 km. Moreover, slide volume is 6.4 km^3 (Tappin *et al*., 2008) and an underwater slump is consist of 4 km^3 of sedimentary material (Okal *et al*., 2003).

Stromboli (2002, December 30)

On 30 December 2002, the coast of the volcanic is land of Stromboli, in the Tyrrhenian sea, was hit by two tsunamis generated by landslides that occurred on the northwest flank of the volcano. Two basic landslides were recorded by the seismic network along the steep slope of Sciara del Fuoco. The tsunamis were generated by the mass movements (Tinti *et al*., 2005).

4. THE MARMARA SEA

4.1. Morphological and Tectonic Features of the Sea of Marmara

The Marmara Sea is an oval shaped interior sea situated between Asia (Anatolia) and Europe (Thrace) (Yılmaz *et al*., 2010). In addition, it is tectonically active basin located the branches of the North Anatolian Fault (Özeren *et al*., 2010) (NAF). The morphological properties of the Marmara Sea Basin: the shelves, slopes, and the deeper parts of the basin show different properties at different sites (Yılmaz *et al*., 2010). There are two well developed shelves in the northern and the southern sides of the Marmara Sea. These shelves are about -100 m deep, and they cover the largest areas within the Marmara Sea region. The northern shelf is about 3-5 km wide. When it is compared to the southern shelf , it is very narrow and exceeds 30 km in width. The latter covers an area of 1883 km^2 (Yılmaz *et al*., 2010).

The Marmara Sea is bordered in the east and west by two linear mountain ranges. They are the Armutlu and Ganos Mountains. They rise steeply in front of the sea and because of this, there are no wide shelves along the highs (Yılmaz *et al*., 2010).

The Marmara Sea consists of three sub-basins which are known as the the Çınarcık, Central, and Tekirdağ basins, from east to west.

The Çınarcık Basin (the eastern sub-basin) is the best-known trough in the Sea of Marmara. It is the largest sub-basin and deeper than the others (1270 m) (Yılmaz *et al*., 2010). It is stated that this wedge-shaped sub-basin is opened by the intersection of the NAF with the nortwest-trending Thrace-Eskişehir Fault (Yaltırak *et al*., 2000; Alpar and Yaltırak 2000a). In addition, it is cut through by a number of secondary oblique faults by low-angle to the NAF's northern branch. It is a significant slump-prone area. Moreover, the morphological features of its continental shelf and slopes are different. The northern shelf is covered by the Plio-Quaternary sediments above the Palaeozoic sedimentary basement. On the shelf the thickness of the sub-horizontally stratifed sediments varies 95-

120 m (Alpar *et al*., 2001). The top 3 m of sediments (representing last 18 kyr) are composed of laminated muds interbedded with two main sapropelic and sometimes turbiditic layers (Cağatay *et al*., 2000), consisting potential slide horizons. The southern shelf is very narrow. The thickness of the sub-horizontally stratifed sediments on the shelf varies 15-25 m (Alpar *et al*., 2001) .

The Tekirdağ and The Central sub-basins are 1250 m and 1120 m deep, respectively (Yılmaz *et al*., 2010). The Tekirdağ Basin (the western sub-basin) is the westernmost of these steep-flanked basins (10-30º slopes). It is an elongate and southwest-trending rhombohedral depression. The Central sub-basin is an elongate depression, aligned to the trend of the Main Marmara Fault. In addition, a ridge borders the Central and Kumburgaz sub-basins (Yalçıner *et al*., 2002).

4.2. Causes of Submarine Landslide in the Marmara Sea

There are several reasons for generating tsunamis in the Marmara Sea. Sari *et al.*, (2006) classified these reasons as presented in Table 4.2. According to table; because of high sedimentary rate of slopes and because of the lowering strength along with the historical time, two reasons are realistic such as earthquakes and landslides. In addition, it is possible that slope failure can be usually created because of weathering and rock falls of the extremely surface layers (OYO and IMM, 2007).

For some time it is not impossible but very rare that the weakened slopes can be begin failure by means of triggers of earthquakes and other causes. These cases require very long time such as several thousand years, much longer than the return periods of 200-250 years for big earthquakes in the Sea of Marmara. Thus, earthquakes or active faults which are the reason of tsunamis is the only reason treated here (OYO and IMM, 2007).

Table 4.2. Reasons of submarine landslides in the Marmara Sea (Çınarcık Basin) after Sari *et al.*, 2006 (modified from OYO and IMM, 2007).

Items	Remarks	Evaluation
River Flow	Kocasu River is far (40 km) away from the Basin. Sedimets from the river is dissected by Imreli Platform (-400 m depth) etc. since at least 7000 years before. Submarine canyon in South Slope has been inactive during the latest sea level high stand.	non-realistic
Storm Surge	Influential Depth will be less than 30 m, then Shelf Edge (depth 100 m) is out of the range.	non-realistic
Volcanic Activities	No volcano activities near Marmara Sea during klast 100,000 years. Santorini Volcano in mid Aegean Sea is the nearest, but last eruption was 3,500 years before.	non-relistic
Tide	Usual tidal change Marmara Sea is around 15 cm. Sea level rising from -85 m to present level during these 12,000 years.	non-realistic
Gas Escape	Latest 7,000 years, high sea level an hydrostatic pressure has been high.	non-realistic
Earthquakes	Active faults of NAF exist just under the sea, that has been active and generated numerous earthquakes during the years with magnitude up to 7.4.	realistic
Tsunami	Some tsunami has been generated by big earthquakes, but the strength of tsunami is not so high comparing to other seas of the world like Pacific Ocean.	not impossible but not so realistic.
High Sedimentary Rate	Geology itself is stiff, but turbulance of the sea water, earthquakes may made it more instable.	not impossible

5. METHODOLOGY

5.1. TWO-LAYER

The generation of the submarine landslide generated tsunamis are modeled using TWO-LAYER model in this study. The model TWO LAYER (Imamura and Imteaz, 1995) which was developed in Tohoku University Disaster Control Research Centre in Japan by Prof. Imamura. The model TWO LAYER solves the non-linear long wave equations simultaneously by using the finite difference method and following the Leap-Frog solution procedure (Shuto *et al.,* 1990) within two interfacing layers with appropriate kinematic and dynamic boundary conditions at the sea bed, interface and water surface. The two interfacing layers consists the water body in the sea and the moving mass at the bottom. In addition, after the sensitivity analysis for different input parameters such as the geometry of the basin, the volume and size of the slided mass, and the bottom slope tested in a regular shaped basin (Özbay, 2000, Yalçıner *et al.* 2001c) (Yalçıner *et al*., 2002).

Two-layer flow may originate from density differences within the fluid. This density difference may be owing to temperature differences or dissolved substances as well as suspended material within the liquid. Moreover, in two-layer flow both layers interact and play a significant role in the establishment of control of the flow. The influence of the mixing or entrainment process at a front or an interface becomes significant (Imamura and Imteaz, 1995).

5.1.1. Theoretical Approach

Two-layer flows that take place owing to underwater landslide can be formed using a non-horizontal bottom with a hydrostatic pressure distribution, uniform density distribution, uniform velocity distribution and negligible interfacial mixing in each layer. The definition sketch for two-layer flow is shown in Figure 5.1. In addition, conservation of mass and momentum continuities are integrated in each layer, with the kinetic and

dynamic boundary conditions at the free surface and interface surface (Imamura and Imteaz 1995).

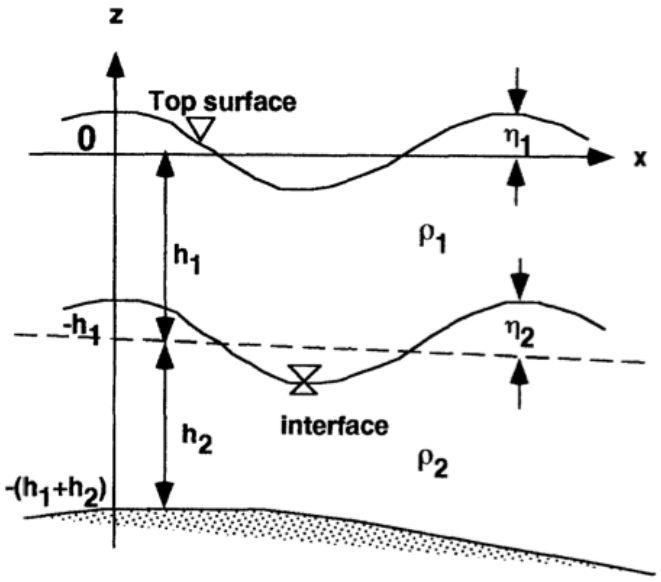

Figure 5.1. Definition sketch for Two-Layer Profile (Imamura and Imteaz, 1995).

Governing equations are consisted of continuity Equation and Equation of motion in two directions (x-y) on horizontal plane. Continuity Equation provides mass conservation and Equation of motion satisfies the momentum conservation. Those Equations for the upper layer are given by:

$$\frac{\partial(\eta_1-\eta_2)}{\partial t}+\frac{\partial M_1}{\partial x}+\frac{\partial N_1}{\partial y}=0 \tag{5.1}$$

$$\frac{\partial M_1}{\partial t}+\frac{\partial\left[\frac{M_1^2}{D_1}\right]}{\partial x}+\frac{\partial\left[\frac{M_1N_1}{D_1}\right]}{\partial y}+gD_1\frac{\partial\eta_1}{\partial x}-gD_1\frac{\partial\eta_2}{\partial x}-\frac{g\eta^2}{D_1^{7/3}}M_1\sqrt{M_1^2+N_1^2}=0 \tag{5.2}$$

$$\frac{\partial N_1}{\partial t}+\frac{\partial\left[\frac{N_1^2}{D_1}\right]}{\partial y}+\frac{\partial\left[\frac{M_1N_1}{D_1}\right]}{\partial y}+gD_1\frac{\partial\eta_1}{\partial x}-gD_1\frac{\partial\eta_2}{\partial x}-\frac{g\eta^2}{D_1^{7/3}}M_1\sqrt{M_1^2+N_1^2}=0 \tag{5.3}$$

and those for the lower layer are:

$$\frac{\partial \eta_2}{\partial t} + \frac{\partial M_2}{\partial x} + \frac{\partial N_2}{\partial y} = 0 \tag{5.4}$$

$$\frac{\partial M_2}{\partial t} + \frac{\partial\left(\frac{M_2^2}{D_2}\right)}{\partial x} + \frac{\partial\left(\frac{M_2 N_2}{D_2}\right)}{\partial y} + gD_2\left\{\partial\left(\frac{\partial \eta}{\partial x} + \frac{\partial h}{\partial x} - \frac{\partial \eta_2}{\partial x}\right) + \frac{\partial \eta_2}{\partial x} - \frac{\partial h}{\partial x}\right\} + \frac{g\eta^2}{D_2^{7/3}} M_2\sqrt{M_2^2 + N_2^2} = 0 \tag{5.5}$$

$$\frac{\partial N_2}{\partial t} + \frac{\partial\left(\frac{N_2^2}{D_2}\right)}{\partial y} + \frac{\partial\left(\frac{M_2 N_2}{D_2}\right)}{\partial y} + gD_2\left\{\partial\left(\frac{\partial \eta}{\partial y} + \frac{\partial h}{\partial y} - \frac{\partial \eta_2}{\partial y}\right) + \frac{\partial \eta_2}{\partial y} - \frac{\partial h}{\partial y}\right\} + \frac{g\eta^2}{D_2^{7/3}} N_2\sqrt{M_2^2 + N_2^2} = 0 \tag{5.6}$$

Where η is referred the surface elevation, D=h+ η the total depth, h is the still water depth, M and N are referred the discharge fluxex in x and y directions respectively, ρ the density of the fluid, $\alpha=\rho_1/\rho_2$, and subscripts 1 and 2 indicate the upper and lower layer respectively (Imamura and Imteaz, 1995). In addition, M_1, N_1, η_1, η_2, M_2, N_2 are solved from the above 6 Equations numerically. At the open boundary the total derivative of surface elevation is set to be equal to zero as :

$$\frac{D\eta}{Dt} = 0 \tag{5.7}$$

The dynamic and kinetic boundary conditions at surface and bottom are difened as follows:

$$p = 0 \qquad atz = \eta \tag{5.8}$$

$$w = \frac{\partial \eta}{\partial t} + u\frac{\partial \eta}{\partial x} + v\,\frac{\partial \eta}{\partial y} \qquad atz = \eta \tag{5.9}$$

$$w = -u\frac{\partial h}{\partial x} - v\frac{\partial h}{\partial y} \qquad atz = -h \tag{5.10}$$

5.1.2. Numerical Approach

The staggered leap-frog scheme (Shuto, Goto, Imamura, 1990) has been used in order to solve the governing equations for long waves numerically. The staggered leap-frog scheme is one of explicit central difference schemes. Furthermore, the staggered scheme considers that the computation point for one variable, η, does not coincide with the computation point for other variable, M. There are some differences, 1/2Δt and 1/2Δx between computation points of two variables. Therefore one variable, η, is at the middle of Δt Δx rectangle, setting other variables at the four corner of rectangle. In the finite difference formulation, 'n' is referred the temporal grid points and 'i' and 'j' are the spatial grid points along x and y directions. Δx, Δy, and Δt are referred spatial grid spacings and time step respectively. The finite difference equations for the governing equations are obtained by using this scheme (Imamura and Imteaz, 1995).

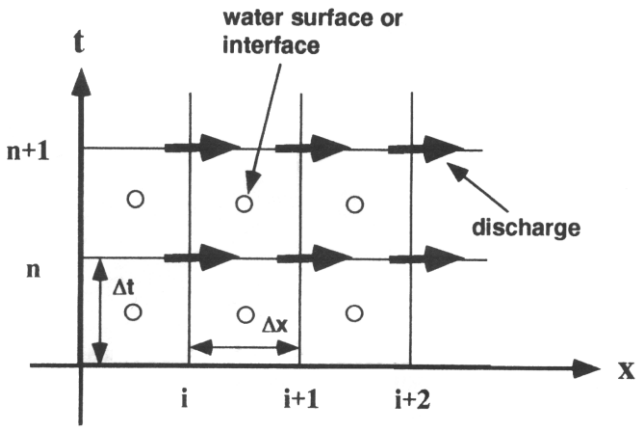

Figure 5.2. Points schematics of the staggered leap-frog scheme (Imamura and Imteaz, 1995).

In spatial direction, all of η_1, η_2 at step 'n+ ½' and all of M_1, M_2 at step 'n' are initial conditions. For all later time steps at left and right boundaries, all values of either discharge or water elevation would be estimated with the values of previous time step or estimated wave celerity. This solution consists of two progressive waves with different celerities and one reflective wave. By using the mass continuity equation for a lower layer, all η_2 at step 'n+3/2' are computed and then all η1 at step 'n+3/2' for an upper layer are computed using

latest values of η_2. All values of M_1, N_1, M_2, N_2 at step 'n+1' are simultaneously computed by using the momentum equation for an upper and a lower layer. Similarly, when new values of η_1, η_2, M_1, N_1, M_2, N_2 are used as initial values for the next time step, the calculations progresses in time up to desired step (Imamura and Imteaz, 1995).

While doing these calculations, it is very hard for the model to obtain a stability condition analytically owing to the interactions between two layers. Courant-Friedrichs-Lewys (CFL) condition is used where two celerities exist as one for a progressive wave and one for reflected wave. Stability is initially researcherd for some arbitrary Δx and Δt. This result proposed that the model is stable up to a certain limit of $\Delta x/\Delta t$. The limit varies with the variation of α and β (Imamura and Imteaz, 1995). It is offered by Imamura and Imteaz (1995) that as for lower 'α' and for higher 'β', an amplification of a top surface goes up and vice versa. h is the water depth and subscripts 1 and 2 indicate the upper and lower layer respectively (Imamura and Imteaz, 1995). According to Imamura and Imteaz (1995), for α= 0.5 and β=4.0, celerity of top surface counted through analytical expression,

$$c_2 = \sqrt{gh_2\ (1-\alpha)/(1+\alpha\beta)} \tag{5.11}$$

controls the stability criteria, while for α= 0.4 and β= 1.0, celerity of interface

$$c_1 = \sqrt{gh_1\ (1+\alpha\beta)} \tag{5.12}$$

corresponds to the stability criteria. It is offered by Imamura and Imteaz (1995) to consider the maximum of c_1 and c_2, to satisfy the stability condition $\Delta t \leq \Delta x/\max(c_1, c_2)$ (Imamura and Imteaz, 1995).

The numerical model TWO-LAYER is more realistic than the previous models in the sense that it combines the impacts of an underwater earthquake and an underwater landslide on the generation and propagation of tsunami waves, which is the case in reality as observed and studied for years for different cases of tsunami events (Imamura and Imteaz, 1995).

5.1.3. Testing of Numerical Model TWO LAYER

There is not specific Benchmark Problem for validation of numerical model TWO LAYER. However, Watts, Imamura and Grilli (2000), proposed three Benchmark cases to study tsunamis created by underwater landslides by applying TWO LAYER model and 2D Boundary Element Model (Grilli *et al.*,1989, 1996) to the laboratory experiments conducted in the University of Rhode Island wavetank. Each model involves distinct center of mass motions and rates of landslide deformation. Computed tsunami amplitudes agree reasonably well for both models, although there are some differences.

In this study, different (subsidence type and subsidence- uplift type) landslide types are applied to the two different regular shaped (simple and oblique) 1:10 sloped bathymetry domains by using TWO LAYER.

5.1.3.1. Curved Shape Erosion Type Landslide on a 1:10 Slope. The landslide with a curved shape 30 m erosion is selected in one of the test applications of TWO LAYER. The location of the landslide on the 1:10 slope is shown in Figure 5.3. The red area indicates that the water depth becomes deeper at the landslide area.

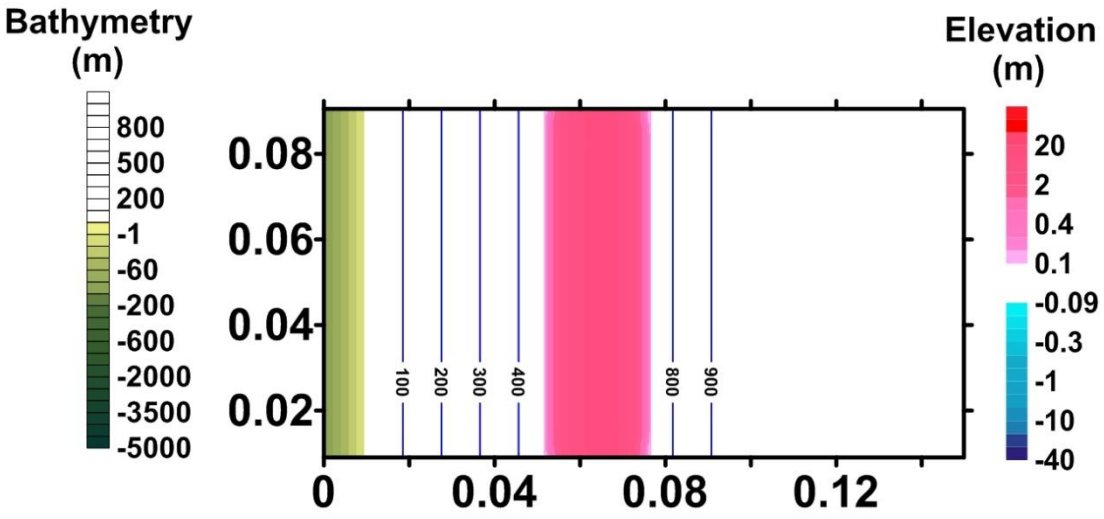

Figure 5.3. The location of curved shape erosion type landslide on the regular shaped simple slope bathymetry.

5.1.3.2. Wave Shape Erosion / Deposition Type Landslide on a 1:10 Slope. The wave shape landslide with 30 m erosion and deposition is selected in the test application of TWO LAYER. The location of the landslide on the 1:10 slope is shown in Figure 5.4. The red area indicates that the water depth becomes deeper at the landslide area and blue area indicates the area of material deposition and decrease of the water depth.

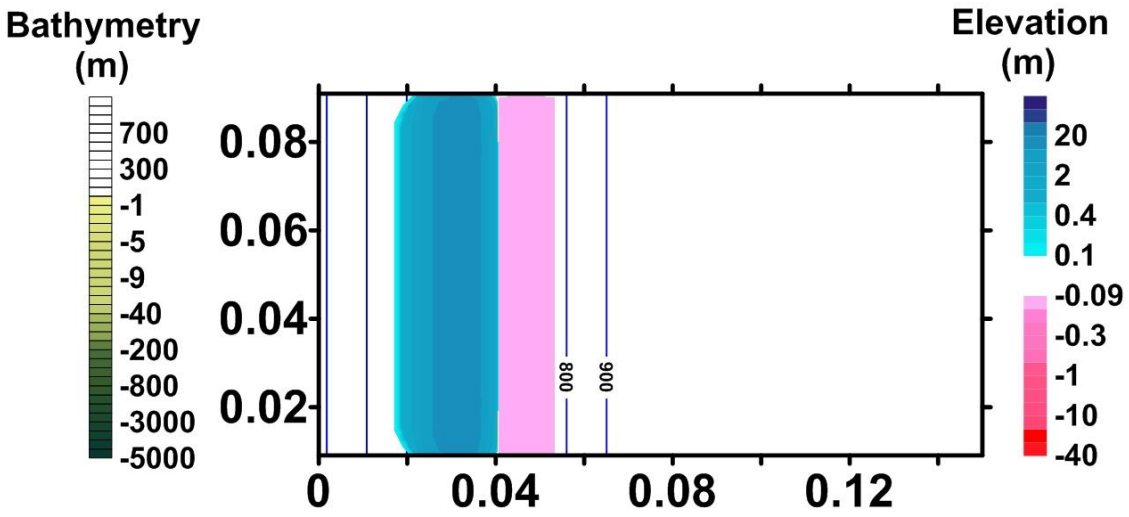

Figure 5.4. The location of wave shape erosion / deposition type landslide on the regular shaped simple slope bathymetry.

5.1.3.3. Curved Shape Erosion Type Landslide on a 1:10 Oblique Slope. The landslide with a curved shape 30 m erosion is selected in one of the test applications of TWO LAYER. The location of the landslide on the 1:10 slope is shown in Figure 5.5. The red area indicates that the water depth becomes deeper at the landslide area.

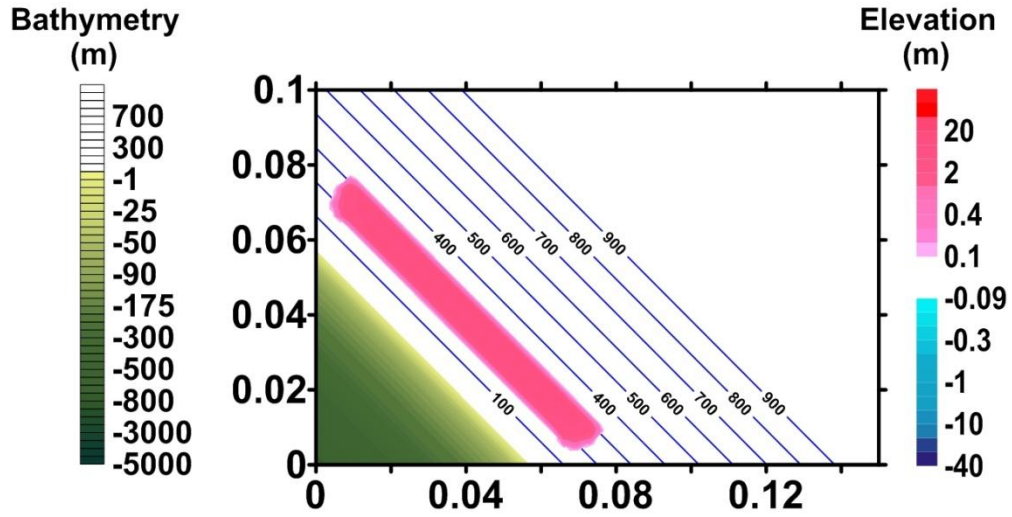

Figure 5.5. The location of curved shape erosion type landslide on the regular shaped oblique slope bathymetry.

5.1.3.4. Wave Shape Erosion / Deposition Type Landslide on a 1:10 Oblique Slope.

The wave shape landslide with 30 m erosion and deposition is selected in the test application of TWO LAYER. The location of the landslide on the 1:10 slope is shown in Figure 5.6. The red area indicates that the water depth becomes deeper at the landslide area and blue area indicates the area of material deposition and decrease of the water depth.

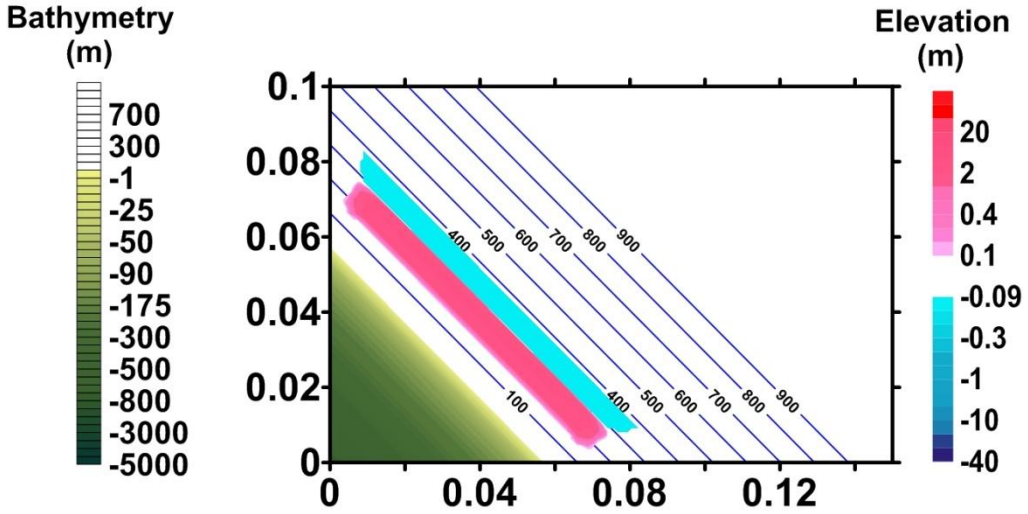

Figure 5.6. The location of wave shape erosion / deposition type landslide on the regular shaped oblique slope bathymetry.

TWO LAYER model is used by inputting above given landslide conditions. The simulation duration is selected 5 minutes. The landslide motion and associated wave evolution are computed together with the landslide and the water velocities. The results of TWO LAYER model are given in the following section.

In Figure 5.7 and 5.8, the motion of the landslide at the sea bottom (left) and water surface (right) are shown at different time steps for the simple sloped bathymetry case. The direction of the velocities are also shown in the Figures. It is seen that the time change of landslide velocity at the center of the landslide shows single peak value (in the magnitude of 19 m/sec) for 30 m thickness of erosion (Figure 5.9). Similar trend is observed for the 30 m erosion and 30 m deposition shape of the landslide. But the peak velocity becomes heigher as 22.5 m/sec (Figure 5.10).

The motion of the landslide at the sea bottom (left) and water surface (right) are shown at different time steps for the oblique sloped bathymetry case in the same sense in Figures 5.11 and 5.12. It is seen that the time change of landslide velocity at the center of the landslide shows single peak value (in the magnitude of 13 m/sec) for 30 m thickness of erosion (Figure 5.13). Similar trend is observed for the 30 m erosion and 30 m deposition shape of the landslide. But the peak velocity becomes 15 m/sec (Figure 5.14). It should be noted that the location of the gauge points for the simple slope bathymetry and oblique slope bathymetry are not at the same locations. Therefore, the computed peak velocities do not match.

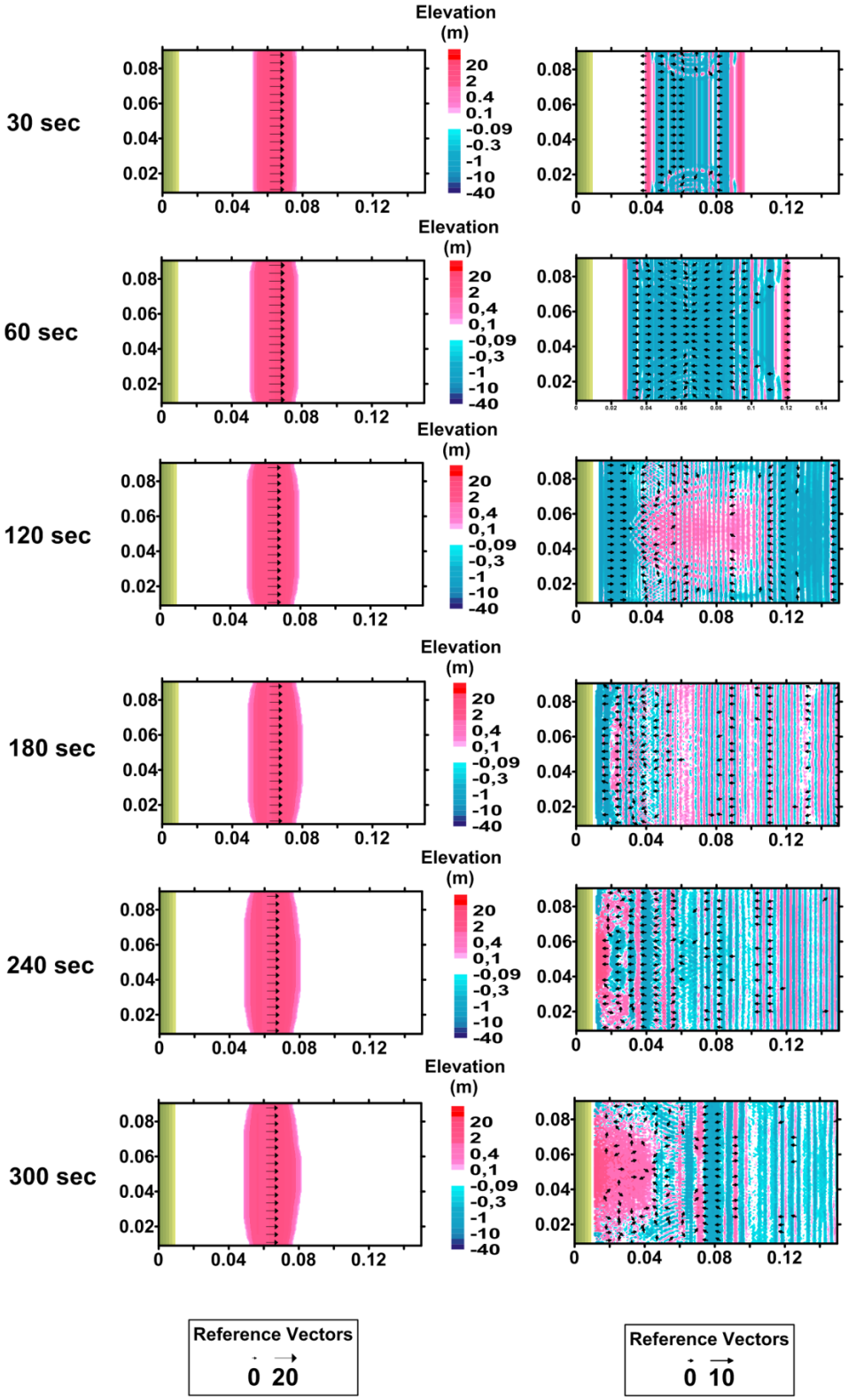

Figure 5.7. The motion of the landslide and water surface with the direction of the velocities at different time steps for the landslide with curved shaped 30 m thickness erosion on simple bottom slope.

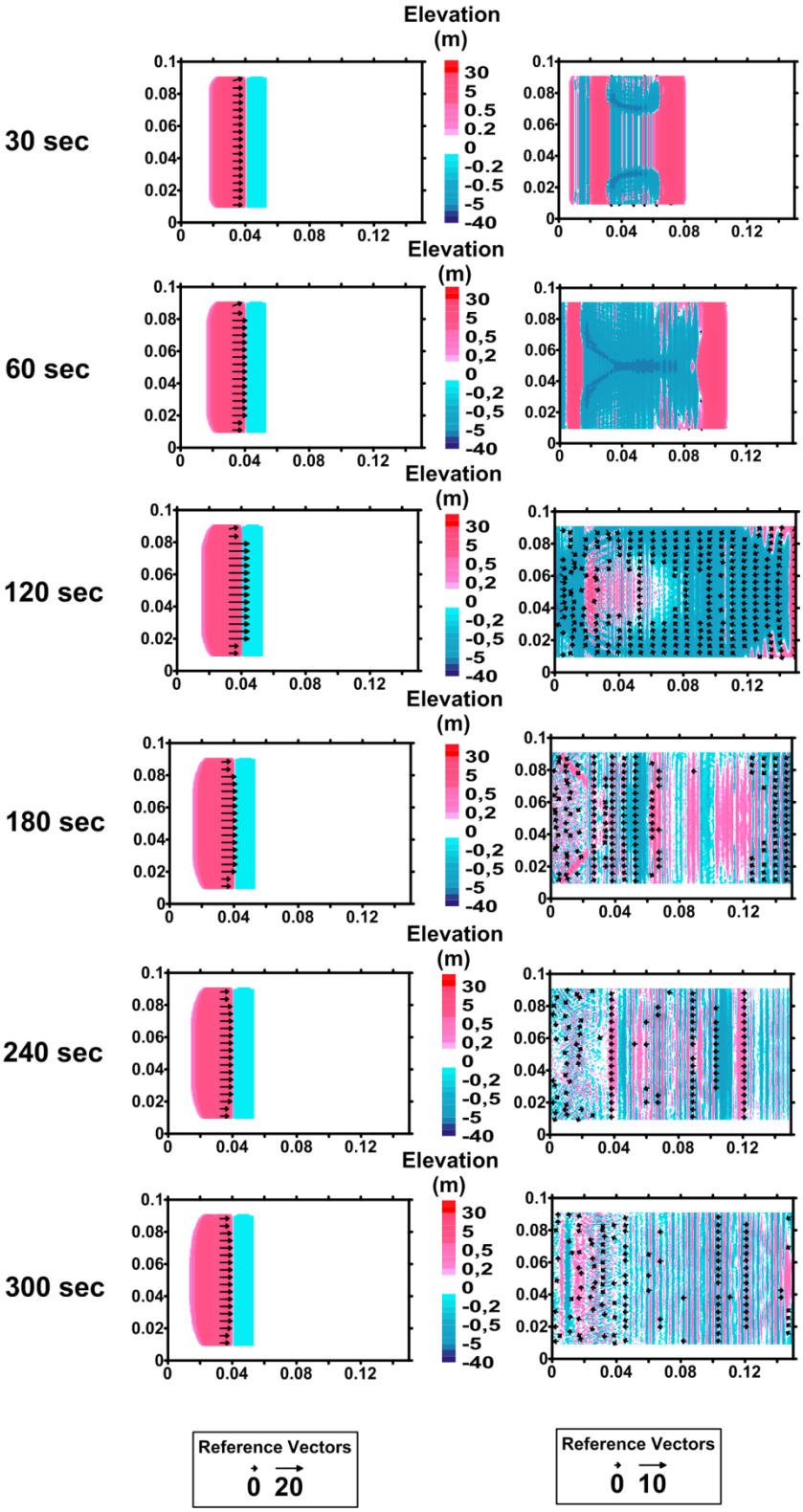

Figure 5.8. The motion of the landslide and water surface with the direction of the velocities at different time steps for the landslide with wave shape 30 m thickness erosion and deposition type landslide on simple bottom slope.

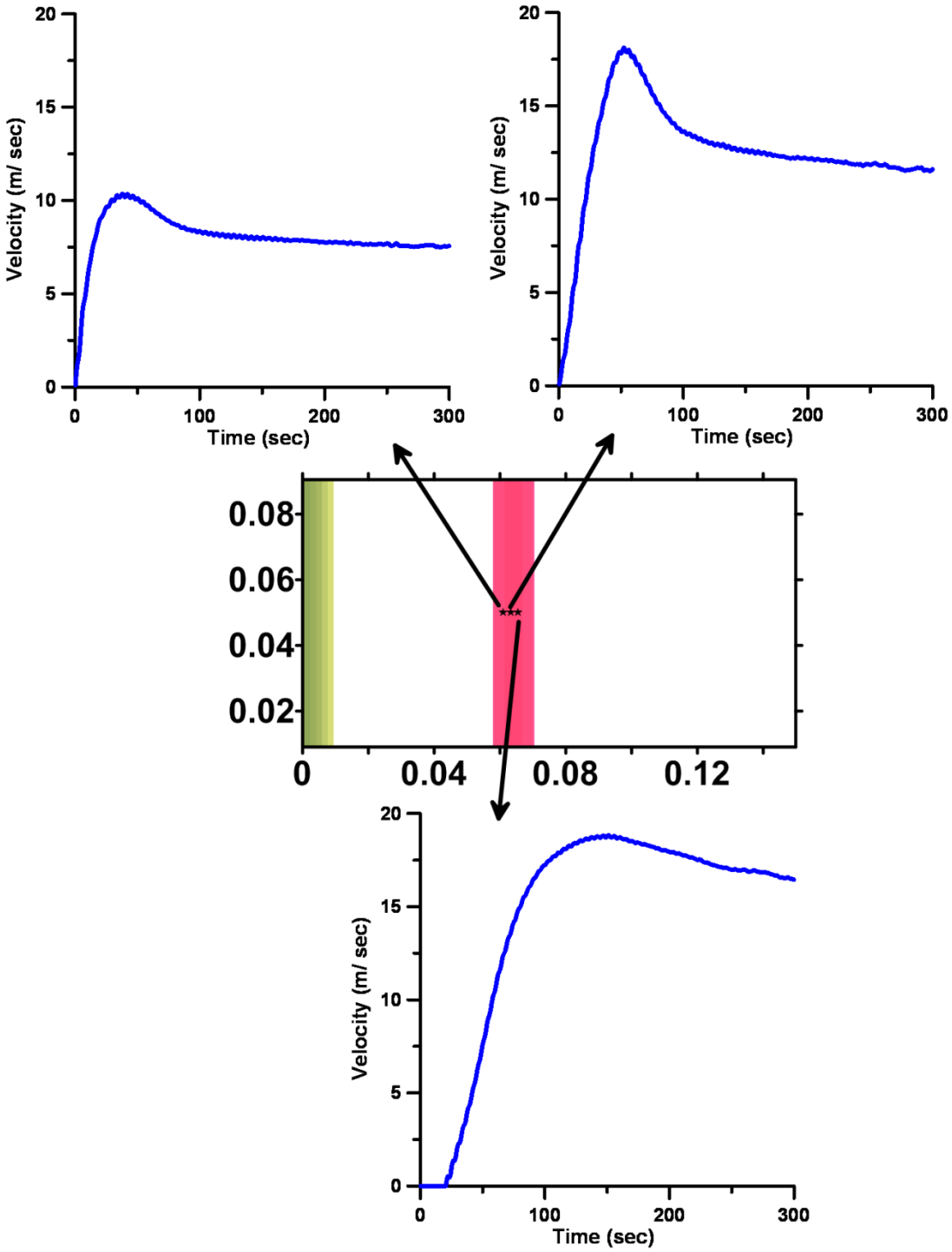

Figure 5.9. Time change of landslide velocity at different locations for the curved shape 30 m thickness erosion landslide on simple bottom slope.

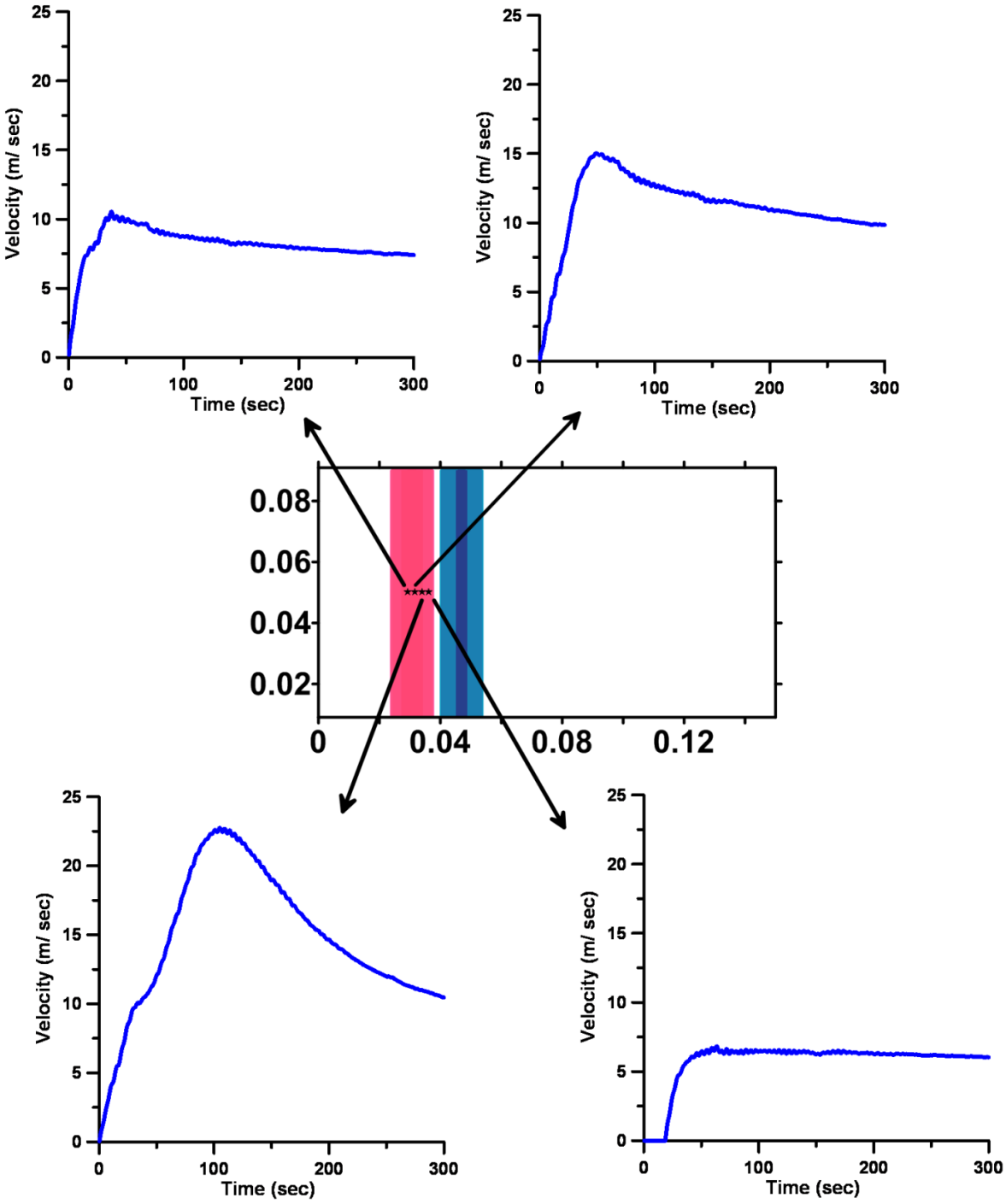

Figure 5.10. Time change of landslide velocity at different locations for the wave shape 30 m thickness erosion and deposition type landslide on simple bottom slope.

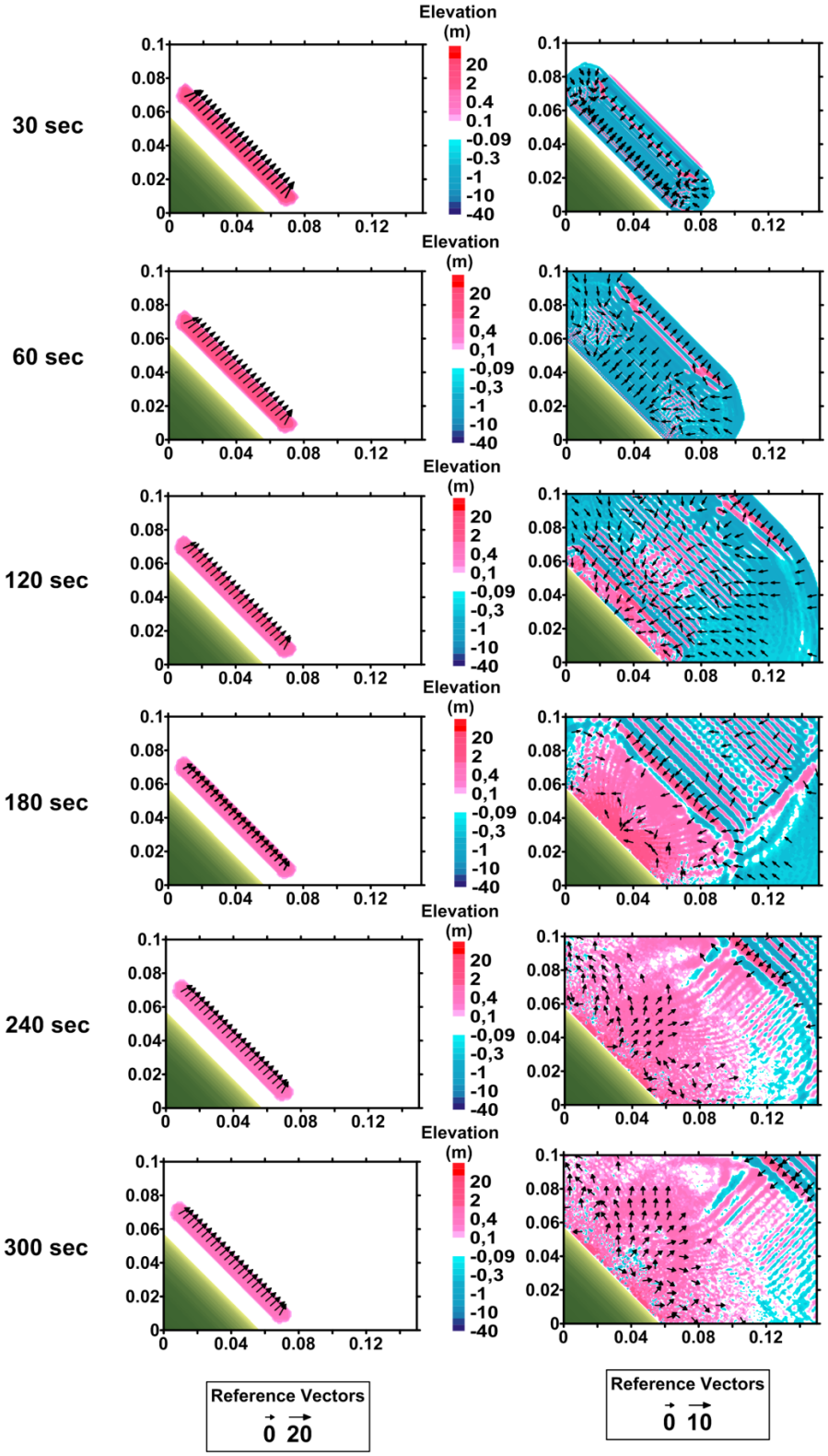

Figure 5.11. The motion of the landslide and water surface with the direction of the velocities at different time steps for the landslide with curved shaped 30 m thickness erosion on oblique slope.

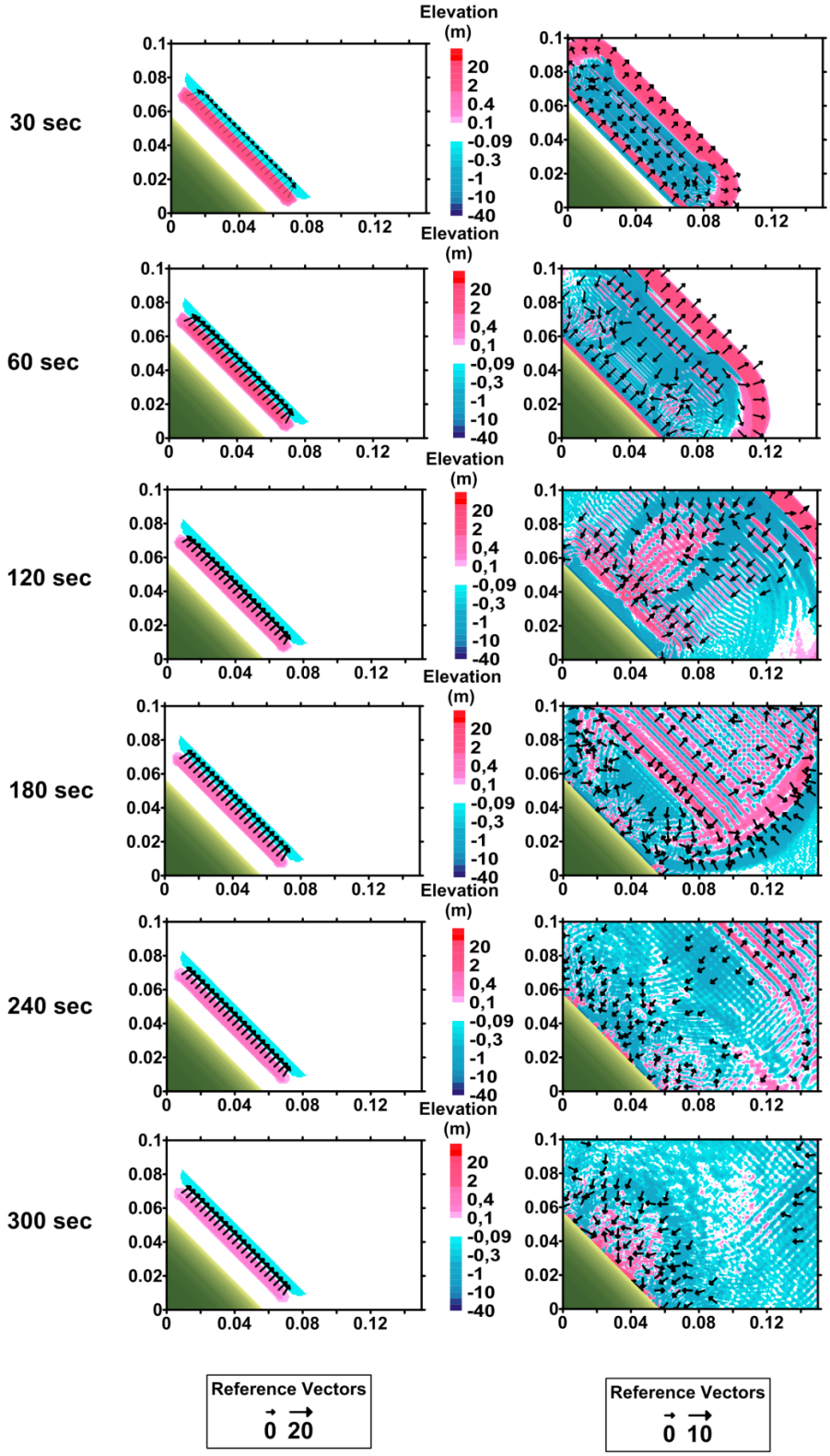

Figure 5.12. The motion of the landslide and water surface with the direction of the velocities at different time steps for the landslide with wave shape 30 m thickness erosion and deposition type landslide on oblique slope.

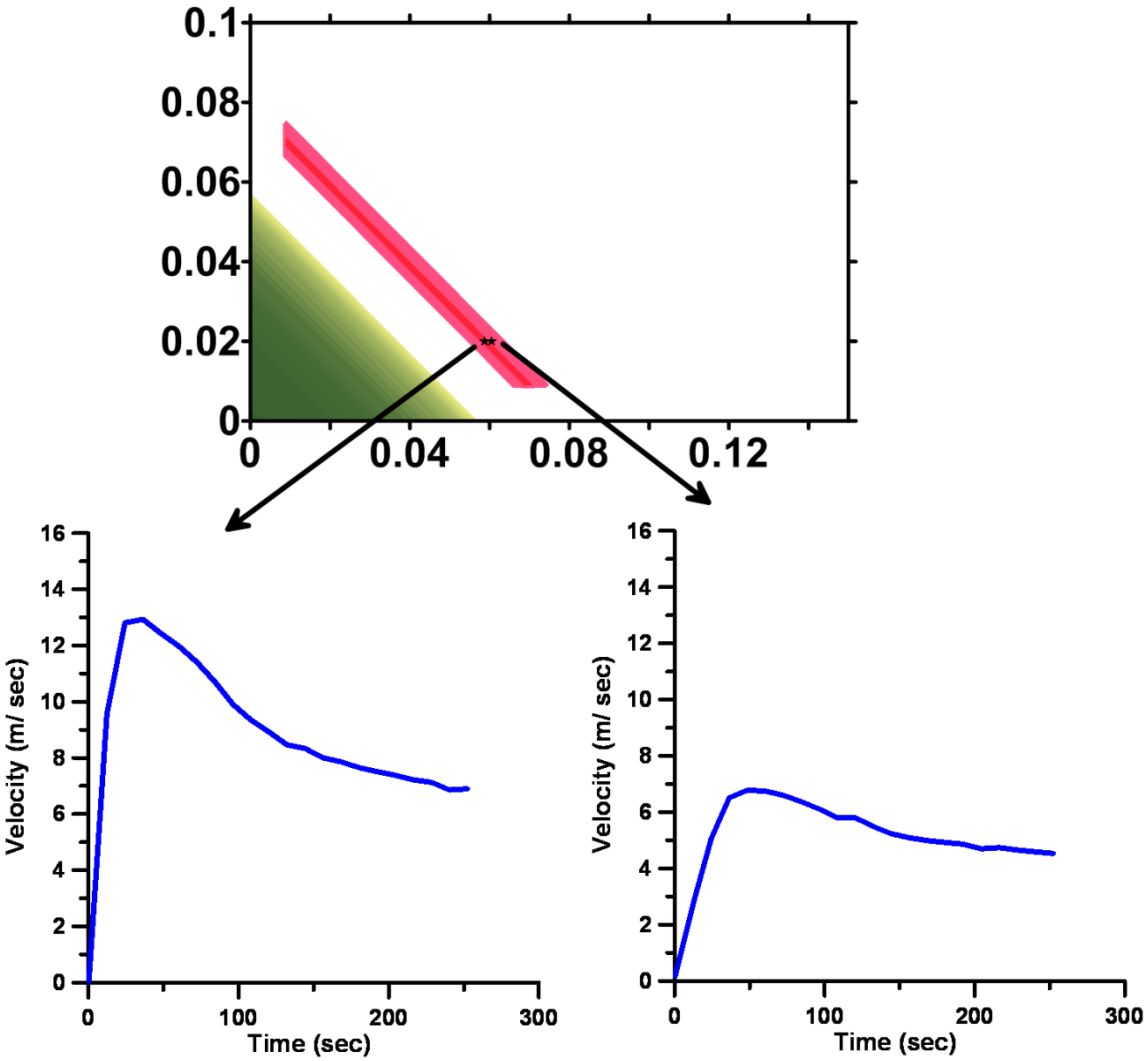

Figure 5.13. Time change of landslide velocity at different locations for the curved shape 30 m thickness erosion landslide on oblique slope.

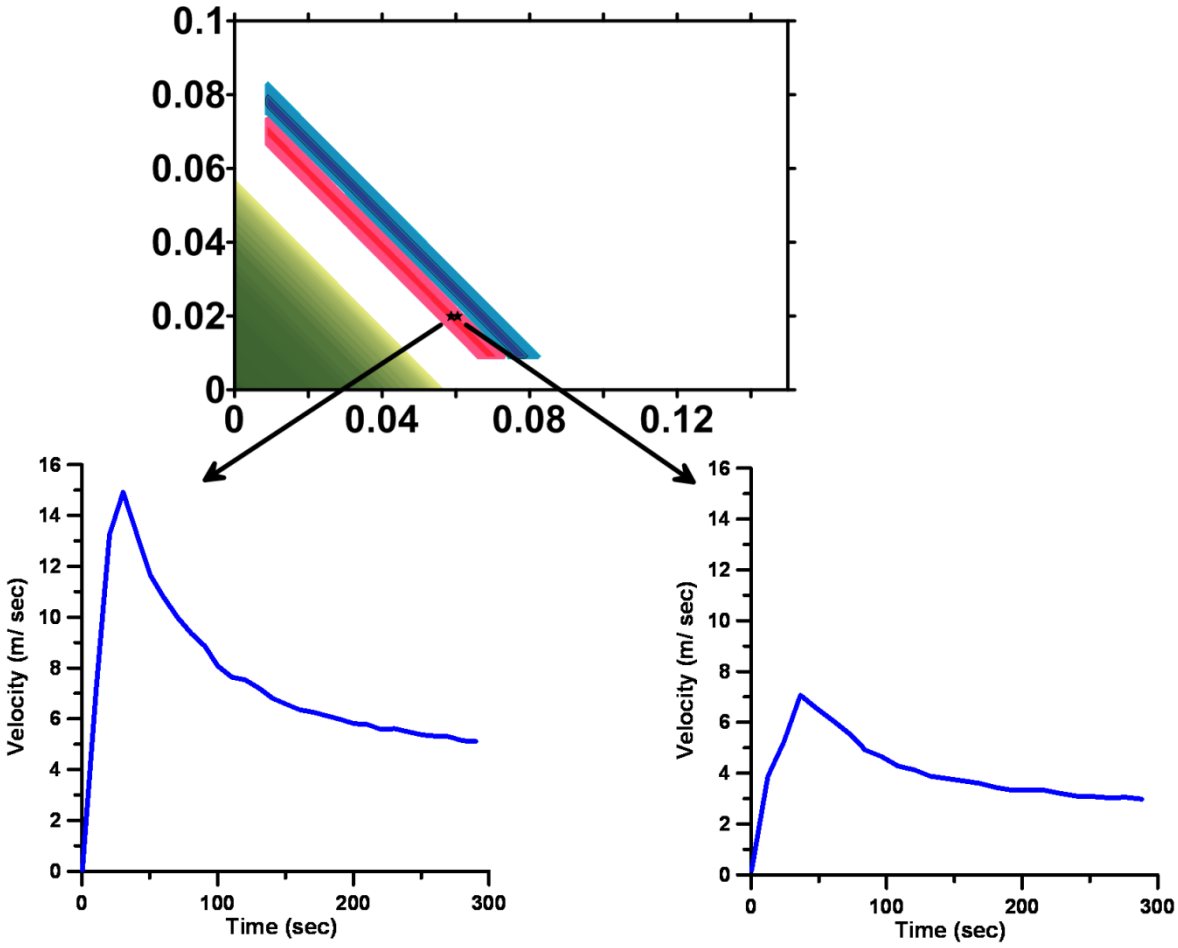

Figure 5.14. Time change of landslide velocity at different locations for the wave shape 30 m thickness erosion and deposition type landslide on oblique slope.

5.2. NAMI-DANCE

In this study, simulation of the landslide generated tsunami with TWO LAYER model, the propagation of the tsunami waves is simulated with NAMI-DANCE. Tsunami numerical modeling by NAMI DANCE is based on the solution of nonlinear form of the long wave equations in terms of related initial and boundary conditions. Generally the explicit numerical solution of Nonlinear Shallow Water (NSW) Equations is preferable for the use since it uses reasonable computer time and memory. Moreover, it als provides the results in acceptable error limit. NAMI DANCE is developed by Profs. Zaytsev, Chernov,

Yalçıner, Pelinovsky and Kurkin using the identical computational procedures of TUNAMI N2. TUNAMI N2 has been achieved by Profs. Shuto and Imamura. Developing model TUNAMI N2 has been the most significant development in tsunami modeling. In addition, TUNAMI N2 identifies the tsunami source characteristics from earthquake rupture characteristics. In addition, it computes all essential parameters of tsunami behavior in shallow water and in the inundation zone allowing for a better understanding of the impact of tsunamis according to bathymetric and topographical conditions (from NAMI-DANCE manual, 2010).

As well as tsunami parameters, NAMI DANCE computes :

i. tsunami source from either rupture characteristics or pre-determined wave form,
ii. propagation,
iii. coastal amplification,
iv. inundation (according to the accuracy of grid size),
v. arrival time,
vi. distribution of current velocities and their directions at selected time intervals,
vii. distribution of water surface elevations (sea state) at selected time intervals,
viii. relative damage levels according to drag force and impact force,
ix. time histories of water surface fluctuations,
x. 3D plot of sea state at selected time intervals from different camera and light positions,
xi. Animation of tsunami propagation between source and target regions (Yalçıner *et al.,* 2006, 2007).

NAMI DANCE has been tested validated by numerous analytical and experimental problems and also verified real event as 2014 Indian Ocean tsunami and 2011 Japon tsunami events (Özer *et al.,* 2011, Yalçıner *et al.,* 2002b, Yalçıner *et al.,* 2004, Yalçıner *et al.,* 2007a, Yalçıner *et al.,* 2007b, Yalçıner *et al.,* 2010, Yalçıner *et al.,* 2011a, Yalçıner *et al.,* 2011b, Yolsal *et al.,* 2007, Zahibo *et al.,* 2003a, Zahibo *et al.,* 2003b, Zaytsev *et al.,* 2008, Zaytsev *et al.,* 2011, Transfer, 2009).

6. MODELING OF SUBMARINE LANDSLIDES

TWO LAYER model has been applied to the sea of Marmara for six tsunami scenarios. The computation domain of the sea of Marmara for these applications is chosen as bounded by the longitudes 27.02ºE and 28.79ºE and the latitudes 40.56ºN and 40.89ºN. Six different scenarios have been applied for hypothetical case studies. They are;

The occurrence of a landslide at offshore Yenikapı

The occurrence of a landslide at offshore Ganos (1-2)

The occurrence of a landslide at CN1; central portion in Central Basin

The occurrence of a landslide offshore Küçükçekmece (1-2).

6.1. Tsunami Due to Submarine Landslide Occurrence at Offshore of Yenikapı

The generation of the landslide generated tsunamis are modeled using TWO-LAYER model. Velocity of the slide is investigated for landslide points using TWO-LAYER code. Yenikapı, Ganos, Küçükçekmece and CN1 (Silivri offshore) points in the Marmara Sea are selected for landslide area. The propagation and coastal amplification of the landslide generated waves are investigated using the tsunami simulation and visualization code NAMI-DANCE. In order to evaluate the evolution of the wave along south-north direction 65 gauge points are selected in the study.

In the Yenikapı case, an underwater landslide scenario is assumed to happen at offshore Yenikapı around the 28.79ºE and 40.89ºN coordinates. The study domain used in modeling of Yenikapı submarine landslide is showed in Figure 6.1.

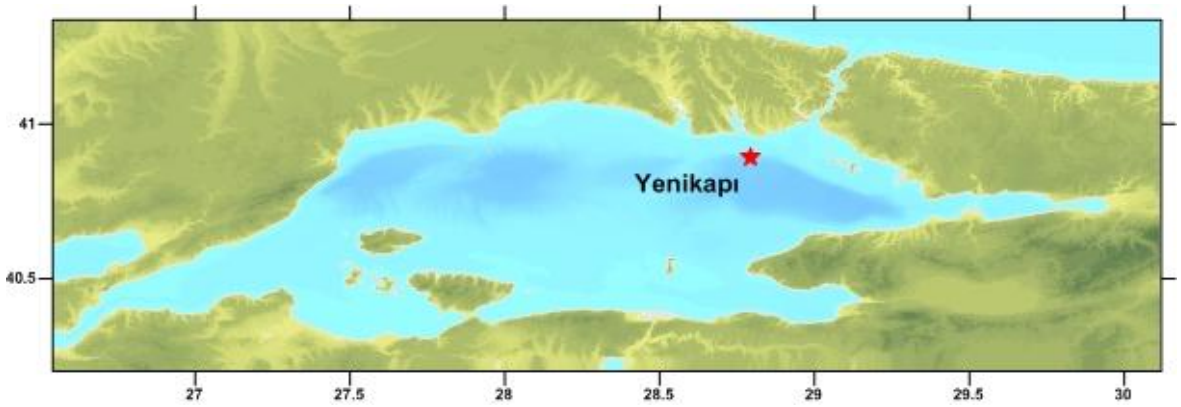

Figure 6.1. Landslide point at the study domain used in modeling of Yenikapı.

Figure 6.2 to 6.6 represent relation between submarine landslide velocity and time. It is seen from Figure 6.2 that landslide velocity is approximately 13.9 m/sec at the center of the landslide for 5 m sediment thickness.It is seen from Figures that velocity is increased for 10 m, 30 m, 60 m and 120 m sediment thicknesses. The landslide velocities are 15 m/ sec, 26.6 m/sec, 44.5 m/sec and 76 m/sec at the sl-10 (center of landslide) gauge point, respectively.

The motion of the sea bottom with respect to the landslide thickness is observed by plotting the landslide velocity of the bottom layer (at the center of the landslide) according to the landslide thicknesses (5, 10, 30, 60 and 120 m) in the Figures 6.2 to 6.7. It should be noted that these Figures show time rate of change of landslide velocity at the center of the landslide. As seen these Figures that the landslide velocity increase quickly with a certain acceleration in the first half minute. The velocity decreases after the peak value with decelaration (negative acceleration) up to a minute duration. After then deceleration continues but at a certain time later it changes. One of the reasons of decelaration change is the material resistance in front of the landslide. When the Figures are compared, it is seen that when the landslide thickness is getting higher the maximum velocity is observed at second peak. The relation between peak velocity of submarine landslide and its thickness is shown in Figure 6.7. According to Figure 6.7, there is linear relation between velocity and thickness for Yenikapı.

Along the coast of the Sea of Marmara, 25 numerical wave gauges are located and which are shown in Figure 6.8 and the coordinates and depths of these points are given in

Table 6.1. Furthermore, 22 gauge points are selected in perpendicular direction to landslide axis and around the landslide area.

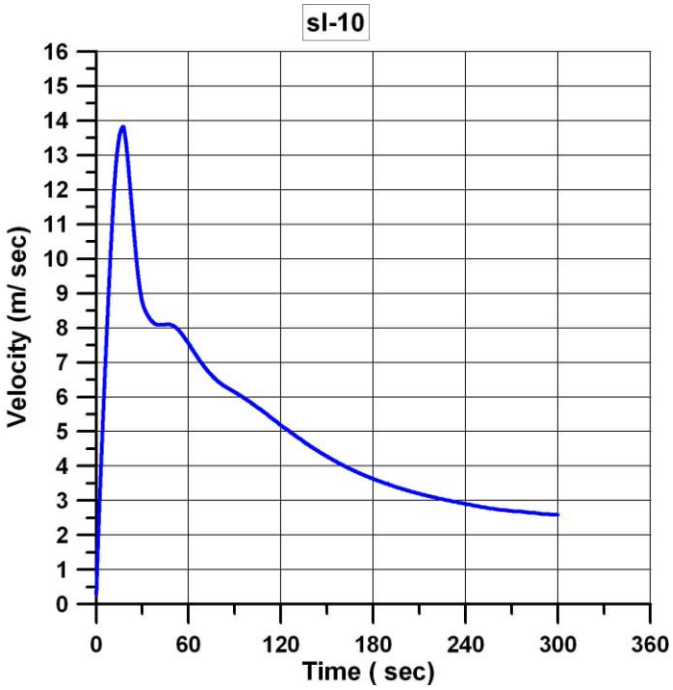

Figure 6.2. Time change of submarine landslide velocity at the center of the slide area (sl-10) due to slide of 5 m sediment thickness (Yenikapı).

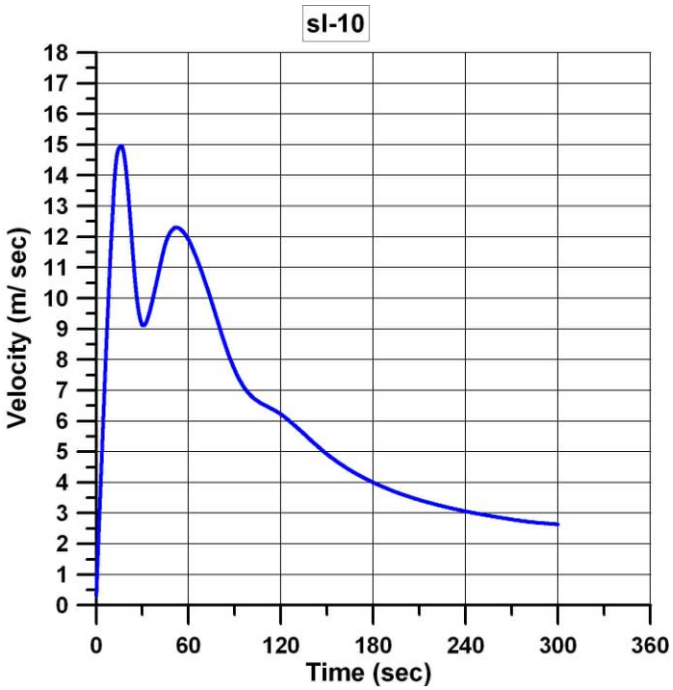

Figure 6.3. Time change of submarine landslide velocity at the center of the slide area (sl-10) due to slide of 10 m sediment thickness (Yenikapı).

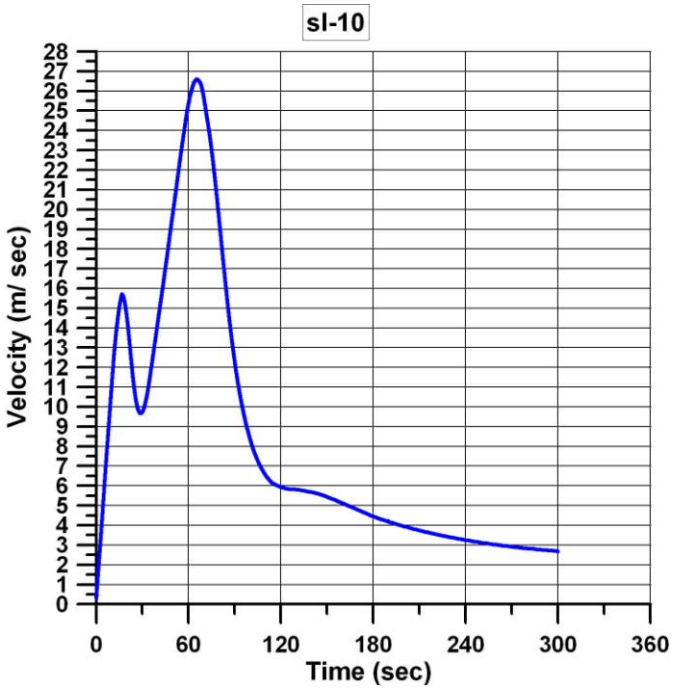

Figure 6.4. Time change of submarine landslide velocity at the center of the slide area (sl-10) due to slide of 30 m sediment thickness (Yenikapı).

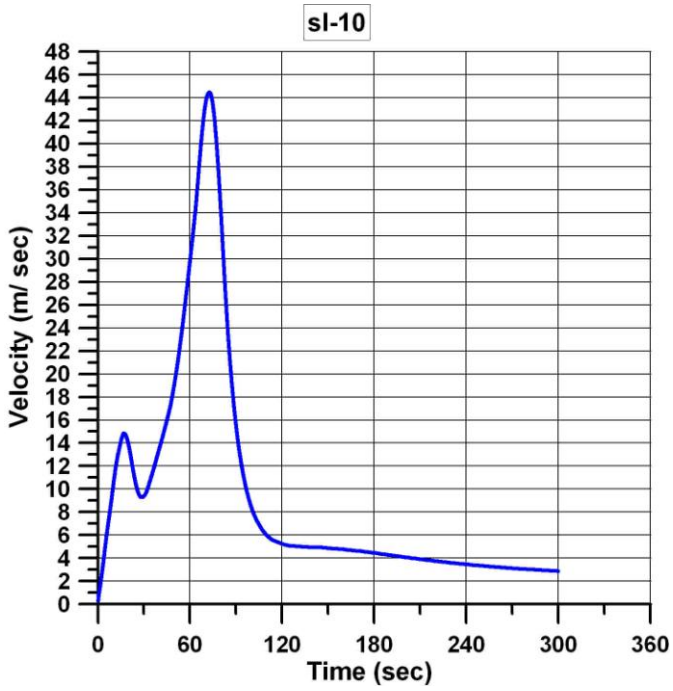

Figure 6.5. Time change of submarine landslide velocity at the center of the slide area (sl-10) due to slide of 60 m sediment thickness (Yenikapı).

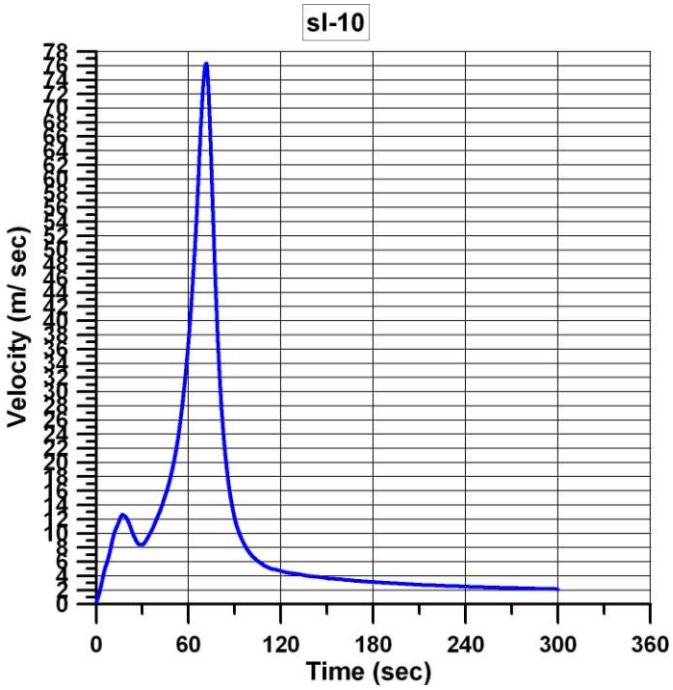

Figure 6.6. Time change of submarine landslide velocity at the center of the slide area (sl-10) due to slide of 120 m sediment thickness (Yenikapı).

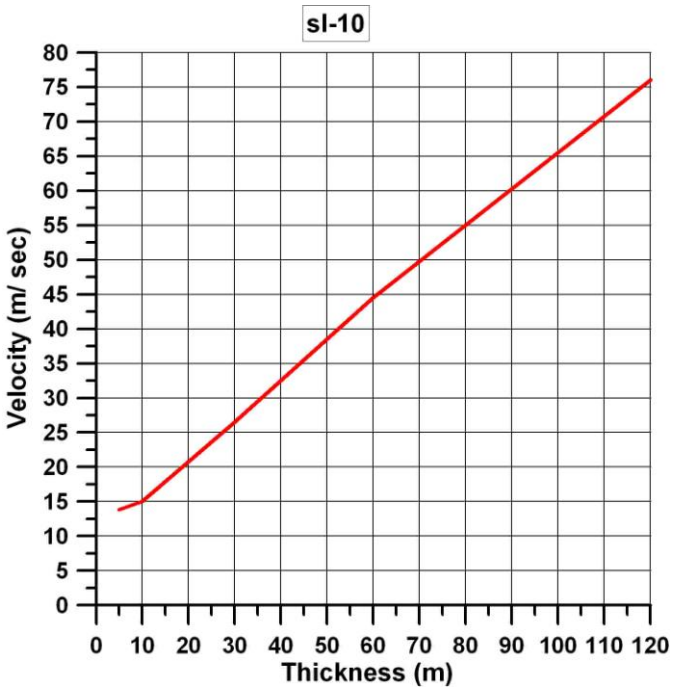

Figure 6.7. Submarine landslide velocity - thickness relation for center of the landslide (sl-10-Yenikapı).

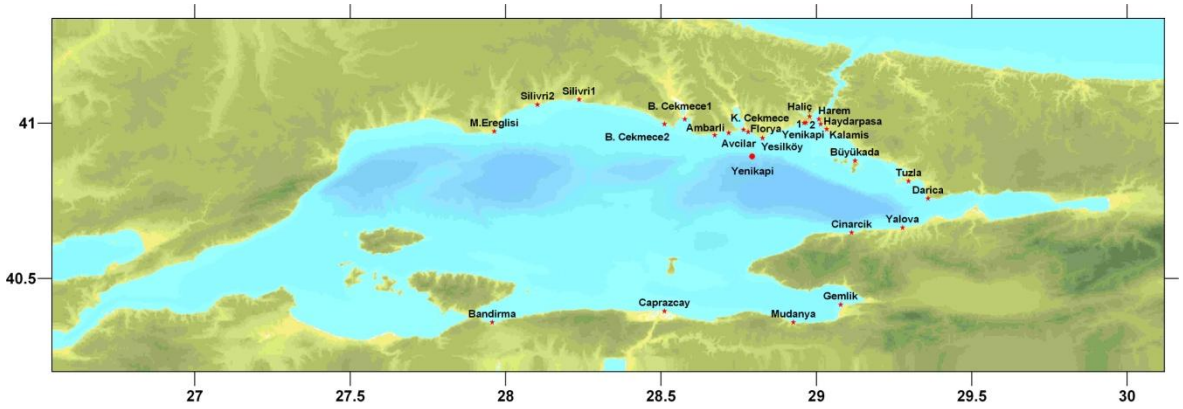

Figure 6.8. The locations of the selected gauge points for the simulations of Yenikapı submarine landslide.

The water surface elevation for 5 m, 10 m, 30 m, 60 m and 120 m sediment thicknesses are indicated in Figure 6.9 to 6.18. As it can be seen from the Figure 6.9, for 5 m sediment thickness, the water surface elevation is 0.2 m at Yeşilköy. It is 0.1 m at sl-11. For 10 m, 30 m, 60 m and 120 m sediment thicknesses, they are 0,4 m, 1.3 m, 2.5 m and 3.9 m at Yeşilköy respectively. According to sl-11, for 5 m, 10 m, 30 m, 60 m and 120 m sediment thicknesses, they are 0.1 m, 0.2 m, 0.5 m, 2.3 m and 4.9 m, respectively.

According to the simulation results, it can be seen that the tsunami wave reaches Yeşilköy, Florya and Ambarlı in 5 minutes. The depths, arrival times of first waves, maximum and minimum water elevation for the 41 selected gauge points are summarized in Table 6.2 for 5 m, 10 m, 30 m, 60 m and 120 m sediment thicknesses.

The aerial view of sea bottom change and water surface change are shown in Figures 6.19, 6.20 and 6.21 for different landslide thickesses at different time steps. In the Figures the sea bottom change with the direction vectors of landslide velocities are shown at left Figure of each thickness. Similarly the water surface is shown at right Figure with the direction of the water velocities. It is seen from these Figures that there is direct relationship between landslide thickness, magnitude of the landslide and water parameters (height and velocities) that also confirms the linear relationship shown in Figure 6.7.

The distributions of maximum surface elevation that the waves result in the shoreline along north and south coasts in the Marmara Sea are displayed in Figure 6.22 to 6.26. According to Figure 6.22, the maximum positive tsunami amplitudes are 0.25 m at the north shore and 0.1 m at the south coast for 5 m sediment thickness. For 10 m sediment

thickness, positive tsunami amplitudes are 0.6 m at the north and 0.2 m at the south coast. For 30 m sediment thickness, positive tsunami amplitudes are 1.6 m at the north and 0.7 m at the south coast. For 60 m sediment thickness, positive tsunami amplitudes are 2 m at the north and 1.5 m at the south coast. For 120 m sediment thickness, positive tsunami amplitudes are 2.95 m at the north and 2.75 m at the south coast.

Table 6.1. The coordinates and depths of the selected gauge points for the simulations of Yenikapı submarine landslide.

Name	X Coordinate	Y Coordinate	Depth (m)
M.Ereğlisi	27.9638	40.9734	8.3
Silivri 1	28.2364	41.0757	5.7
Silivri 2	28.1024	41.0594	3.2
B.Çekmece 1	28.5768	41.0127	9.9
B.Çekmece 2	28.5109	40.9966	9.2
Ambarlı	28.6730	40.9610	16.9
Avcılar	28.7176	40.9681	13.6
K.Çekmece	28.7657	40.9788	5.1
Florya	28.7799	40.9717	7
Yeşilköy	28.8263	40.9521	10
Yenikapı 1	28.9599	41.0002	8.2
Yenikapı 2	28.9662	41.0015	16.5
Haliç	28.9778	41.0216	29.9
Harem	29.0080	41.0127	7.5
Haydarpasa	29.0134	40.9966	9.1
Kalamış	29.033	40.9806	4.8
Büyükada	29.1239	40.8790	10.1
Tuzla	29.2967	40.8131	10.4
Darıca	29.3589	40.7570	19.4
Yalova	29.2771	40.6634	1.7
Çınarcık	29.1132	40.6473	3.2
Gemlik	29.0775	40.4156	12.9
Mudanya	28.9261	40.3586	1.5
Bandırma	27.9567	40,3586	1.7
Çaprazçay	28.5110	40.3946	0.2
Y-sl-01	28.7929	40.7952	1171.7
Y-sl-02	28.7929	40.8052	1170.3
Y-sl-03	28.7929	40.8152	1133.4
Y-sl-04	28.7929	40.8252	1085.1
Y-sl-05	28.7929	40.8352	1037.6
Y-sl-06	28.7929	40.8452	1026.6
Y-sl-07	28.7929	40.8552	1011.1
Y-sl-08	28.7929	40.8652	1052.1
Y-sl-09	28.7929	40.8752	1025.5
Y-sl-10 (Center of Landslide)	28.7929	40.8852	851.9
Y-sl-11	28.7929	40.8952	631
Y-sl-12	28.7929	40.9052	454.7
Y-sl-13	28.7929	40.9152	120.1
Y-sl-14	28.7929	40.9252	92.3
Y-sl-15	28.7929	40.9352	83.2
Y-sl-16	28.7929	40.9452	64
Y-sl-17	28.7929	40.9552	44.4

Table 6.1 (continued). The coordinates and depths of the selected gauge points for the simulations of Yenikapı submarine landslide.

Y-sl-18	28.7929	40.9652	8.9
Y-sl-19	28.7849	40.8938	777.4
Y-sl-20	28.8003	40.8985	596.9
Y-sl-21	28.7729	40.8839	985
Y-sl-22	28.8086	40.8909	729.3

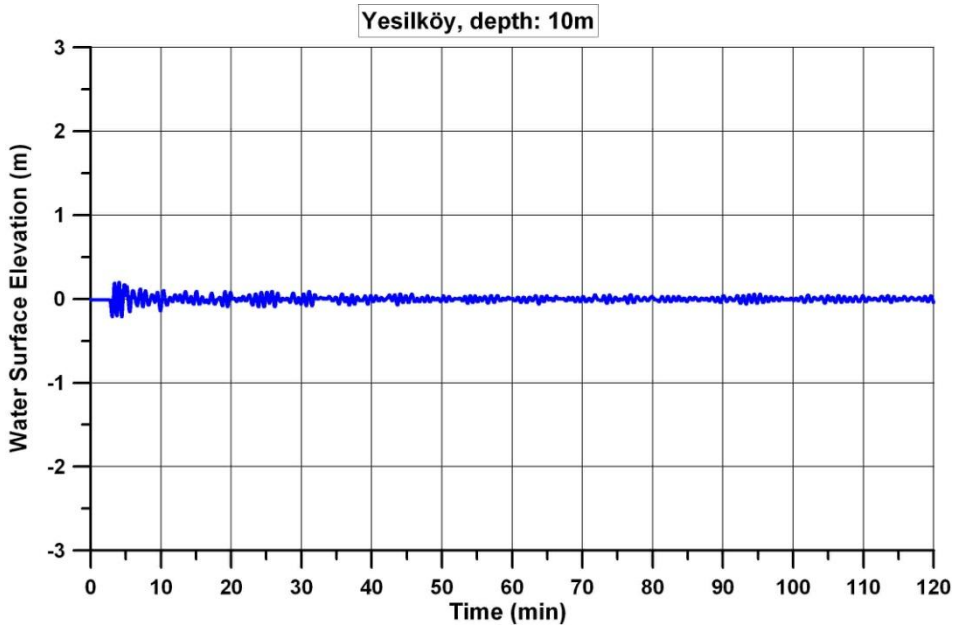

Figure 6.9. The time histories of water surface fluctuations computed at selected gauge point (Yeşilköy) for the simulation due to landslide of 5 m submarine sediment thickness at offshore of Yenikapı.

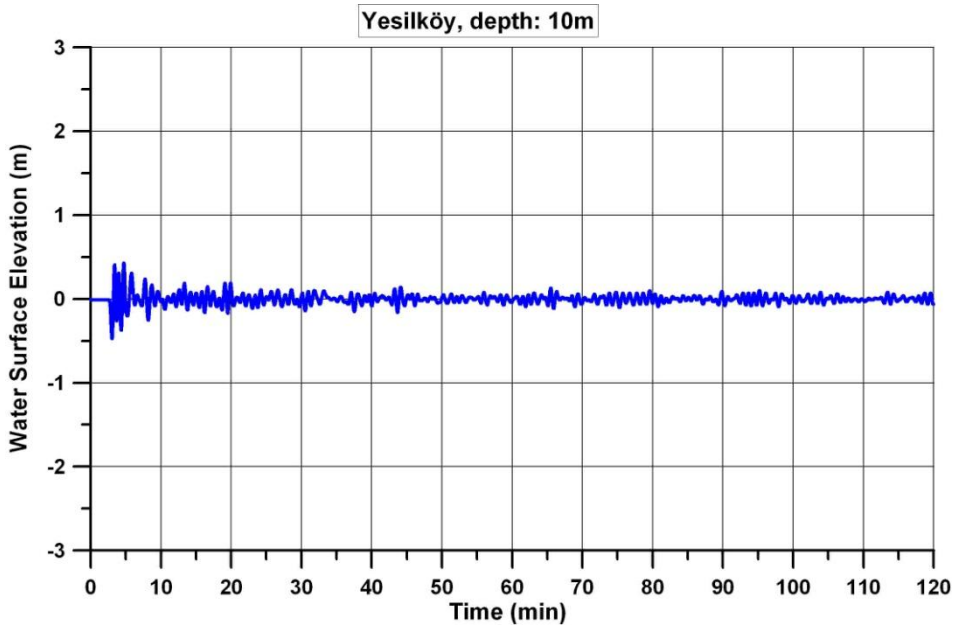

Figure 6.10. The time histories of water surface fluctuations computed at selected gauge point (Yeşilköy) for the simulation due to landslide of 10 m submarine sediment thickness at offshore of Yenikapı.

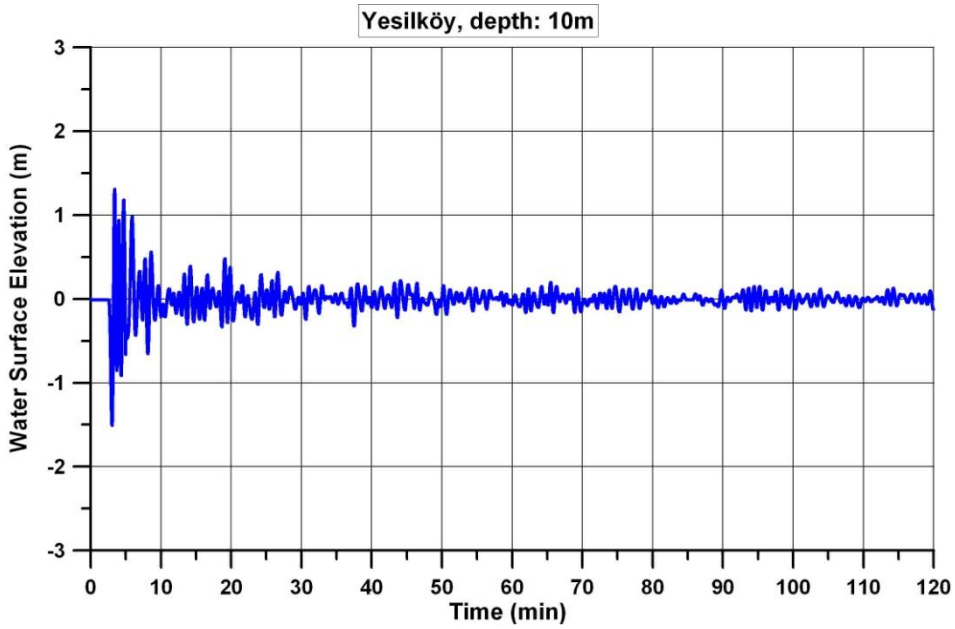

Figure 6.11. The time histories of water surface fluctuations computed at selected gauge point (Yeşilköy) for the simulation due to landslide of 30 m submarine sediment thickness at offshore of Yenikapı.

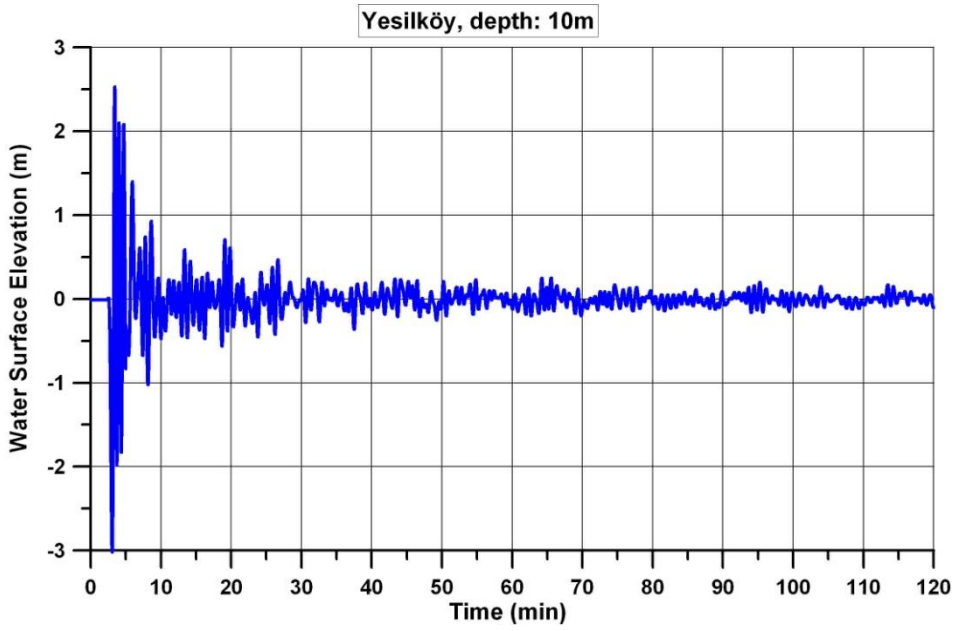

Figure 6.12. The time histories of water surface fluctuations computed at selected gauge point (Yeşilköy) for the simulation due to landslide of 60 m submarine sediment thickness at offshore of Yenikapı.

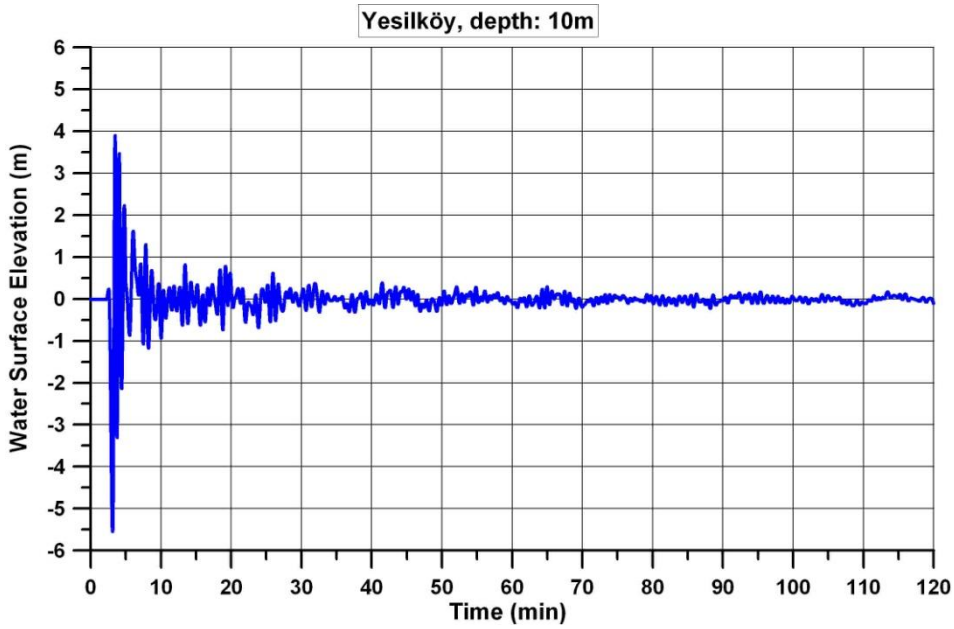

Figure 6.13. The time histories of water surface fluctuations computed at selected gauge point (Yeşilköy) for the simulation due to landslide of 120 m submarine sediment thickness at offshore of Yenikapı.

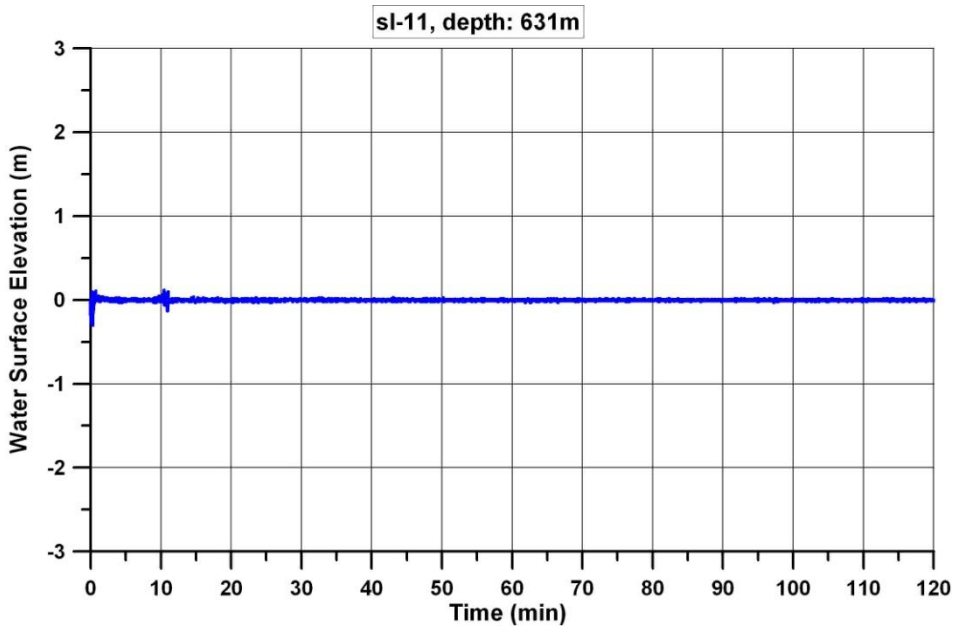

Figure 6.14. The time histories of water surface fluctuations computed at selected gauge point (sl-11) for the simulation due to landslide of 5 m submarine sediment thickness at offshore of Yenikapı.

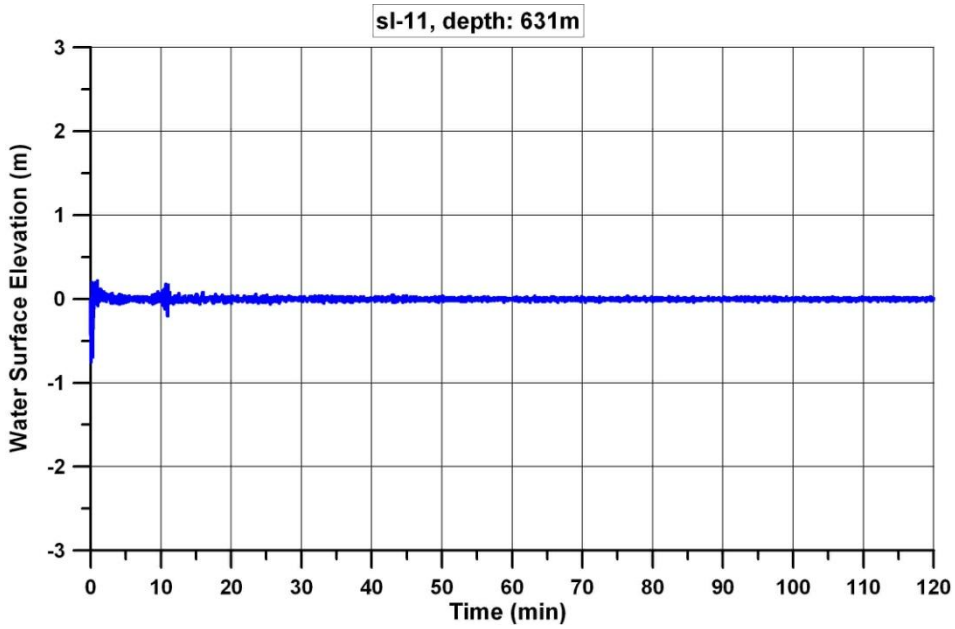

Figure 6.15. The time histories of water surface fluctuations computed at selected gauge point (sl-11) for the simulation due to landslide of 10 m submarine sediment thickness at offshore of Yenikapı.

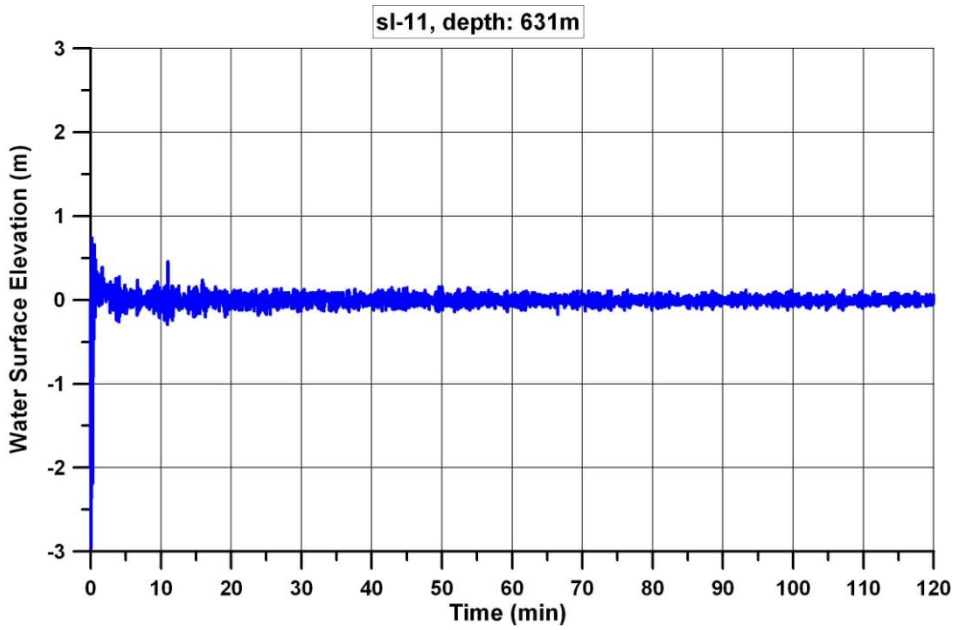

Figure 6.16. The time histories of water surface fluctuations computed at selected gauge point (sl-11) for the simulation due to landslide of 30 m submarine sediment thickness at offshore of Yenikapı.

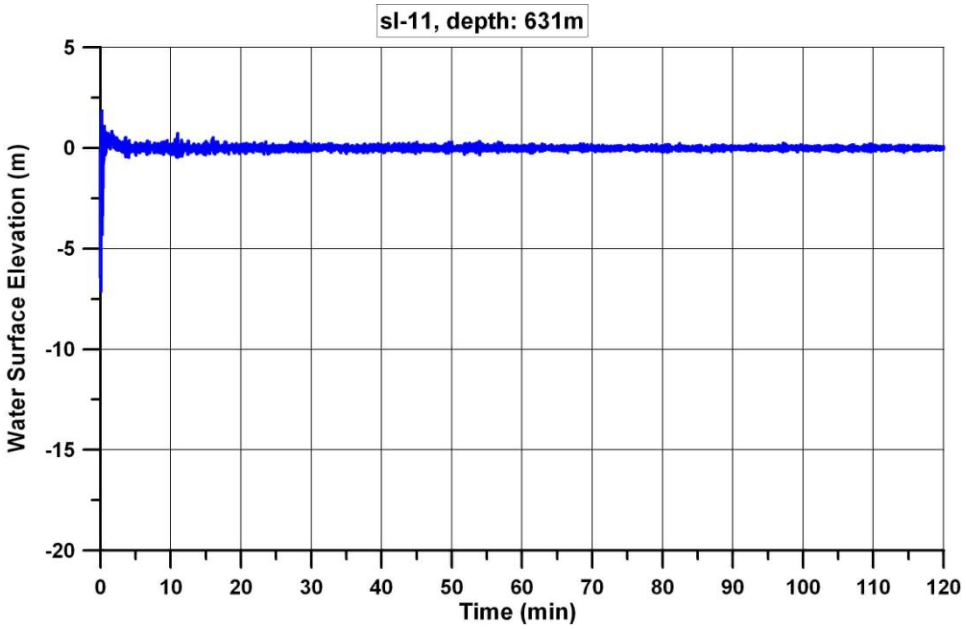

Figure 6.17. The time histories of water surface fluctuations computed at selected gauge point (sl-11) for the simulation due to landslide of 60 m submarine sediment thickness at offshore of Yenikapı.

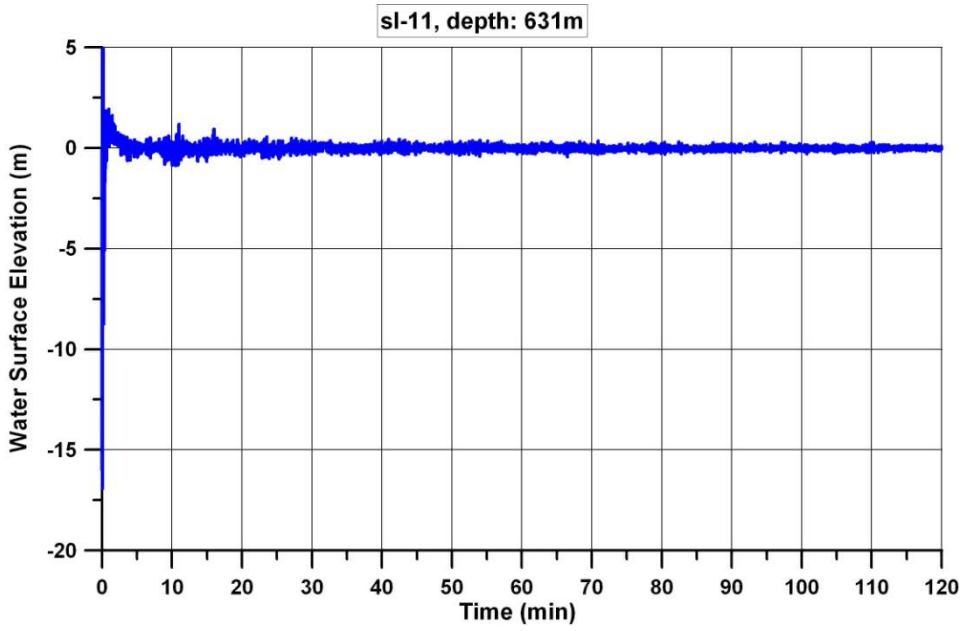

Figure 6.18. The time histories of water surface fluctuations computed at selected gauge point (sl-11) for the simulation due to landslide of 120 m submarine sediment thickness at offshore of Yenikapı.

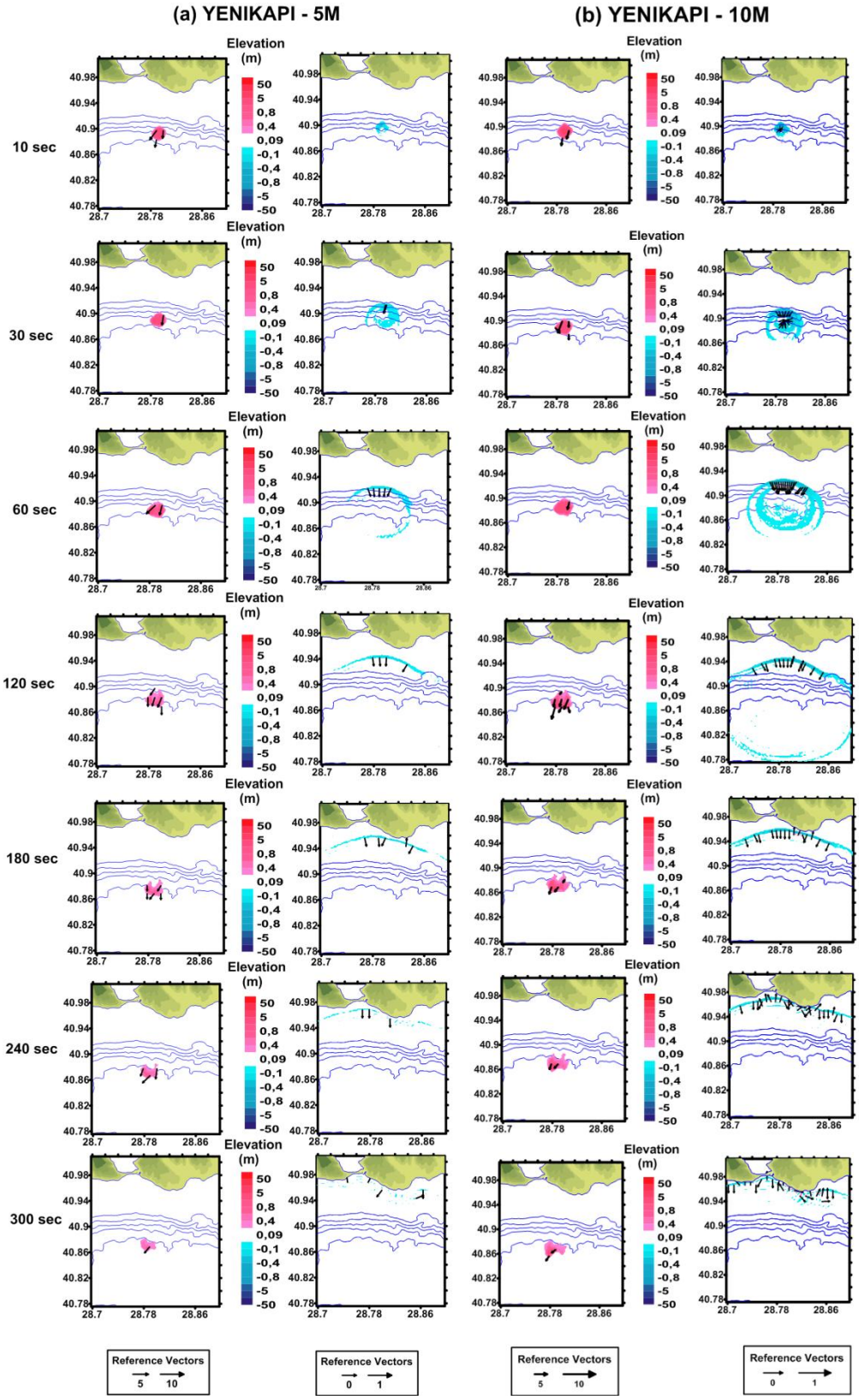

Figure 6.19. The view of the sea bottom material and corresponding water surface elevation at different time steps due to 5 m (a) and 10 m (b) sediment thicknesses of submarine landslide at Yenikapı.

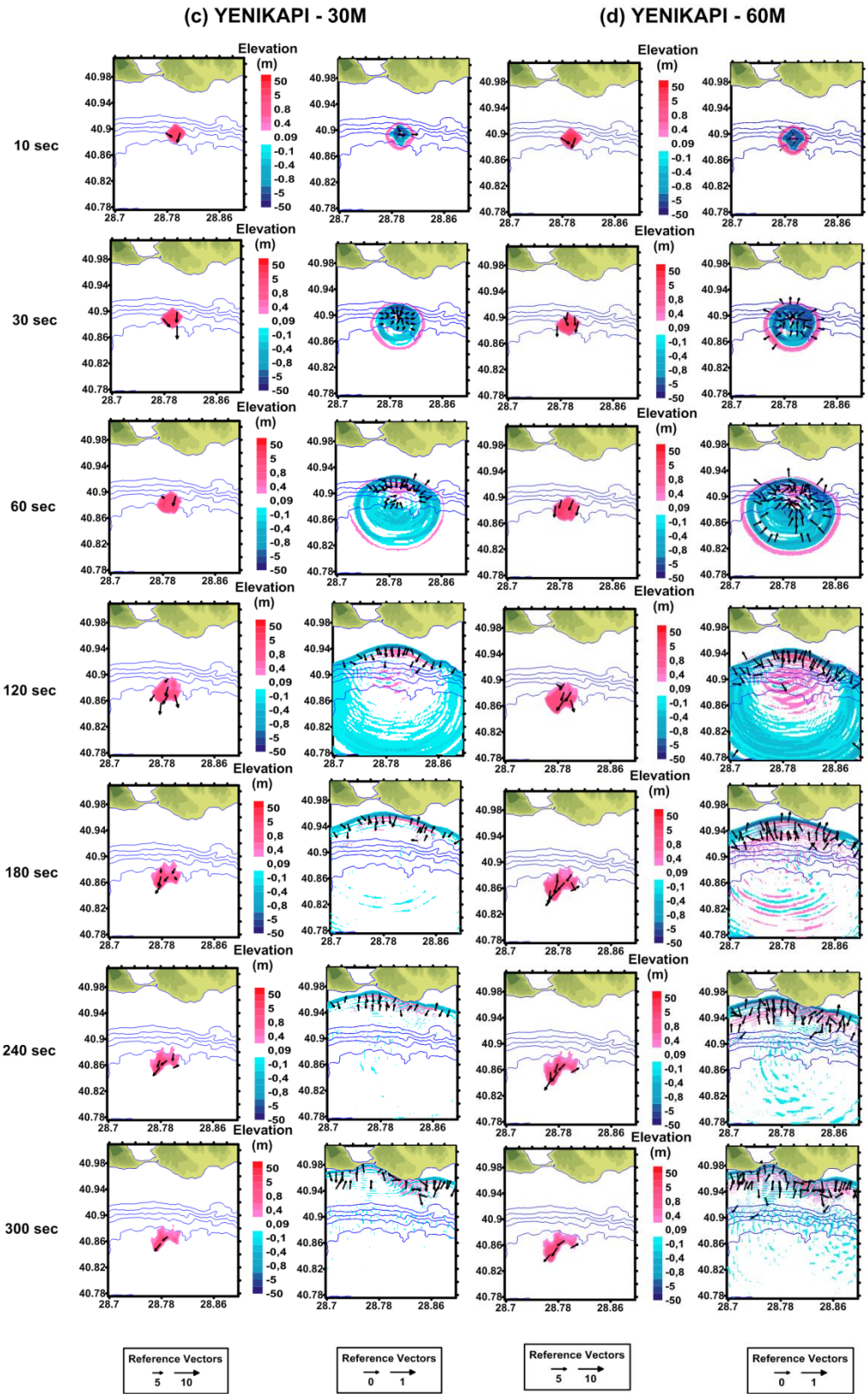

Figure 6.20. The view of the sea bottom material and corresponding water surface elevation at different time steps due to 30 m (c) and 60 m (d) sediment thicknesses of submarine landslide at Yenikapı.

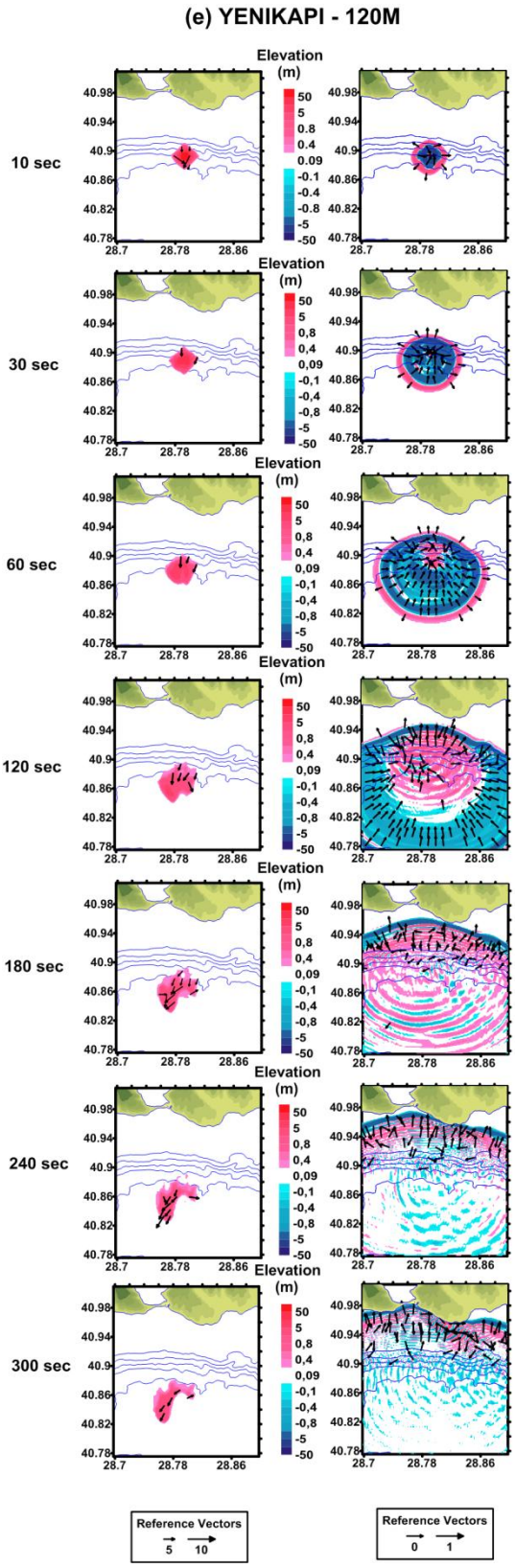

Figure 6.21. The view of the sea bottom material and corresponding water surface elevation at different time steps due to 120 m (e) sediment thickness of submarine landslide at Yenikapı.

Table 6.2. The summary sheet of the simulation results of submarine landslide tsunami at Yenikapı.

		5M			10M			30M			60M			120M		
Gauge Point	Depth (m)	T_first (min)	Amplitude (+) (m)	Amplitude (-) (m)	T_first (min)	Amplitude (+) (m)	Amplitude (-) (m)	T_first (min)	Amplitude (+) (m)	Amplitude (-) (m)	T_first (min)	Amplitude (+) (m)	Amplitude (-) (m)	T_first (min)	Amplitude (+) (m)	Amplitude (-) (m)
Silivri 1	5.7	8	0.02	-0.02	8	0.04	-0.04	7	0.1	-0.1	7	0.2	-0.2	7	0.4	-0.3
Silivri 2	3.2	9	0.03	-0.02	8	0.1	-0.1	8	0.1	-0.1	8	0.3	-0.3	8	0.5	-0.5
B.Çekmece1	9.9	9	0.04	-0.04	8	0.1	-0.1	8	0.1	-0.2	8	0.3	-0.4	8	0.6	-0.6
B.Çekmece2	9.2	7	0.1	-0.04	7	0.1	-0.1	7	0.2	-0.2	7	0.4	-0.4	7	0.7	-0.9
Ambarlı	16.9	5	0.2	-0.2	5	0.2	-0.2	5	0.6	-0.7	5	1.2	-1.4	5	1.7	-2
Avcılar	13.6	5	0.1	-0.1	5	0.2	-0.2	5	0.4	-0.6	5	0.8	-1.1	5	1.1	-2.7
K. Çekmece	5.1	5	0.1	-0.1	5	0.2	-0.4	5	0.5	-1.1	5	0.7	-1.8	5	1	-3
Florya	7	5	0.1	-0.1	5	0.4	-0.3	5	0.8	-0.8	5	1.2	-1.5	5	1.6	-2
Yeşilköy	10	5	0.2	-0.2	5	0.3	-0.3	5	1	-0.7	5	1.4	-1	5	1.6	-1.2
Yenikapı 1	8.2	6	0.1	-0.04	6	0.1	-0.1	6	0.2	-0.3	6	0.3	-0.4	6	0.5	-0.9
Haliç	30	6	0.04	-0.03	6	0.04	-0.1	6	0.1	-0.1	6	0.2	-0.2	6	0.3	-0.3
Harem	7.5	6	0.03	-0.03	5	0.1	-0.1	5	0.1	-0.1	5	0.2	-0.2	5	0.3	-0.3
Haydarpaşa	9.1	5	0.1	-0.1	5	0.1	-0.1	5	0.2	-0.2	5	0.4	-0.3	5	1.1	-0.7
Kalamış	4.8	11	0.04	-0.04	11	0.1	-0.1	11	0.4	-0.4	11	0.6	-0.8	11	1.1	-1.4
Büyükada	10.1	6	0.03	-0.03	6	0.1	-0.1	6	0.2	-0.1	6	0.3	-0.2	6	0.6	-0.4
Tuzla	10.4	6	0.03	-0.02	6	0.04	-0.03	5	0.1	-0.1	5	0.1	-0.2	5	0.2	-0.4
Yalova	1.7	14	0.01	-0.02	10	0.04	-0.04	8	0.2	-0.1	8	0.2	-0.3	8	0.4	-0.6
Çınarcık	3.2	7	0.03	-0.03	7	0.1	-0.1	6	0.2	-0.3	6	0.4	-0.6	6	0.9	-1.6
Mudanya	1.5	14	0.03	-0.02	13	0.1	-0.04	13	0.1	-0.1	13	0.2	-0.2	13	0.4	-0.5
sl-01	1171.7	5	0.03	-0.02	5	0.1	-0.03	5	0.1	-0.1	5	0.2	-0.2	5	0.3	-4
sl-02	1170.3	5	0.03	-0.02	5	0.04	-0.04	5	0.1	-0.1	5	0.1	-0.2	5	0.3	-0.3
sl-03	1133.4	5	0.03	-0.02	5	0.04	-0.04	5	0.1	-0.1	5	0.2	-0.2	5	0.3	-0.4
sl-04	1085.1	5	0.03	-0.03	5	0.04	-0.1	5	0.1	-0.1	5	0.2	-0.3	5	0.3	-0.4
sl-05	1037.6	5	0.03	-0.03	5	0.04	-0.04	5	0.1	-0.1	5	0.2	-0.2	5	0.3	-0.5
sl-06	1026.6	5	0.03	-0.03	5	0.1	-0.1	5	0.1	-0.1	5	0.2	-0.2	5	0.4	-0.4

Table 6.2 (continued). The summary sheet of the simulation results of submarine landslide tsunami at Yenikapı.

sl-07	1011.1	5	0.04	-0.03	5	0.1	-0.1	5	0.1	-0.1	5	0.2	-0.2	5	0.4	-0.5
sl-08	1052.1	5	0.04	-0.04	5	0.1	-0.1	5	0.1	-0.1	5	0.2	-0.2	5	0.4	-0.4
sl-09	1025.5	5	0.1	-0.04	5	0.1	-0.1	5	0.1	-0.2	5	0.2	-0.3	5	0.5	-0.5
sl-10	851.9	5	0.1	-0.1	5	0.1	-0.2	5	0.2	-0.2	5	0.3	-0.4	5	0.5	-1.1
sl-11	631	5	0.1	-0.1	5	0.2	-0.2	5	0.5	-0.3	5	2.3	-0.5	5	4.9	-0.9
sl-12	454.7	5	0.1	-0.1	5	0.2	-0.1	5	0.3	-0.3	5	0.5	-0.5	5	0.8	-0.9
sl-13	120.1	5	0.1	-0.1	5	0.1	-0.1	5	0.3	-0.2	5	0.5	-0.4	5	0.9	-0.8
sl-14	92.3	5	0.1	-0.1	5	0.1	-0.1	5	0.3	-0.2	5	0.4	-0.4	5	0.7	-0.9
sl-15	83.2	5	0.1	-0.1	5	0.1	-0.1	5	0.2	-0.3	5	0.4	-0.5	5	0.8	-0.9
sl-16	64	5	0.1	-0.1	5	0.1	-0.2	5	0.3	-0.4	5	0.6	-0.5	5	1.3	-1.2
sl-17	44.4	5	0.1	-0.1	5	0.2	-0.2	5	0.6	-0.5	5	1	-1	5	1.6	-1.5
sl-18	8.9	5	0.2	-0.2	5	0.4	-0.5	5	0.9	-1.1	5	1.5	-1.7	5	1.9	-2
sl-19	777.4	5	0.1	-0.1	5	0.2	-0.2	5	0.4	-0.2	5	0.5	-0.6	5	0.8	-1.1
sl-20	596.9	5	0.1	-0.1	5	0.2	-0.1	5	0.3	-0.3	5	0.6	-0.5	5	0.8	-0.9
sl-21	984.9	5	0.04	-0.03	5	0.1	-0.1	5	0.2	-0.2	5	0.3	-0.3	5	0.4	-0.5
Sl-22	729.4	5	0.1	-0.04	5	0.1	-0.1	5	0.2	-0.2	5	0.3	-0.3	5	0.5	-0.5

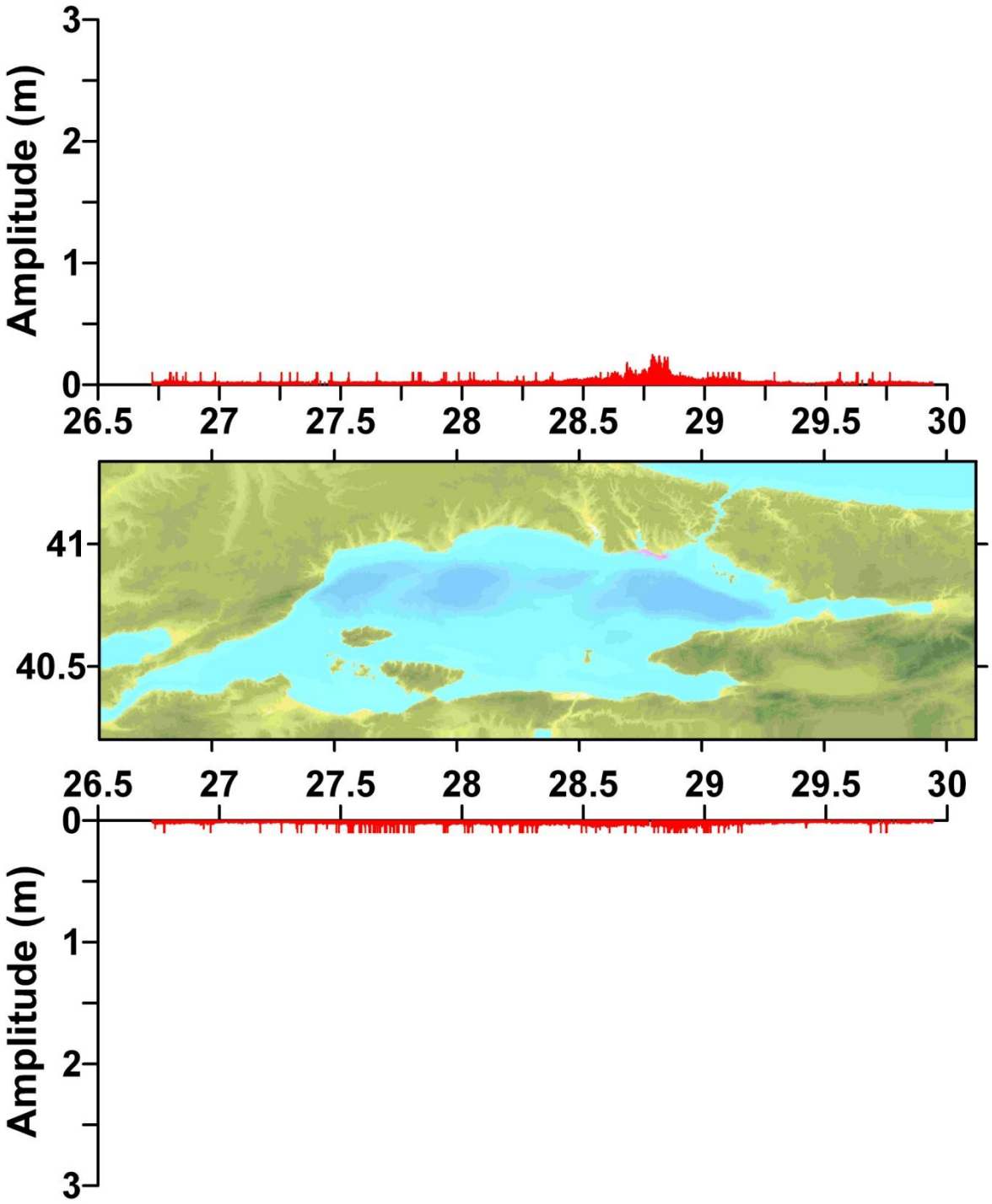

Figure 6.22. Maximum water level distributions (m) along North and South coasts of Marmara computed by the 120 minutes simulations due to the 5 m thickness of submarine landslide at Yenikapı.

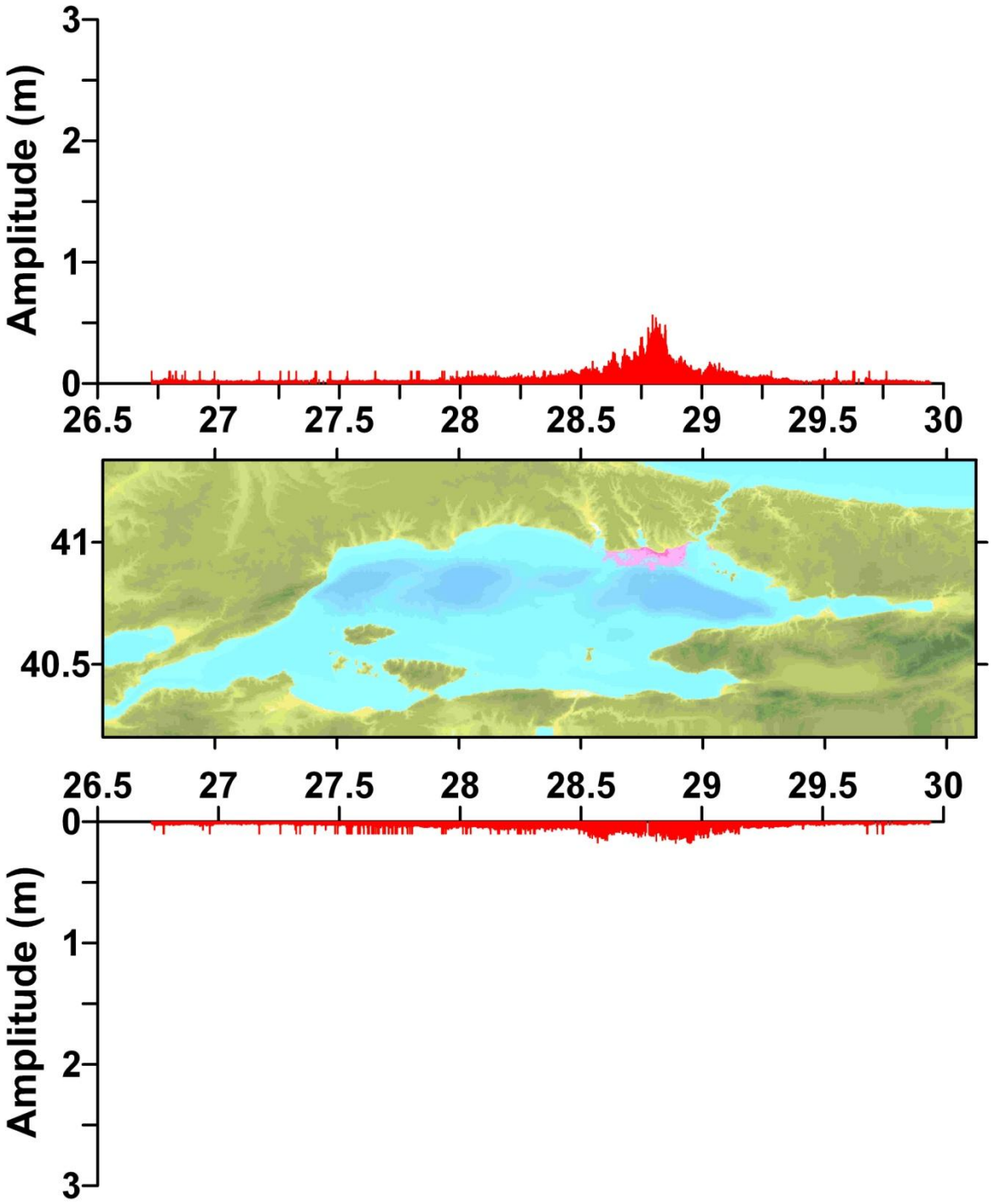

Figure 6.23. Maximum water level distributions (m) along North and South coasts of Marmara computed by the 120 minutes simulations due to the 10 m thickness of submarine landslide at Yenikapı.

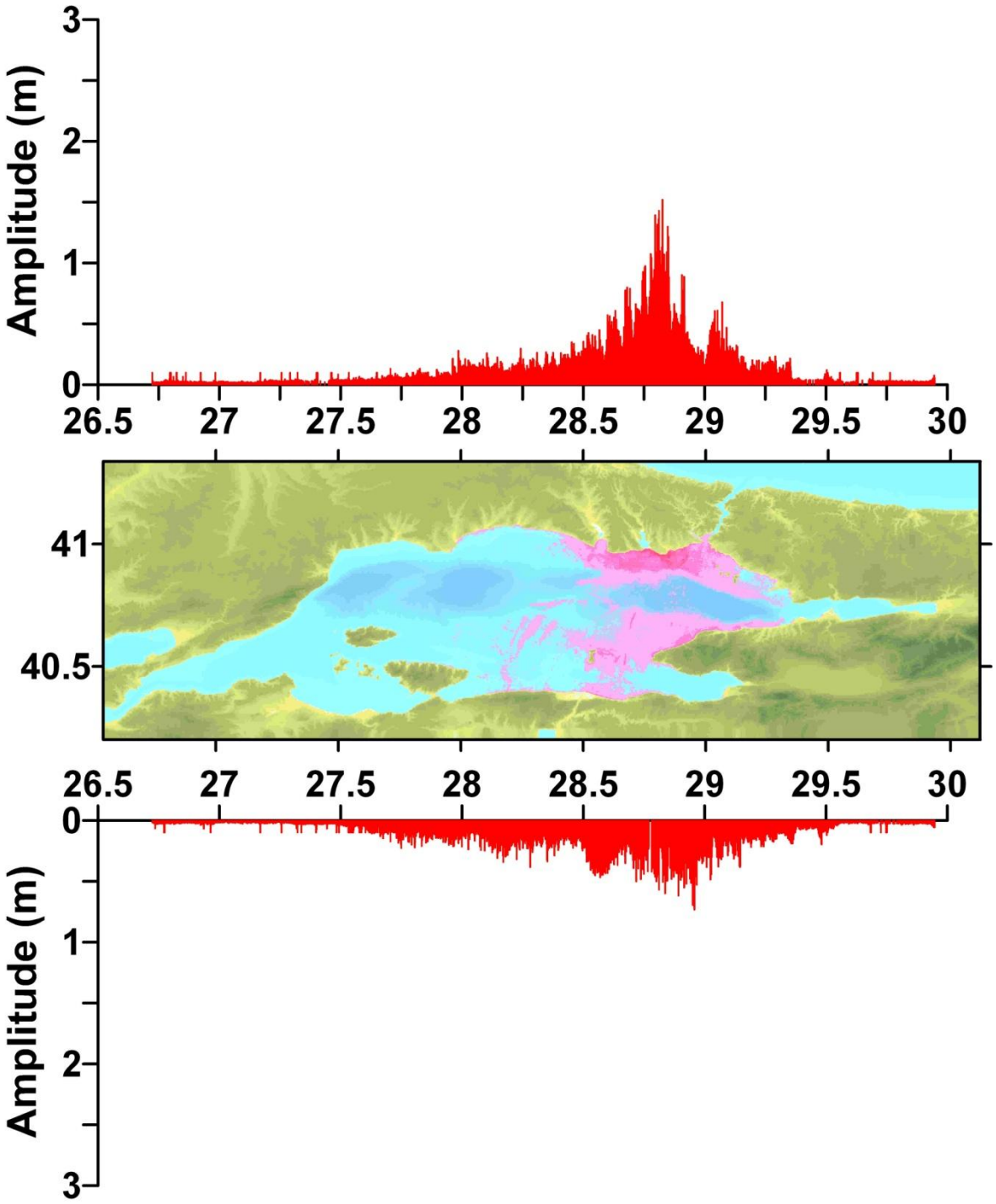

Figure 6.24. Maximum water level distributions (m) along North and South coasts of Marmara computed by the 120 minutes simulations due to the 30 m thickness of submarine landslide at Yenikapı.

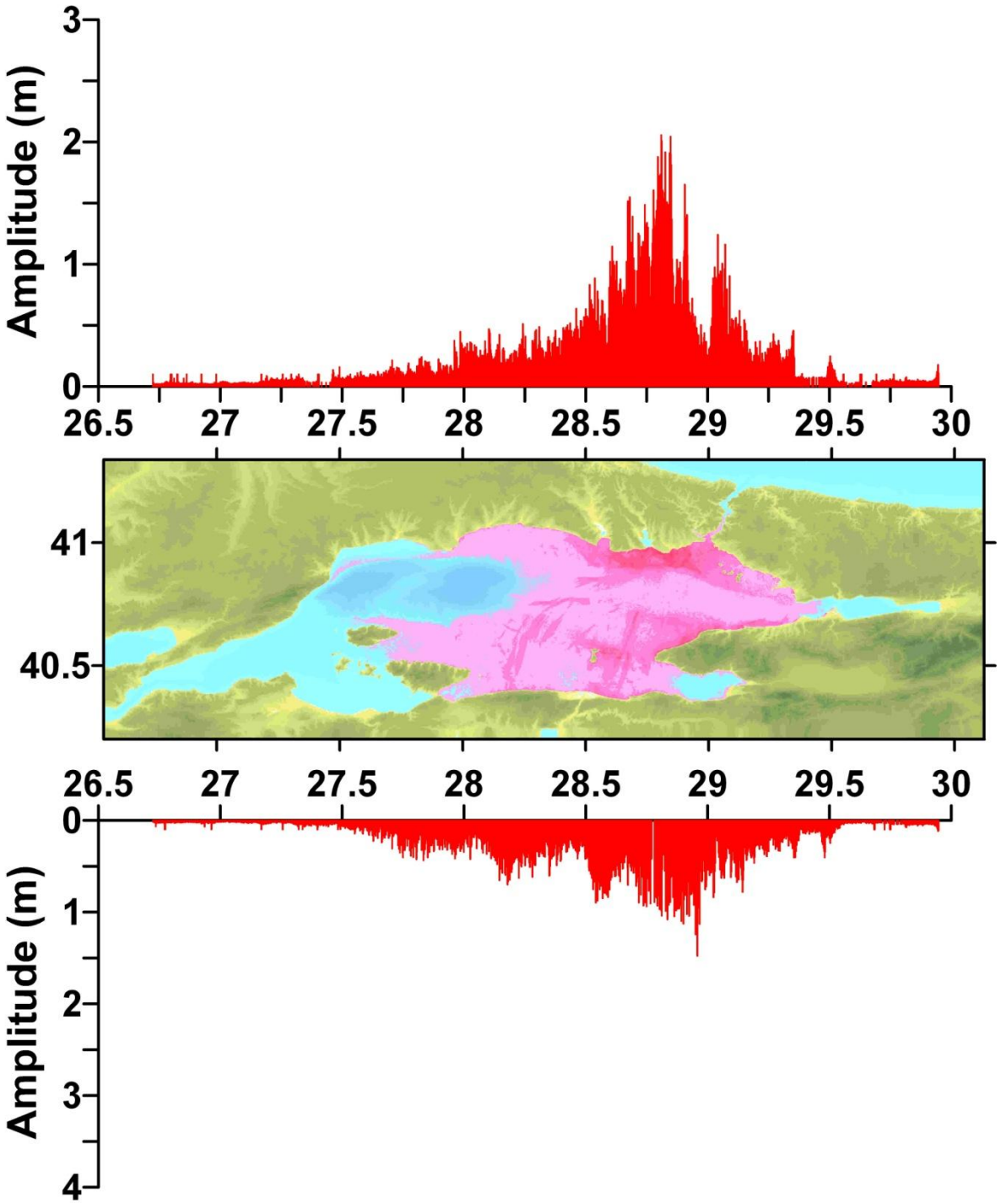

Figure 6.25. Maximum water level distributions (m) along North and South coasts of Marmara computed by the 120 minutes simulations due to the 60 m thickness of submarine landslide at Yenikapı.

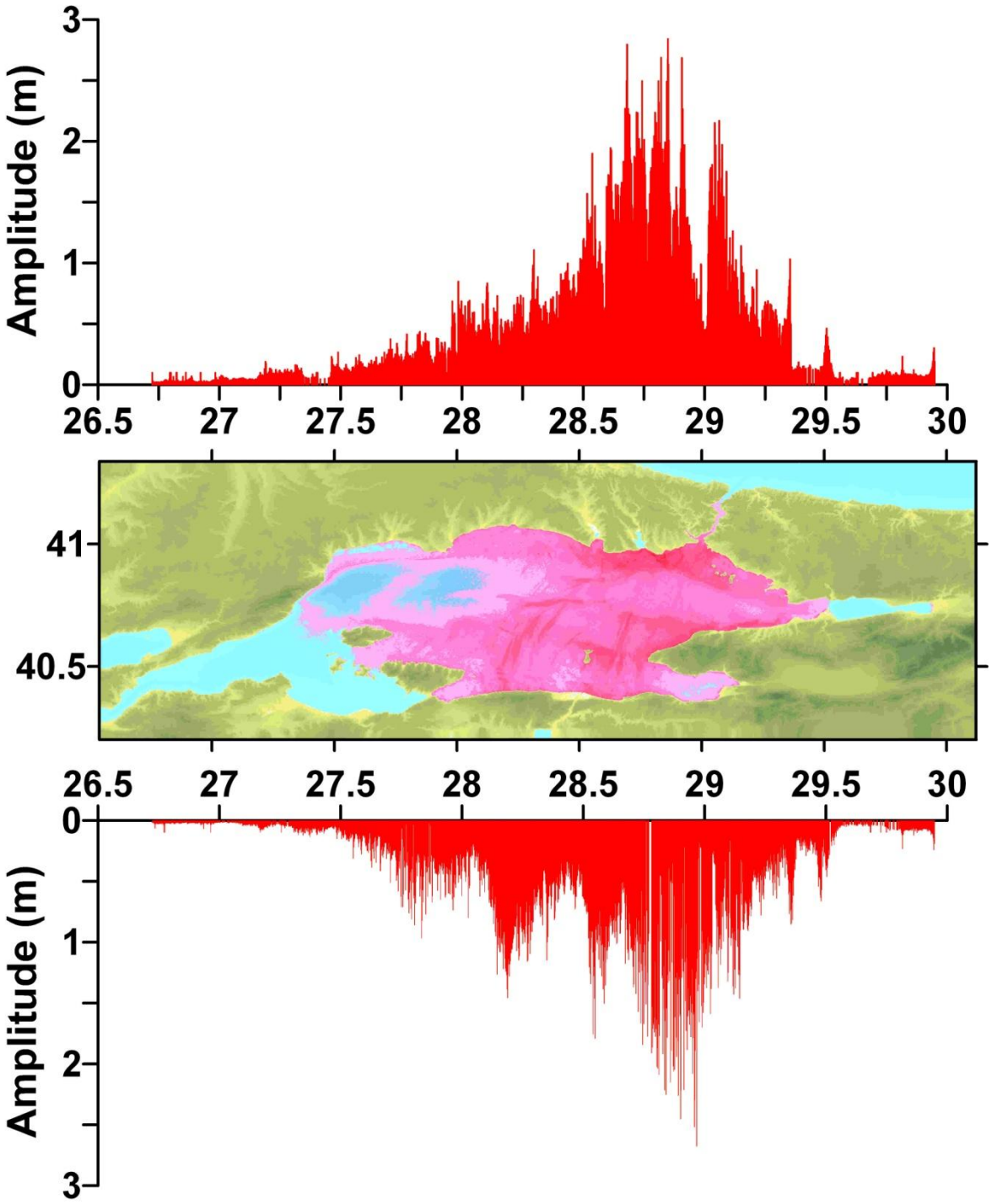

Figure 6.26. Maximum water level distributions (m) along North and South coasts of Marmara computed by the 120 minutes simulations due to the 120 m thickness of submarine landslide at Yenikapı.

The view of sea bottom material and corresponding water surface elevations (sea state) at different time steps are plotted in Figure 6.27. The depression and elevation patterns of the water surface are seen compatible with the motion of the sea bottom. The lateral motion of the bottom material is seen to be compatible with the bathymetry.

The sea bottom and the water surface profiles from south (left) to north (right) at different time steps from the start time of landslide are shown in the Figure 6.27. In the Figures, the left side is the offshore region and the right is the nearshore region at Yenikapı. As seen from the Figures that the sea bottom level changes due to landslide motion and there is cavern pattern at the sea bottom is shown together with the wave evolution (water surface). Wave propagates at both direction. The leading depression wave form is seen clearly moving towards shore direction as usual for the submarine landslide generated tsunamis. Within 5 minutes duration of the simulation, the wave amplitude diminishes while propagating towards shore but it amplifies when water depth get shallower.

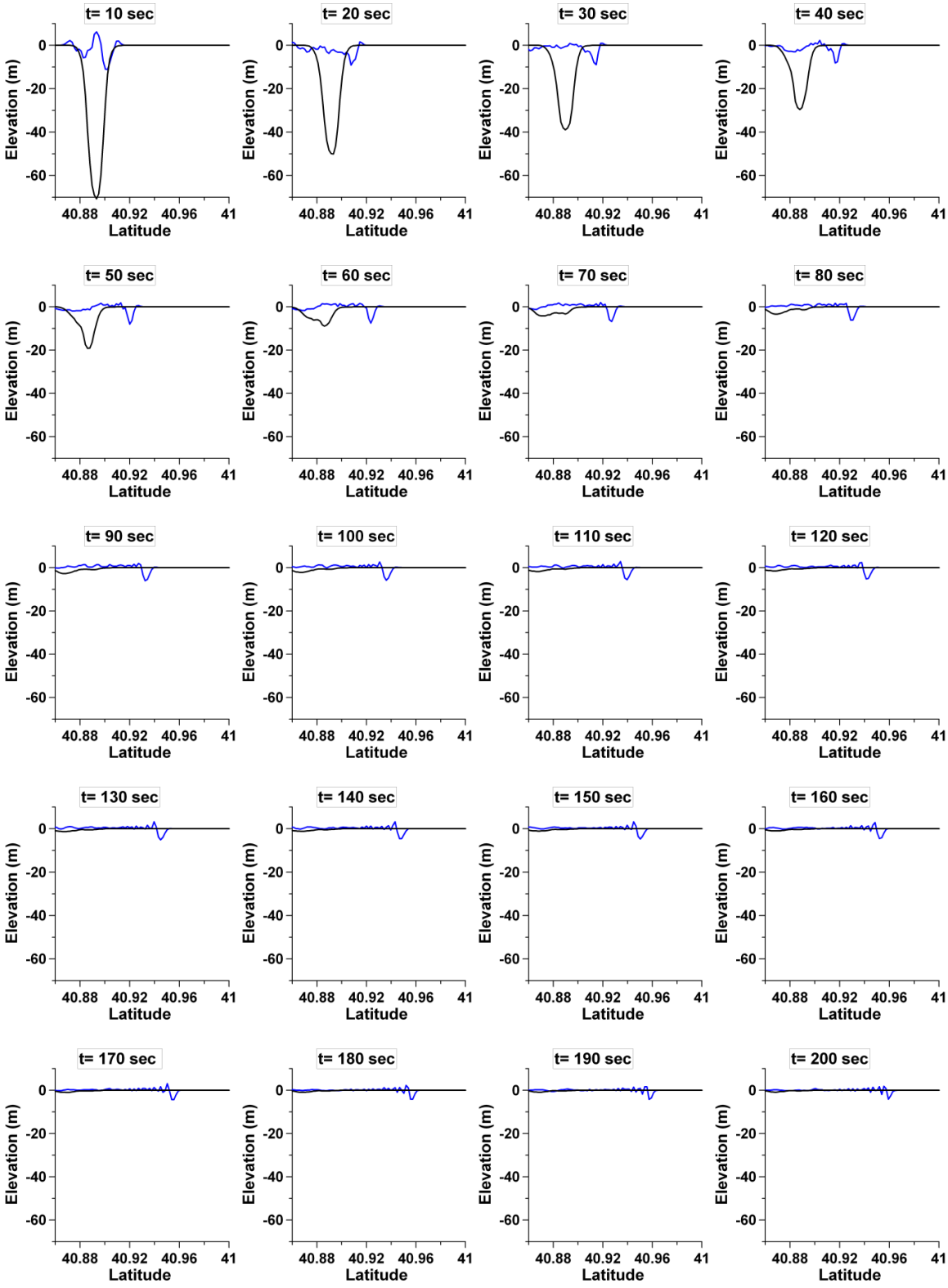

Figure 6.27. The profiles of sea bottom (black) and water surface (blue) at different time steps from the start of the landslide along the cross section from offshore (left) and shore (right).

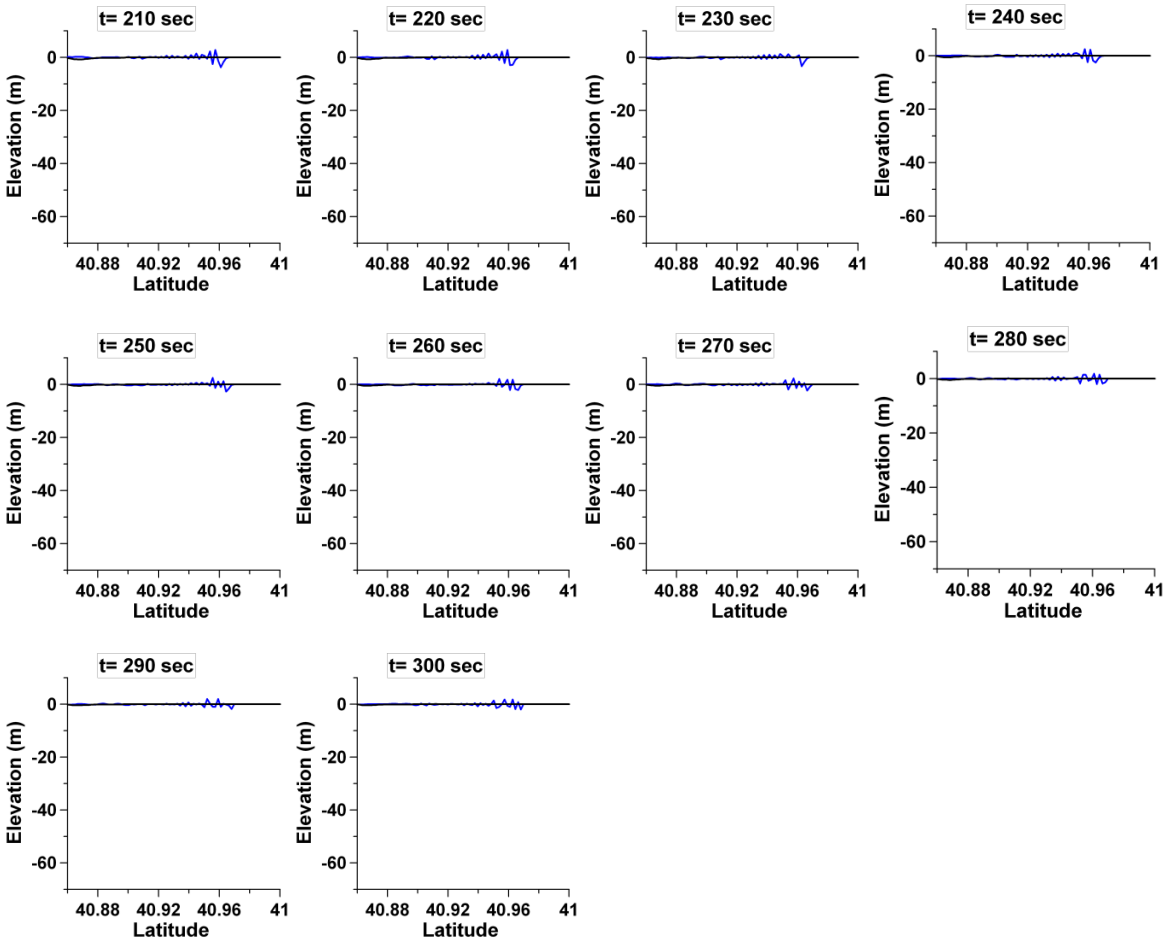

Figure 6.27 (continued). The profiles of sea bottom (black) and water surface (blue) at different time steps from the start of the landslide along the cross section from offshore (left) and shore (right).

6.2. Tsunami Due to Submarine Landslide Occurrence at Offshore of Ganos1

In Ganos1 case, an underwater landslide scenario is assumed to occur at offshore Ganos around the 27.02ºE and 40.56 ºN coordinates. The study domain used in modeling of Ganos1 submarine landslide is shown in Figure 6.28. Sediment thicknesses for Ganos are 10 m and 50 m in the model. The model is applied to the submarine failure scenario of Ganos1 choosing a simulation duration of 120 minutes in real time.

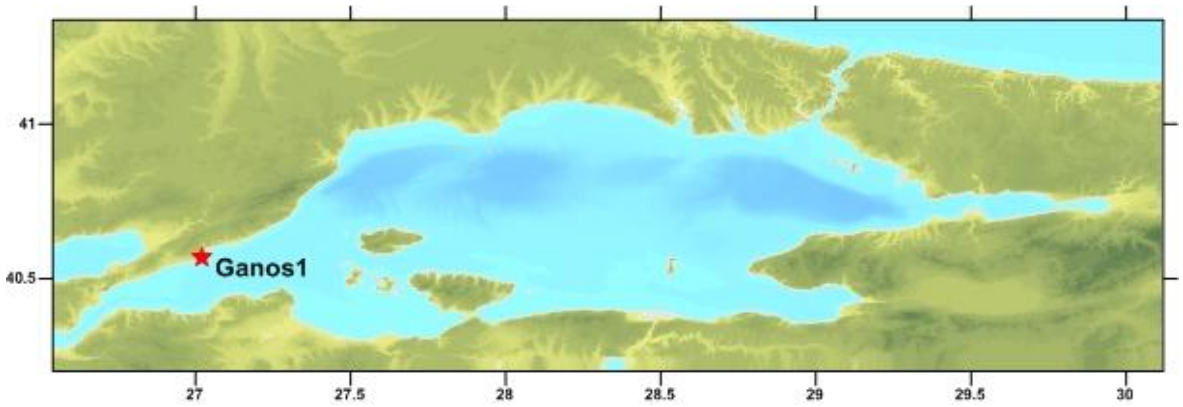

Figure 6.28. Landslide point at the study domain used in modeling of Ganos1.

Figure 6.29 and 6.30 represent relation between submarine landslide velocity and time. For 10 m sediment thickness, sl-07 gauge point is at the center of the landslide. It is seen from Figure 6.29 that landslide velocity is approximately 6.4 m/sec at the middle of the landslide. Velocity is reduced from the landslide center to the boundary of the sliding surface (rupture surface). It is seen from Figure 6.30 that velocity is increased for 50 m sediment thickness. The landslide velocity is approximately 21 m/sec at the sl-07 gauge point.

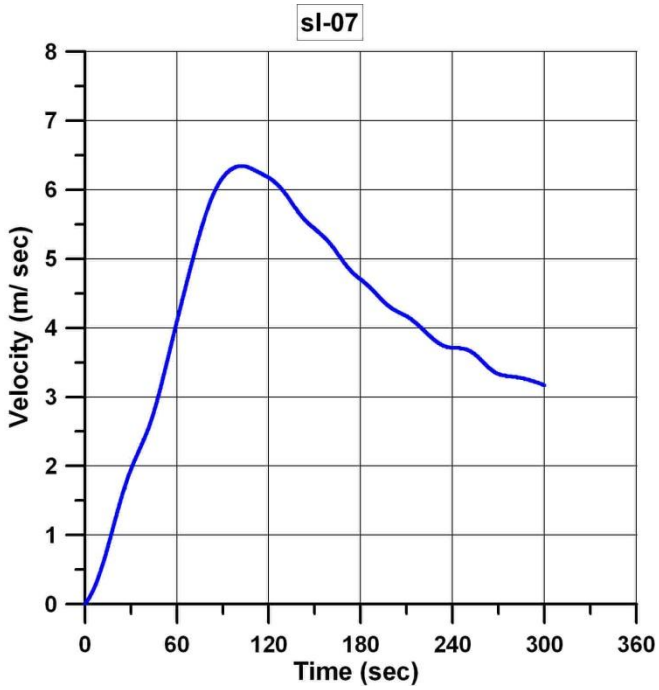

Figure 6.29. Time change of submarine landslide velocity at the center of the slide area (sl-07) due to slide of 10 m sediment thickness (Ganos1).

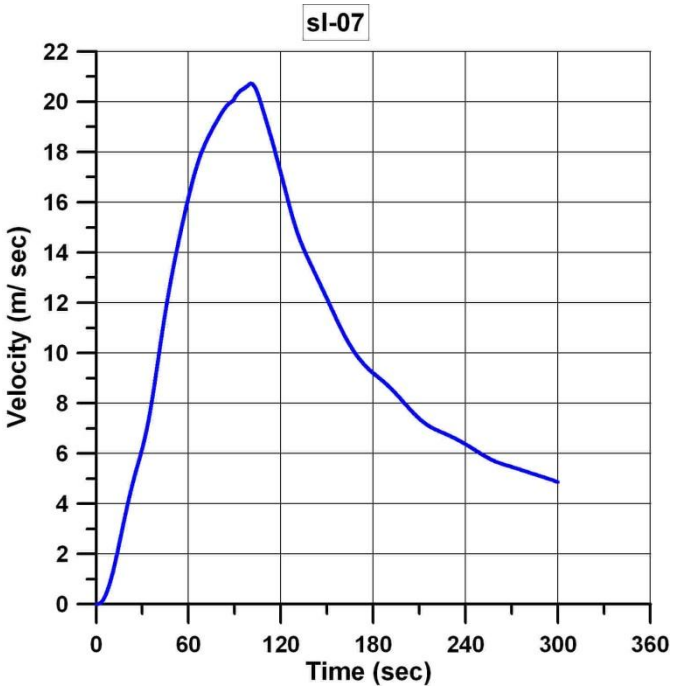

Figure 6.30. Time change of submarine landslide velocity at the center of the slide area (sl-07) due to slide of 50 m sediment thickness (Ganos1).

In this part, the propagation of the tsunami wave induced by offshore Ganos (Ganos1) landslide and its effects are observed. After 5 minutes of simulation of the submarine landslide generated tsunami with TWO LAYER model, the propagation of the tsunami waves is simulated with NAMI-DANCE. For input, the 150 m grid size Marmara bathymetry and gauge point locations files are inserted to the model.

Along the coast of the Sea of Marmara, 30 gauge points are selected which are shown in Figure 6.31 and the coordinates and depths of these points are given in Table 6.3. Furthermore, 15 gauge points are selected which are perpendicular direction to landslide axis and around the landslide area.

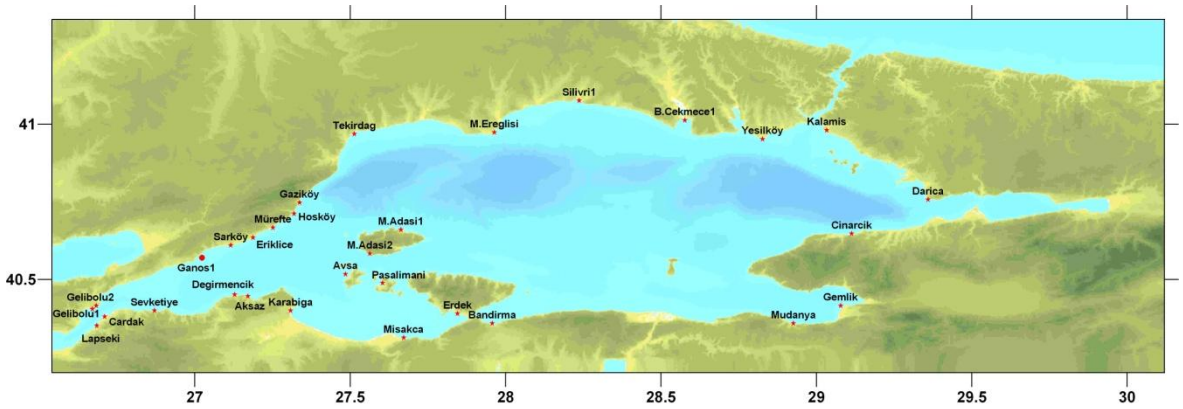

Figure 6.31. The locations of the selected gauge points for the simulations of Ganos1 submarine landslide.

The water surface elevation for 10 m and 50 m sediment thicknesses are shown in Figure 6.32 to 6.35. As it can be seen from the Figure, for 10 m sediment thickness, the water surface elevations are 0.5 m and 0.5 m at Şarköy, sl-08 gauge points, respectively. When the sediment thickness is 50 m, the water surface elevations increase. Thus, the water surface elevations are 2.7 m and 2.9 m at Şarköy, sl-08 gauge points for 50 m sediment thickness, respectively. In addition, the most affected areas by the landslide are the south and north coast along the location the slide happens.

Table 6.3. The coordinates and depths of the selected gauge points for the simulations of Ganos1 submarine lanslide.

Name	X Coordinate	Y Coordinate	Depth (m)
M.Adası 1	27.6626	40.6598	2.7
M.Adası 2	27.5629	40.5832	26.1
Avşa	27.4844	40.5172	9.8
Paşalimanı	27.6038	40.4887	9
Erdek	27.8451	40.3899	9.6
Misakça	27.6716	40.3123	0.9
Karabiga	27.3080	40.3996	2.7
Aksaz	27.1708	40.4459	2.5
Değirmencik	27.1281	40.4513	1.9
Şevketiye	26.8697	40.3996	1.3
Çardak	26.7093	40.380	4.2
Lapseki	26.6843	40.3515	8.7
Gelibolu1	26.6701	40.4049	22.9
Gelibolu2	26.6826	40.4156	6.4
Şarköy	27.1156	40.6099	12.4
Eriklice	27.1869	40.6348	4.7
Mürefte	27.2510	40.6669	7.8
Hoşköy	27.3187	40.7115	8.2
Gaziköy	27.3365	40.7471	2.3
Tekirdağ	27.5130	40.9681	8.5
M. Ereğlisi	27.9638	40.9734	8.3
Silivri 1	28.2364	41.0757	5.7
B. Çekmece 1	28.5768	41.0127	9.9
Yeşilköy	28.8263	40.9521	10
Kalamış	29.0330	40.9806	4.8
Darıca	29.3589	40.7570	19.4
Çınarcık	29.1132	40.6473	3.2
Gemlik	29.0775	40.4156	12.9
Mudanya	28.9261	40.3586	1.5
Bandırma	27.9567	40.3586	1.7
G1-sl-01	27.0229	40.5093	53.8
G1-sl-02	27.0229	40.5193	52.1
G1-sl-03	27.0229	40.5293	51.4
G1-sl-04	27.0229	40.5393	49.5
G1-sl-05	27.0229	40.5493	41.1
G1-sl-06	27.0229	40.5593	28.1
G1-sl-07 (Center of Landslide)	27.0229	40.5693	15.7
G1-sl-08	27.0229	40.5793	7.9
G1-sl-09	27.0104	40.5671	9.6
G1-sl-10	27.0158	40.5636	20
G1-sl-11	27.0247	40.5707	16.9
G1-sl-12	27.0194	40.5689	14.1

Table 6.3 (continued). The coordinates and depths of the selected gauge points for the simulations of Ganos1 submarine lanslide.

G1-sl-13	27.0265	40.5778	15.7
G1-sl-14	27.0354	40.5832	17.3
G1-sl-15	27.0288	40.5702	18.2

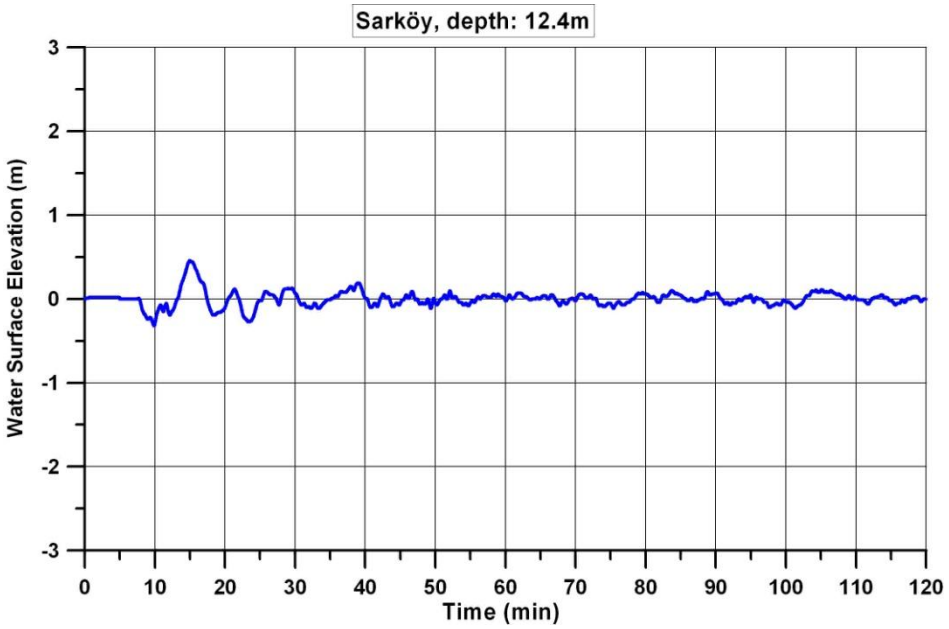

Figure 6.32. The time histories water surface fluctuations computed at selected gauge point (Şarköy) for the simulation due to landslide of 10 m submarine sediment thickness at offshore of Ganos1.

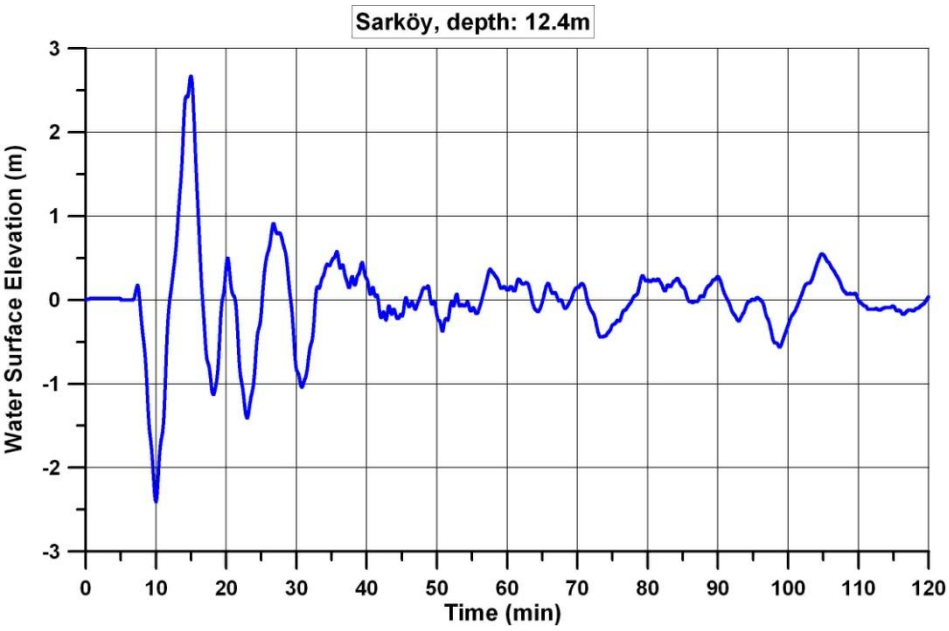

Figure 6.33. The time histories water surface fluctuations computed at selected gauge point (Şarköy) for the simulation due to landslide of 50 m submarine sediment thickness at offshore of Ganos1.

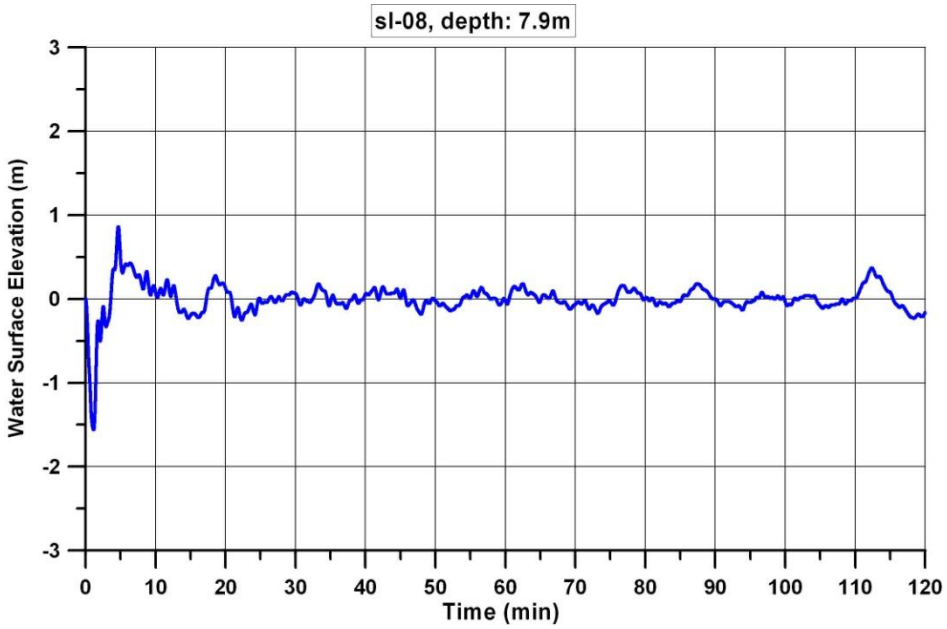

Figure 6.34. The time histories water surface fluctuations computed at selected gauge point (sl-08) for the simulation due to landslide of 10 m submarine sediment thickness at offshore of Ganos1.

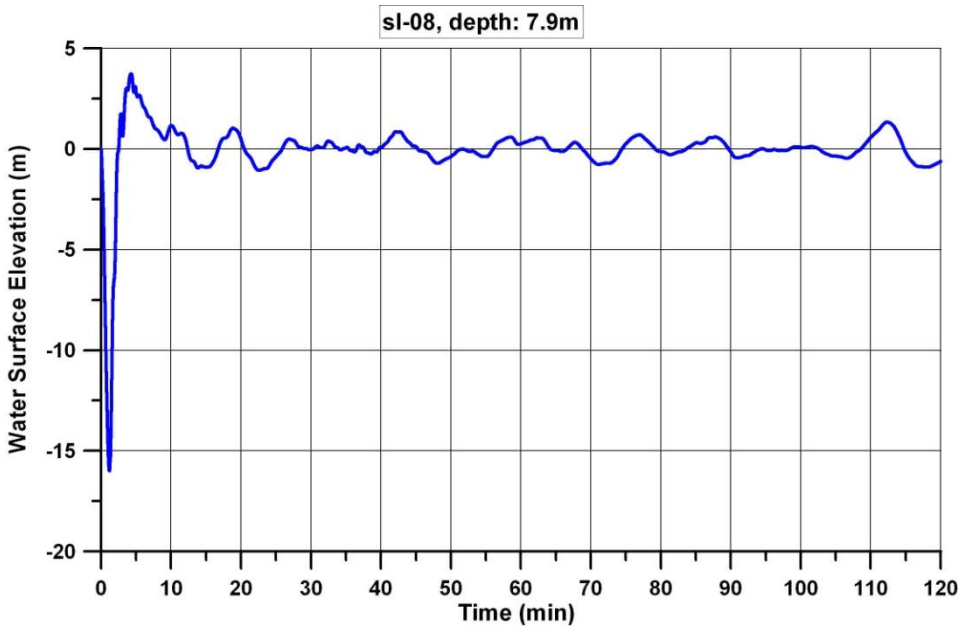

Figure 6.35. The time histories water surface fluctuations computed at selected gauge point (sl-08) for the simulation due to landslide of 50 m submarine sediment thickness at offshore of Ganos1.

According to the simulation results, it can be observed that the tsunami wave reaches Avşa, Aksaz, Gelibolu and Hoşköy in 5 minutes, Şarköy, Erdek, Tekirdağ and Silivri in 7 minutes. The depths, arrival times of first waves, maximum and minimum water elevation for the 37 selected gauge points are summarized in Table 6.4 for 10 m and 50 m sediment thicknesses. According to simulation results, Şarköy and Aksaz are in danger.

The distributions of maximum surface elevation that the waves lead to the shoreline along north and south coasts in the Marmara Sea are indicated in Figure 6.36 and 6.37. According to Figure, the maximum positive tsunami amplitudes are 1.5 m at the north shore and 0.7 m at the south coast for 10 m sediment thickness. For 50 m sediment thickness, positive tsunami amplitudes are 7 m at the north and 4 m at the south coast.

Table 6.4. The summary sheet of the simulation results of submarine landslide tsunami at Ganos1.

		10M			50M		
Gauge Point	**Depth (m)**	**T_first (min)**	**Amplitude (+) (m)**	**Amplitude (-) (m)**	**T_first (min)**	**Amplitude (+) (m)**	**Amplitude (-) (m)**
M. Adası 1	2.7	8	0.1	-0.1	8	0.6	-0.6
M. Adası 2	26.1	6	0.1	-0.1	6	0.5	-0.4
Avşa	9.8	5	0.1	-0.1	5	0.7	-0.5
Paşalimanı	9	13	0.2	-0.3	13	0.8	-1.2
Erdek	9.6	7	0.1	-0.1	7	0.5	-0.4
Misakça	0.9	20	0.1	-0.2	20	0.5	-0.8
Karabiga	2.7	21	0.2	-0.2	21	0.8	-0.6
Aksaz	2.5	5	0.2	-0.4	5	1.8	-2.6
Değirmencik	1.9	11	0.4	-0.4	9	1.9	-1.9
Şevketiye	1.3	18	0.4	-0.2	16	1.9	-1.4
Çardak	4.2	26	0.2	-0.1	26	0.5	-0.4
Lapseki	8.7	6	0.1	-0.1	6	0.7	-0.4
Gelibolu 1	23	5	0.1	-0.1	5	0.2	-0.4
Gelibolu 2	6.4	12	0.1	-0.1	12	0.5	-0.5
Şarköy	12.4	7	0.5	-0.3	6	2.7	-2.4
Eriklice	4.7	6	0.3	-0.3	6	1.5	-2.2
Mürefte	7.8	6	0.2	-0.3	6	1.5	-1.8
Hoşköy	8.2	5	0.2	-0.2	5	1.3	-1.1
Gaziköy	2.3	15	0.2	-0.2	15	1.3	-1
Tekirdağ	8.5	7	0.1	-0.1	7	0.5	-0.6
M. Ereğlisi	8.3	12	0.1	-0.1	12	0.4	-0.5
Silivri 1	5.7	7	0.1	-0.1	7	0.2	-0.2
G1-sl-01	53.8	5	0.2	-0.2	5	0.9	-1.5
G1-sl-02	52.1	5	0.2	-0.2	5	1	-1.5
G1-sl-03	51.4	5	0.3	-0.1	5	1.1	-0.9
G1-sl-04	49.5	5	0.3	-0.1	5	1.3	-0.4
G1-sl-05	41.1	5	0.4	-0.1	5	1.6	-0.6
G1-sl-06	28.1	5	0.4	-0.2	5	1.8	-0.7
G1-sl-07	15.7	5	0.6	-0.2	5	2.7	-0.7
G1-sl-08	7.9	5	0.5	-0.3	5	2.9	-1.1
G1-sl-09	9.6	5	1	-0.3	5	3.2	-1.1
G1-sl-10	20	5	0.7	-0.2	5	2.6	-0.7
G1-sl-11	16.9	5	0.6	-0.2	5	2.6	-0.7
G1-sl-12	14.1	5	0.8	-0.2	5	2.9	-0.8
G1-sl-13	15.7	5	0.6	-0.2	5	2.8	-0.9
G1-sl-14	17.3	5	0.6	-0.2	5	2	-0.8
G1-sl-15	18.2	5	0.5	-0.2	5	2.6	-0.7

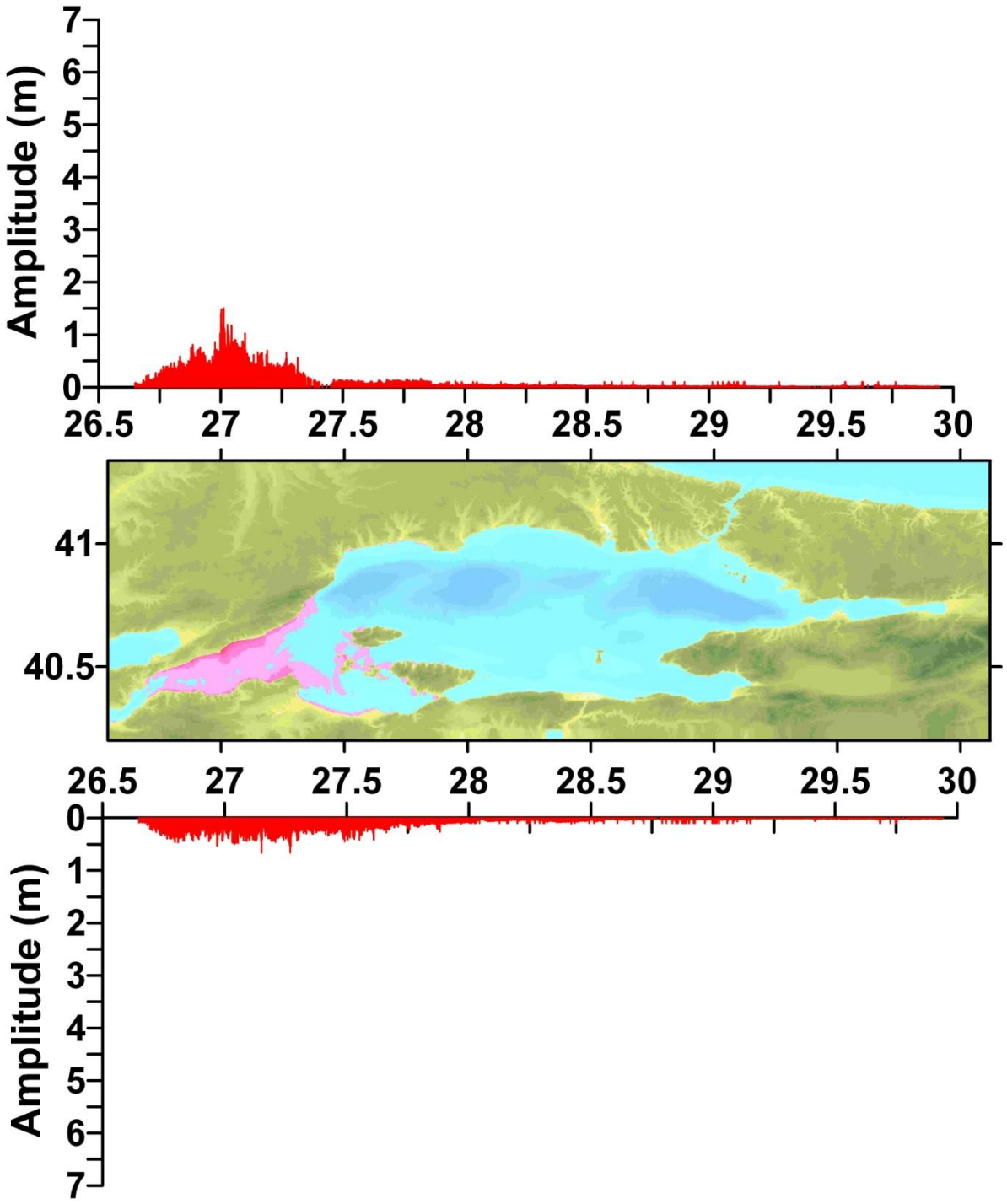

Figure 6.36. Maximum Water level distributions (m) along North and South coasts of Marmara computed by the 120 minutes simulations due to the 10 m thickness of submarine landslide at Ganos1.

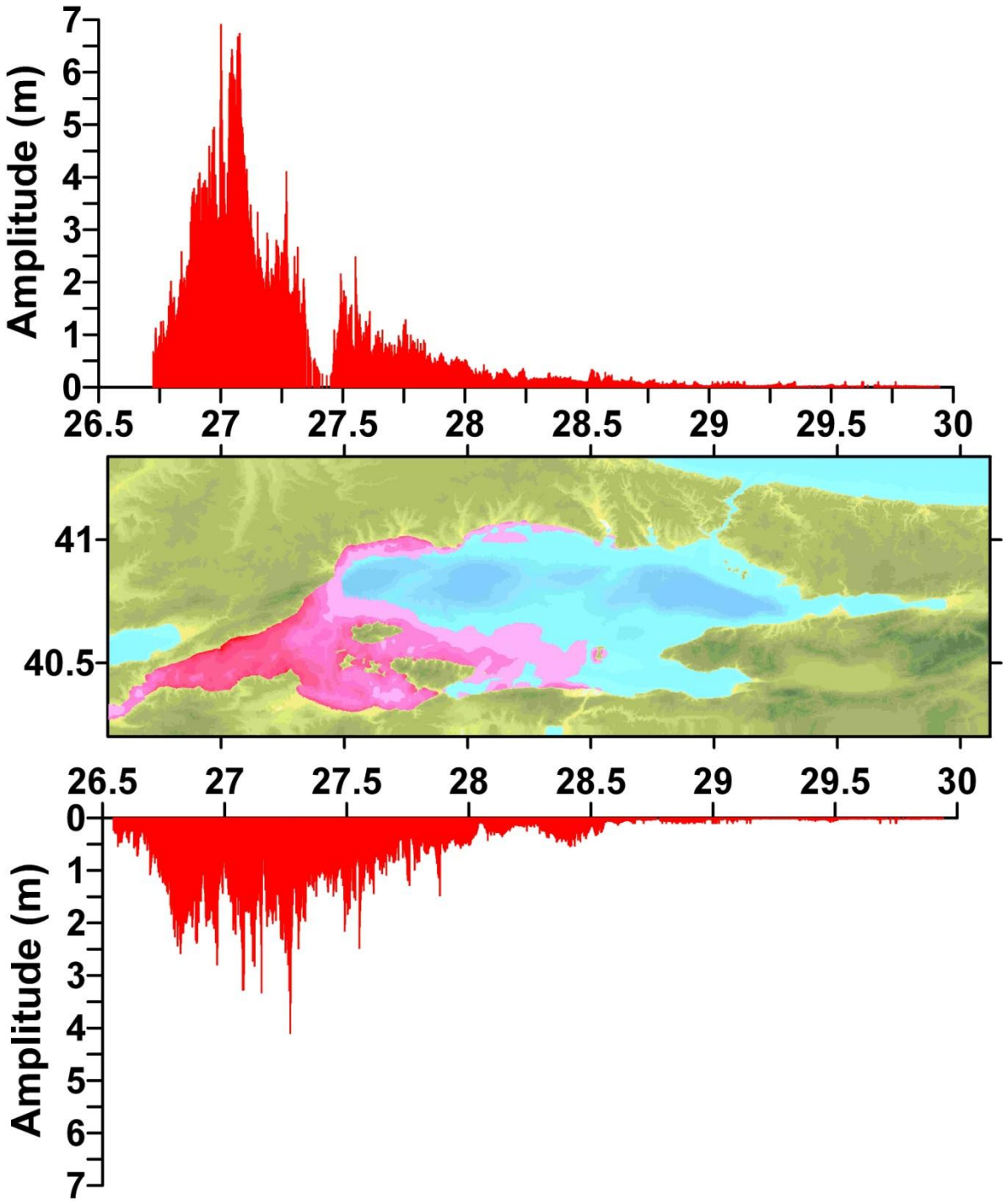

Figure 6.37. Maximum water level distributions (m) along North and South coasts of Marmara computed by the 120 minutes simulations due to the 50 m thickness of submarine landslide at Ganos1.

6.3. Tsunami Due to Submarine Landslide Occurrence at Offshore of Ganos2

In the second case, an underwater landslide scenario is assumed to happen at offshore Ganos around the 27.34ºE and 40.60ºN coordinates. The study domain used in modeling of Ganos2 submarine landslide is indicated in Figure 6.38.

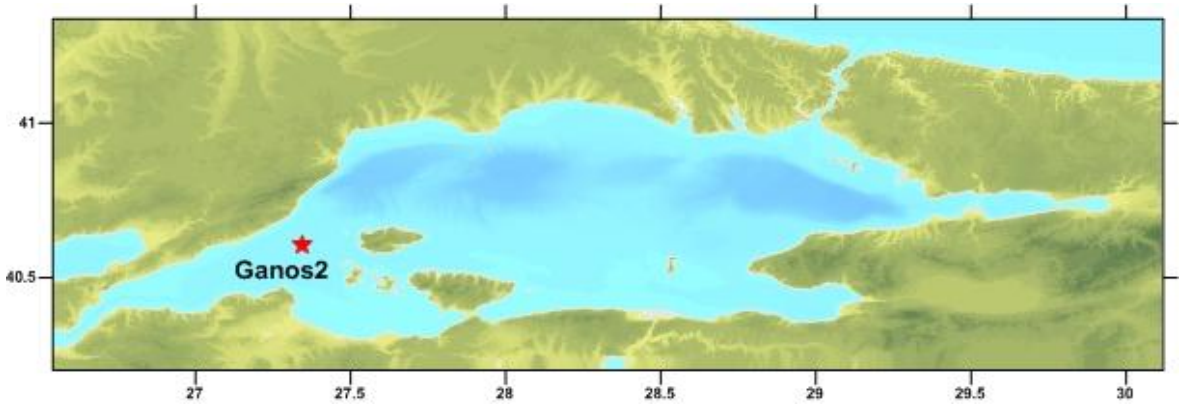

Figure 6.38. Landslide point at the study domain used in modeling of Ganos2.

Figure 6.39 and 6.40 represent relation between submarine landslide velocity and time. For 10 m sediment thickness, sl-03 gauge point is at the center of the landslide. It is seen from Figure 6.39 that landslide velocity is approximately 11.7 m/sec at the middle of the landslide. As it can be seen from the Figure 6.40, for 50 m sediment thickness, landslide velocity is 15 m/sec.

Along the coast of the Sea of Marmara, 30 gauge points are selected which are indicated in Figure 6.41 and the coordinates and depths of these points are given in Table 6.5. Furthermore, 15 gauge points are selected which are perpendicular direction to landslide axis and around the landslide area.

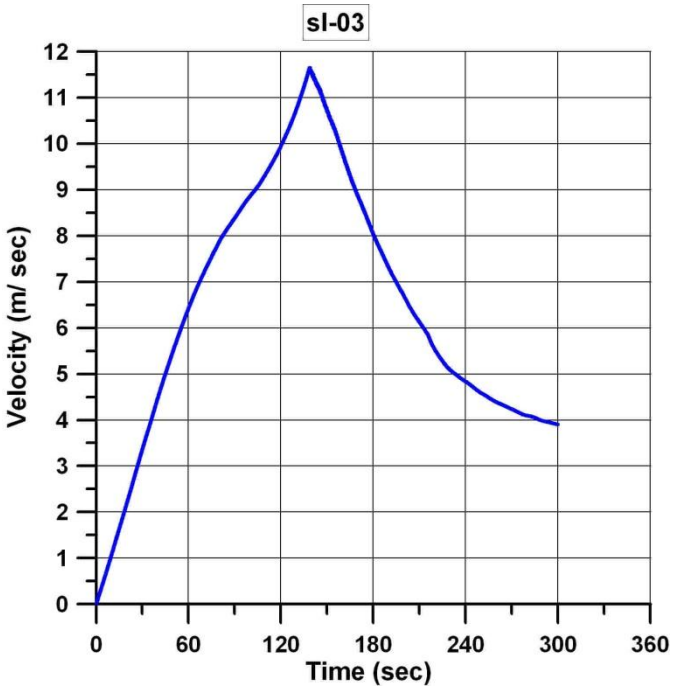

Figure 6.39. Time change of submarine landslide velocity at the center of the slide area (sl-03) due to slide of 10 m sediment thickness (Ganos2).

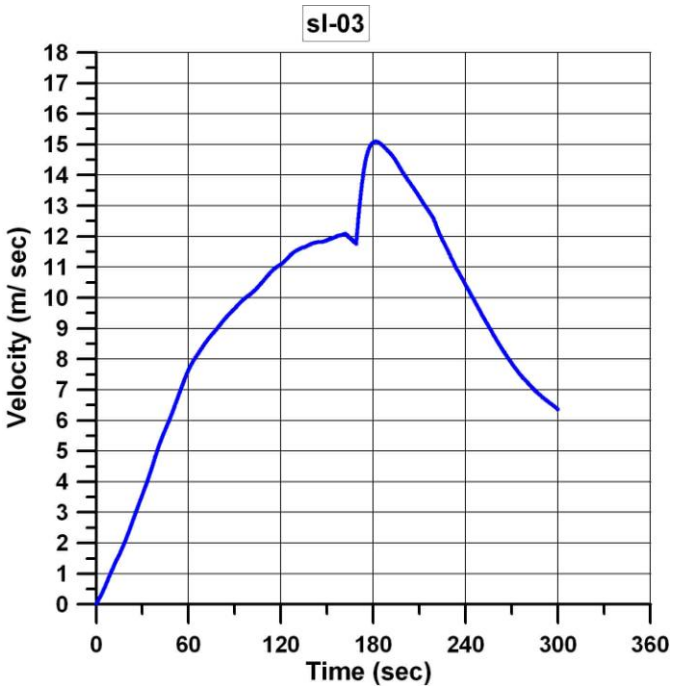

Figure 6.40. Time change of submarine landslide velocity at the center of the slide area (sl-03) due to slide of 50 m sediment thickness (Ganos2).

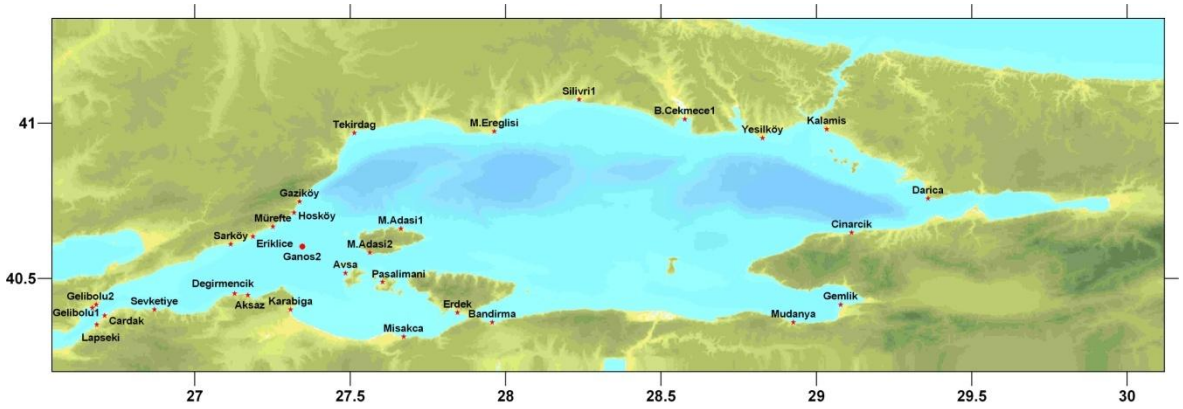

Figure 6.41. The locations of the selected gauge points for the simulations of Ganos2 submarine landslide.

The water surface elevation for 10 m and 50 m sediment thicknesses are displayed in Figure 6.42 and 6.43. As it can be seen from the Figure, for 10 m sediment thickness, the water surface elevation is 0.4 m at Gaziköy. When the sediment thickness is 50 m, the water surface elevation increases. Thus, the water surface elevation is 2.3 m at Gaziköy. In addition, the most affected areas by the landslide are the south and north coast along the location the slide happens.

According to the simulation results, it can be seen that the tsunami wave reaches Aksaz and Hoşköy in 5 minutes, Mürefte in 6 minutes, Tekirdağ in 7 minutes. The depths, arrival times of first waves, maximum and minimum water elevation for the 36 selected gauge points are summarized in Table 6.6 for 10 m and 50 m sediment thicknesses. Gaziköy, Şarköy and Aksaz are in danger.

The distributions of maximum surface elevation that the waves result in the shoreline along north and south coasts in the Marmara Sea are displayed in Figure 6.44 and 6.45. According to Figure 6.44, the maximum positive tsunami amplitudes are 0.75 m at the north shore and 0.5 m at the south coast for 10 m sediment thickness. For 50 m sediment thickness, positive tsunami amplitudes are 3.9 m at the north and 3.4 m at the south coast in Figure 6.45.

Table 6.5. The coordinates and depths of the selected gauge points for the simulations of Ganos2 submarine landslide.

Name	X Coordinate	Y Coordinate	Depth (m)
M.Adası 1	27.6626	40,6598	2.7
M.Adası 2	27.5629	40,5832	26.1
Avşa	27.4844	40,5172	9.8
Paşalimanı	27.6038	40,4887	9
Erdek	27.8451	40,3899	9.6
Misakça	27.6716	40,3123	0.9
Karabiga	27.308	40,3996	2.7
Aksaz	27.1708	40,4459	2.5
Değirmencik	27.1281	40,4513	1.9
Şevketiye	26.8697	40,3996	1.3
Çardak	26.7093	40,3800	4.2
Lapseki	26.6843	40,3515	8.7
Gelibolu 1	26.6701	40,4049	22.9
Gelibolu 2	26.6826	40,4156	6.4
Şarköy	27.1156	40,6099	12.4
Eriklice	27.1869	40,6348	4.7
Mürefte	27.2510	40,6669	7.8
Hoşköy	27.3187	40,7115	8.2
Gaziköy	27.3365	40,7471	2.3
Tekirdağ	27.5130	40.9681	8.5
M. Ereğlisi	27.9638	40.9734	8.3
Silivri 1	28.2364	41.0757	5.7
B. Çekmece 1	28.5768	41.0127	9.9
Yeşilköy	28.8263	40.9521	10
Kalamış	29.0330	40.9806	4.8
Darıca	29.3589	40.7570	19.4
Çınarcık	29.1132	40.6473	3.2
Gemlik	29.0775	40.4156	12.9
Mudanya	28.9261	40.3586	1.5
Bandırma	27.9567	40.3586	1.7
G2-sl-01	27.3455	40.5825	82.2
G2-sl-02	27.3455	40.5925	92.2
G2-sl-03 (Center of Landslide)	27.3455	40.6025	109.5
G2-sl-04	27.3455	40.6125	118.1
G2-sl-05	27.3455	40.6225	117.7
G2-sl-06	27.3455	40.6325	102.5
G2-sl-07	27.3455	40.6425	91.5
G2-sl-08	27.3455	40.6525	84.1
G2-sl-09	27.3455	40.6625	77.3
G2-sl-10	27.3285	40.6153	113.6
G2-sl-11	27.3474	40.6166	119.5
G2-sl-12	27.3340	40.6048	116.3

Table 6.5 (continued). The coordinates and depths of the selected gauge points for the simulations of Ganos2 submarine landslide.

G2-sl-13	27.3196	40.5983	108.2
G2-sl-14	27.3573	40.6272	123.7
G2-sl-15	27.3663	40.6166	126.2

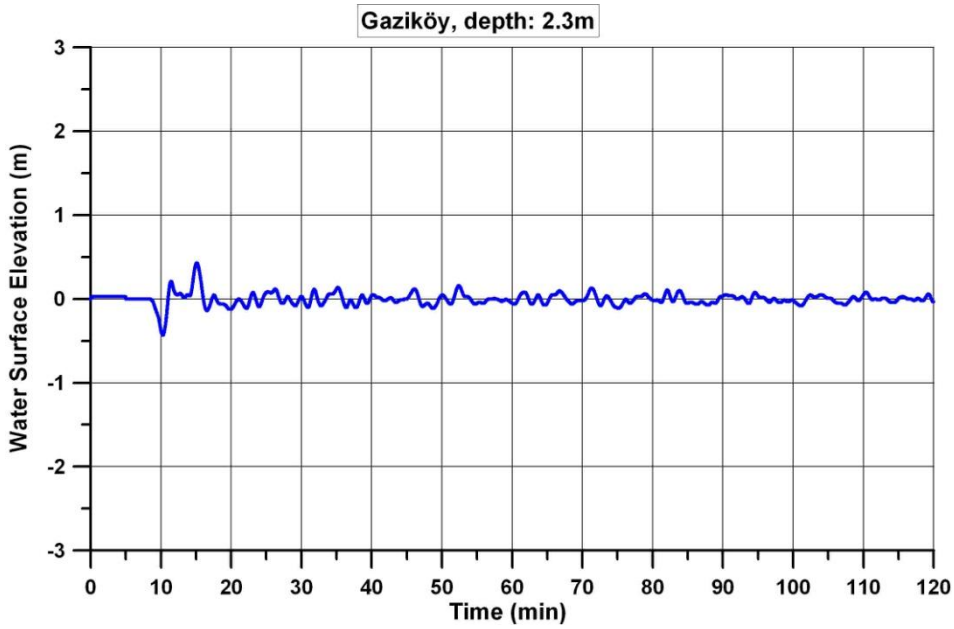

Figure 6.42. The time histories water surface fluctuations computed at selected gauge point (Gaziköy) for the simulation due to landslide of 10 m submarine sediment thickness at offshore of Ganos2.

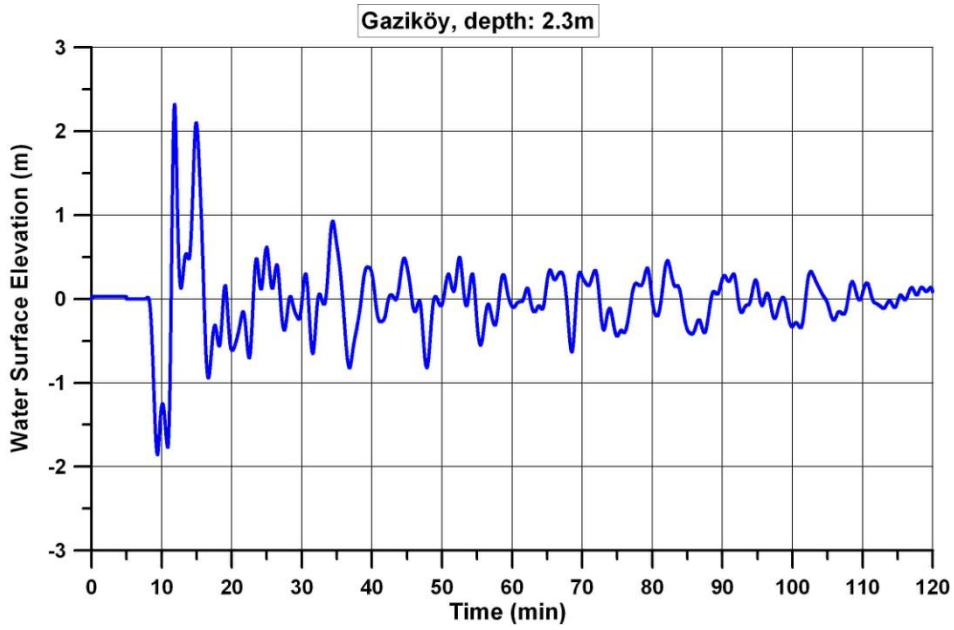

Figure 6.43. The time histories water surface fluctuations computed at selected gauge point (Gaziköy) for the simulation due to landslide of 50 m submarine sediment thickness at offshore of Ganos2.

Table 6.6. The summary sheet of the simulation results of submarine landslide tsunami at Ganos2.

		10M			50M		
Gauge Point	**Depth (m)**	**T_first (min)**	**Amplitude (+) (m)**	**Amplitude (-) (m)**	**T_first (min)**	**Amplitude (+) (m)**	**Amplitude (-) (m)**
M. Adası 1	2.7	8	0.2	-0.2	8	0.8	-1.3
M. Adası 2	26.1	6	0.1	-0.1	6	0.8	-1
Avşa	9.8	5	0.1	-0.2	5	0.4	-1.1
Paşalimani	9	13	0.1	-0.1	13	0.7	-0.6
Erdek	9.6	7	0.1	-0.1	7	0.5	-0.3
Misakça	0.9	20	0.2	-0.1	20	1	-0.8
Karabiga	2.7	17	0.2	-0.2	16	0.6	-1.1
Aksaz	2.5	5	0.3	-0.3	5	1.8	-2.1
Değirmencik	1.9	16	0.3	-0.2	15	1.4	-1.7
Şevketiye	1.3	34	0.2	-0.2	33	0.8	-0.8
Çardak	4.2	26	0.1	-0.1	26	0.2	-0.4
Lapseki	8.7	6	0.1	-0.1	6	0.3	-0.3
Gelibolu 1	22.9	5	0.1	-0.1	5	0.2	-0.3
Gelibolu 2	6.4	12	0.1	-0.1	12	0.3	-0.3
Şarköy	12.4	8	0.2	-0.2	8	1	-1
Eriklice	4.7	6	0.2	-0.3	6	0.7	-1.7
Mürefte	7.8	6	0.2	-0.5	5	1.3	-2.6
Hoşköy	8.2	5	0.3	-0.3	5	1.9	-2.3
Gaziköy	2.3	8	0.4	-0.4	7	2.3	-1.9
Tekirdağ	8.5	7	0.1	-0.1	7	0.4	-0.5
M. Ereğlisi	8.3	12	0.1	-0.1	12	0.2	-0.3
G2-sl-01	82.2	5	0.1	-0.1	5	0.5	-0.4
G2-sl-02	92.2	5	0.2	-0.1	5	0.5	-0.4
G2-sl-03	109.5	5	0.2	-0.1	5	0.6	-0.4
G2-sl-04	118.1	5	0.2	-0.1	5	0.6	-0.4
G2-sl-05	117.7	5	0.2	-0.1	5	0.5	-0.4
G2-sl-06	102.5	5	0.1	-0.1	5	0.5	-0.4
G2-sl-07	91.5	5	0.1	-0.1	5	0.6	-0.3
G2-sl-08	84.1	5	0.1	-0.1	5	0.5	-0.3
G2-sl-09	77.3	5	0.1	-0.1	5	0.4	-0.3
G2-sl-10	113.6	5	0.1	-0.1	5	0.5	-0.3
G2-sl-11	119.5	5	0.2	-0,1	5	0.6	-0.4
G2-sl-12	116.3	5	0.2	-0,1	5	0.6	-0.4
G2-sl-13	108.2	5	0.2	-0.1	5	0.5	-0.3
G2-sl-14	123.7	5	0.2	-0.1	5	0.5	-0.4
G2-sl-15	126.2	5	0.1	-0.1	5	0.5	-0.4

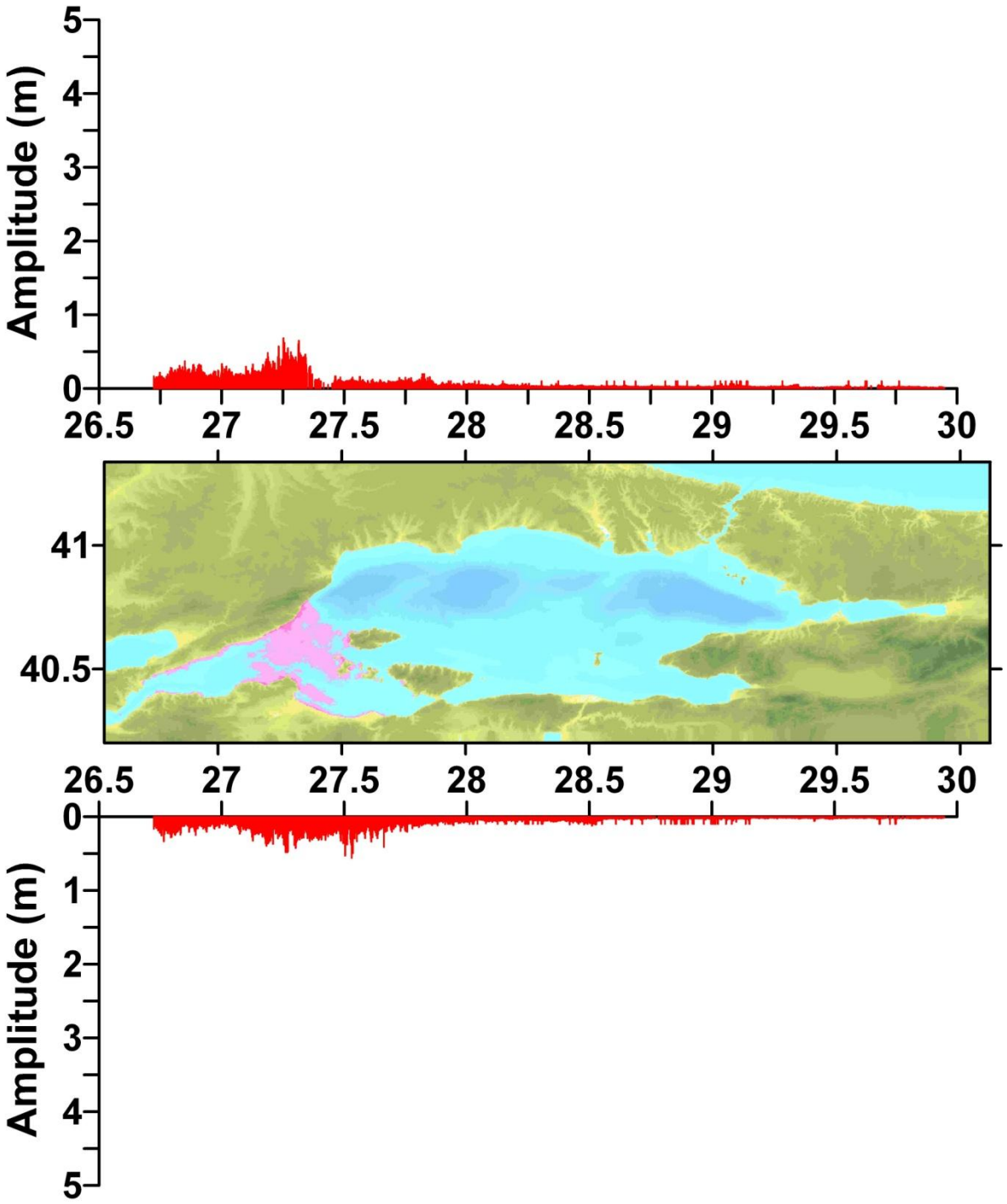

Figure 6.44. Maximum water level distributions (m) along North and South coasts of Marmara computed by the 120 minutes simulations due to the 10 m thickness of submarine landslide at Ganos2.

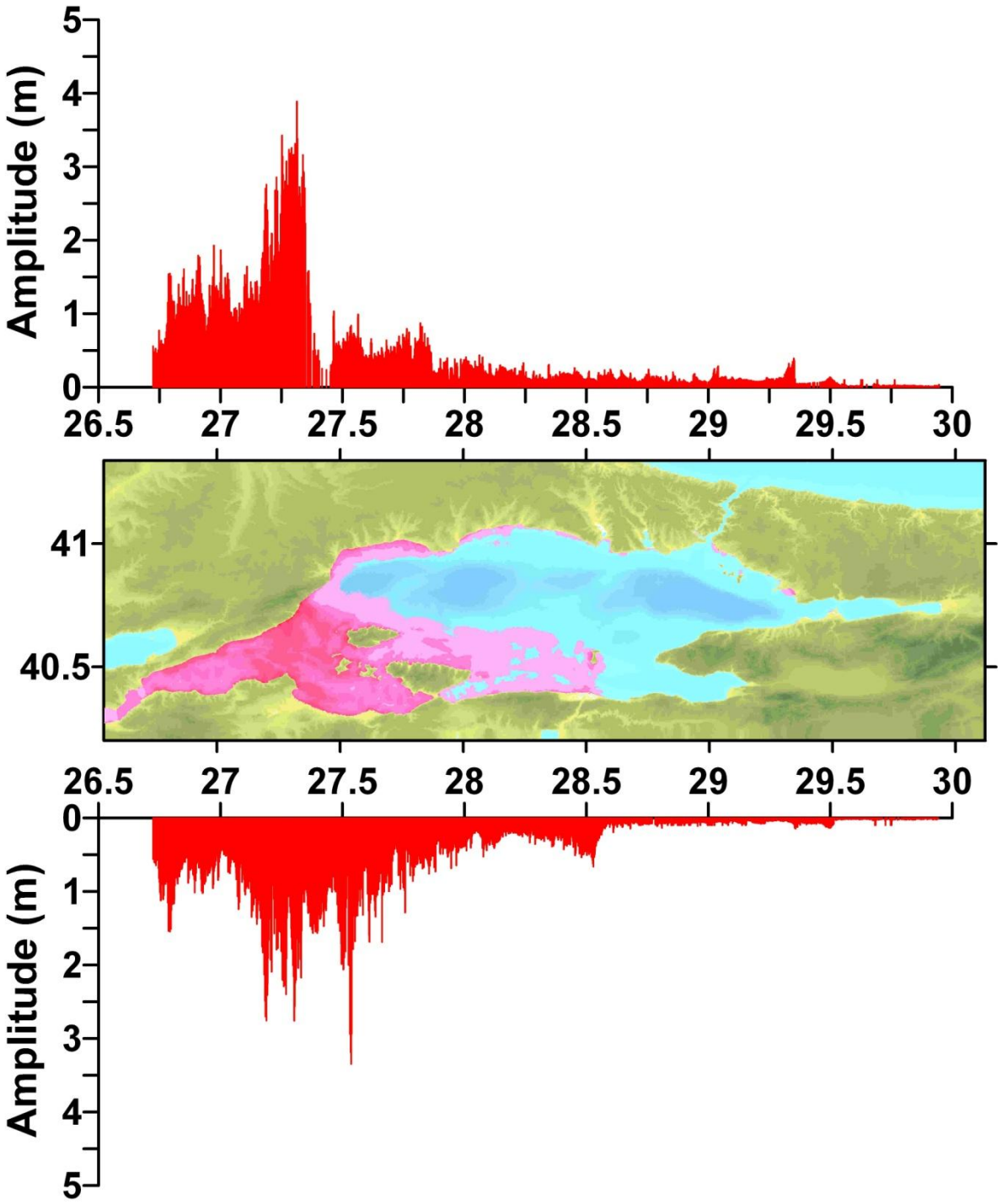

Figure 6.45. Maximum water level distributions (m) along North and South coasts of Marmara computed by the 120 minutes simulations due to the 50 m thickness of submarine landslide at Ganos2.

6.4. Tsunami Due to Submarine Landslide Occurrence at Offshore of CN1

In the CN1 case, an underwater landslide scenario is assumed to happen at offshore Ganos around the 28.19ºE and 40.92 ºN coordinates. The study domain used in modeling of CN1 submarine landslide is indicated in Figure 6.46.

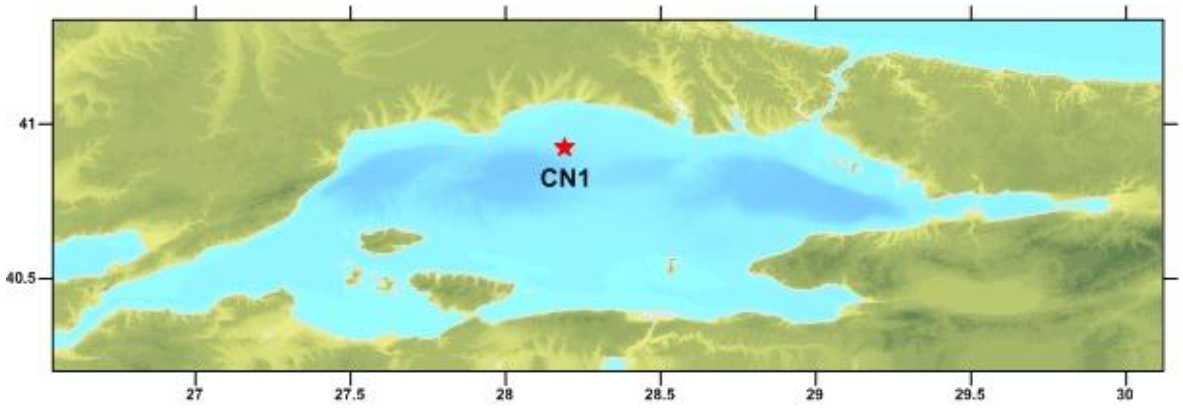

Figure 6.46. Landslide point at the study domain used in modeling of CN1.

Figure 6.47 and 6.48 represent relation between submarine landslide velocity and time. For 10 m sediment thickness, sl-06 gauge point is at the center of the landslide. It is seen from Figure 6.47 that landslide velocity is approximately 25.5 m/sec at the center of the landslide. It is seen from Figure 6.48 that velocity is increased for 50 m sediment thickness. The landslide velocity is approximately 31 m/sec at the sl-06 gauge point.

Along the coast of the Sea of Marmara, 30 gauge points are selected which are indicated in Figure 6.49 and the coordinates and depths of these points are given in Table 6.7. Furthermore, 20 gauge points are selected which are perpendicular direction to landslide axis and around the landslide area.

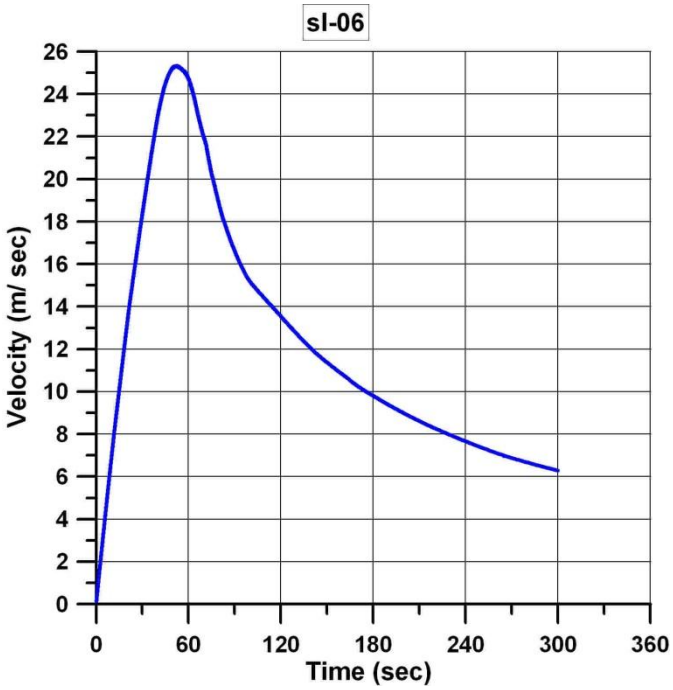

Figure 6.47. Time change of submarine landslide velocity at the center of the slide area (sl-06) due to slide of 10 m sediment thickness (CN1).

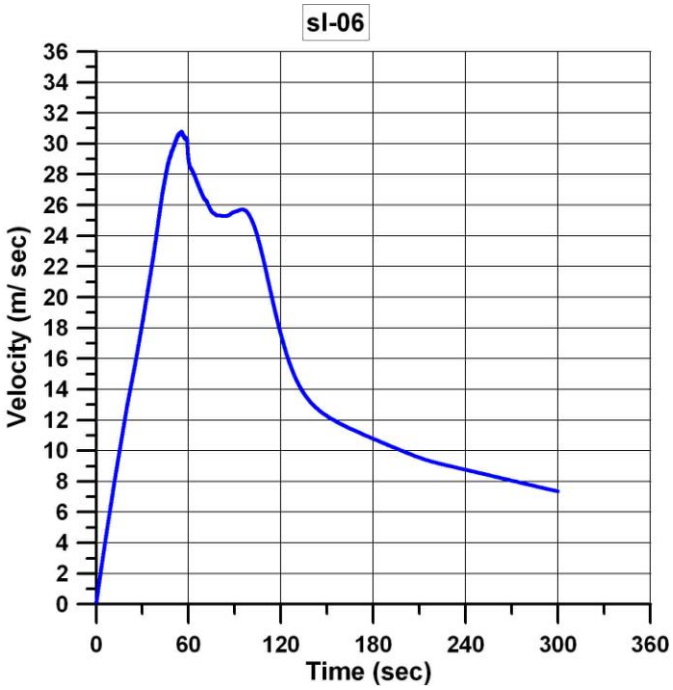

Figure 6.48. Time change of submarine landslide velocity at the center of the slide area (sl-06) due to slide of 50 m sediment thickness (CN1).

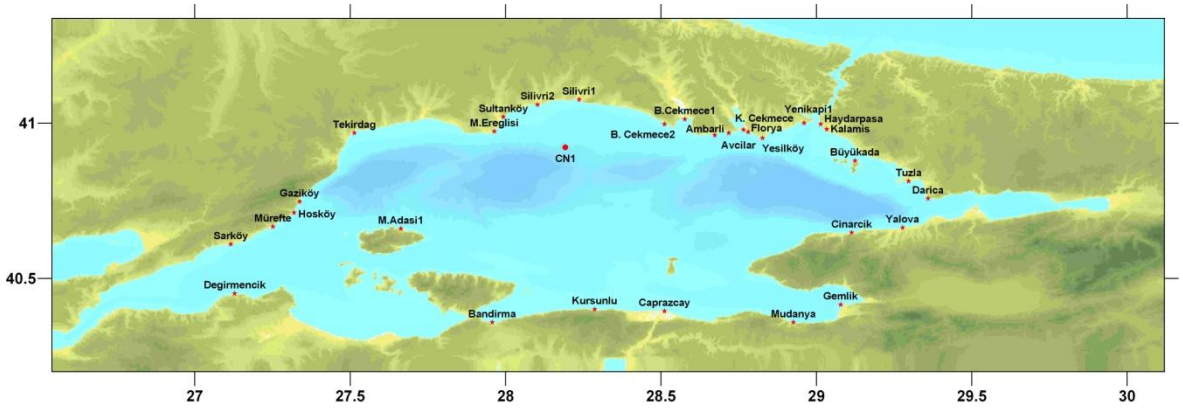

Figure 6.49. The locations of the selected gauge points for the simulations of CN1 submarine landslide.

The water surface elevation for 10 m and 50 m sediment thicknesses are showed in Figure 6.50 and 6.51. As it can be seen from the Figure 6.50, for 10 m sediment thickness, the water surface elevation is 0.9 m at Silivri. In Figure 6.51, when the sediment thickness is 50 m, the water surface elevation increases. Thus, the water surface elevation is 1.8 m at Silivri. In addition, the most affected areas by the landslide are the south and north coast along the location the slide happens.

According to the simulation results, it can be seen that the tsunami wave reaches Sultanköy and Marmara Ereğlisi in 6 minutes, Silivri in 8 minutes. The depths, arrival times of first waves, maximum and minimum water elevation for the 46 selected gauge points are summarized in Table 6.8 for 10 m and 50 m sediment thicknesses.

The distributions of maximum surface elevation that the waves result in the shoreline along north and south coasts in the Marmara Sea are displayed in Figure 6.52 and 6.53. According to Figure 6.52, the maximum positive tsunami amplitudes are 1.9 m at the north shore and 0.9 m at the south coast for 10 m sediment thickness. For 50 m sediment thickness, positive tsunami amplitudes are 5.1 m at the north and 4 m at the south coast in Figure 6.53.

Table 6.7. The coordinates and depths of the selected gauge points for the simulations of CN1 submarine landslide.

Name	X Coordinate	Y Coordinate	Depth (m)
M. Adası 1	27.6626	40.6598	2.7
Şarköy	27.1156	40.6099	12.4
Mürefte	27.2510	40.6669	7.8
Hoşköy	27.3187	40.7115	8.2
Gaziköy	27.3365	40.7471	2.3
Tekirdağ	27.5130	40.9681	8.5
M. Ereğlisi	27.9638	40.9734	8.3
Sultanköy	27.9926	41.0195	1.9
Silivri 1	28.2364	41.0757	5.7
Silivri 2	28.1024	41.0594	3.2
B. Çekmece 1	28.5768	41.0127	9.9
B.Çekmece 2	28.5109	40.9966	9.2
AmbarlI	28.6730	40.9610	16.9
Avcılar	28.7176	40.9681	13.6
K. Çekmece	28.7657	40.9788	5.1
Florya	28.7799	40.9717	7
Yeşilköy	28.8263	40.9521	10
Yenikapı 1	28.9599	41.0002	8.2
Haydarpaşa	29.0134	40.9966	9
Kalamış	29.0330	40.9806	4.8
Büyükada	29.1239	40.8790	10.1
Tuzla	29.2967	40.8131	10.4
Darıca	29.3589	40.7570	19.4
Yalova	29.2771	40.6634	1.7
Çınarcık	29.1132	40.6473	3.2
Gemlik	29.0775	40.4156	12.9
Mudanya	28.9261	40.3586	1.5
Bandırma	27.9567	40.3586	1.7
Kurşunlu	28.2865	40.4008	3.6
Çaprazçay	28.5110	40.3946	0.2
CN1-sl-01	28.1906	40.8613	960.2
CN1-sl-02	28.1906	40.8713	954.2
CN1-sl-03	28.1906	40.8813	862.6
CN1-sl-04	28.1906	40.8913	782
CN1-sl-05	28.1906	40.9013	716.4
CN1-sl-06 (Center of Landslide)	28.1906	40.9113	645
CN1-sl-07	28.1906	40.9213	617.6
CN1-sl-08	28.1906	40.9313	483
CN1-sl-09	28.1906	40.9413	339.3
CN1-sl-10	28.1906	40.9513	223.5
CN1-sl-11	28.1906	40.9613	89.7
CN1-sl-12	28.1906	40.9713	79.3

Table 6.7 (continued). The coordinates and depths of the selected gauge points for the simulations of CN1 submarine landslide.

CN1-sl-13	28.1906	40.9813	66
CN1-sl-14	28.1906	40.9913	55.7
CN1-sl-15	28.2129	40.9337	353.4
CN1-sl-016	28.1765	40.9197	490
CN1-sl-017	28.1889	40.9140	613.3
CN1-sl-018	28.1758	40.9363	439.2
CN1-sl-019	28.1895	40.9244	597.9
CN1-sl-020	28.1978	40.9203	571.6

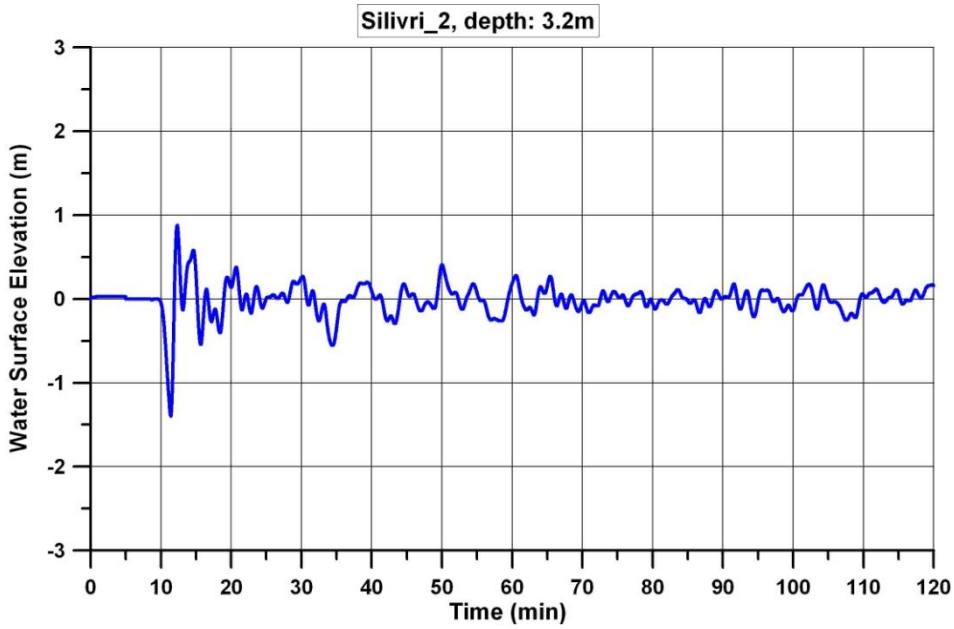

Figure 6.50. The time histories water surface fluctuations computed at selected gauge point (Silivri_2) for the simulation due to landslide of 10 m submarine sediment thickness at offshore of CN1.

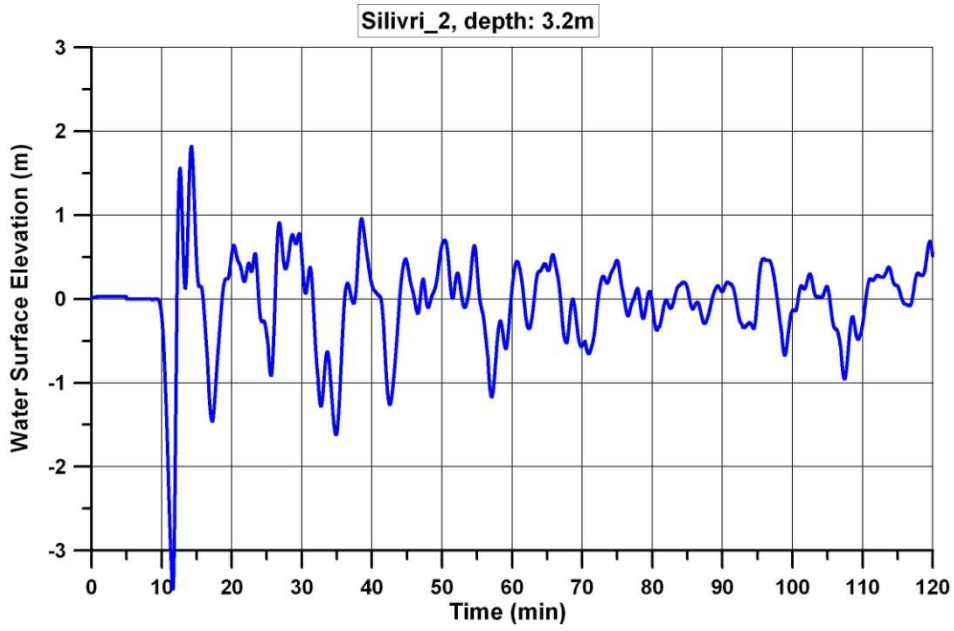

Figure 6.51. The time histories water surface fluctuations computed at selected gauge point (Silivri_2) for the simulation due to landslide of 50 m submarine sediment thickness at offshore of CN1.

Table 6.8. The summary sheet of the simulation results of submarine landslide tsunami at CN1.

		10M			50M		
Gauge Point	**Depth (m)**	**T_first (min)**	**Amplitude (+) (m)**	**Amplitude (-) (m)**	**T_first (min)**	**Amplitude (+) (m)**	**Amplitude (-) (m)**
M. Adası 1	2.7	8	0.2	-0.3	8	0.8	-1.3
Değirmencik	1.9	36	0.1	-0.1	36	0.5	-0.6
Mürefte	7.8	6	0.1	-0.1	6	0.5	-0.5
Hoşköy	8.2	5	0.1	-0.1	5	0.5	-0.7
Gaziköy	2.3	15	0.1	-0.2	15	0.7	-0.8
Tekirdağ	8.5	7	0.2	-0.1	7	0.5	-0.5
M. Ereğlisi	8.3	6	0.3	-0.4	6	1.2	-1.3
Sultanköy	1.9	6	0.6	-0.9	6	1.8	-1.9
Silivri 1	5.7	7	0.7	-1	7	1.6	-4.1
Silivri 2	3.2	8	0.9	-1.4	8	1.8	-3.5
B.Çekmece1	9.9	8	0.2	-0.2	8	0.8	-0.9
B.Çekmece2	9.2	7	0.4	-0.4	7	1.1	-2
Ambarlı	16.9	5	0.2	-0.2	5	0.5	-0.9
Avcılar	13.6	7	0.1	-0.1	7	0.5	-0.6
K. Çekmece	5.1	6	0.2	-0.2	6	0.7	-0.6
Florya	7	6	0.2	-0.1	6	0.6	-0.6
Yeşilköy	10	5	0.1	-0.1	5	0.5	-0.5
Yenikapı 1	8.2	6	0.1	-0.1	6	0.4	-0.4
Kalamış	4.8	11	0.1	-0.1	11	0.5	-0.7
Büyükada	10.1	6	0.1	-0.1	6	0.5	-0.4
Çınarcık	3.2	7	0.1	-0.1	7	0.4	-0.5
Gemlik	12.9	6	0.1	-0.1	6	0.2	-0.2
Mudanya	1.5	13	0.1	-0.2	13	0.4	-0.5
Bandırma	1.7	5	0.1	-0.2	5	0.5	-0.6
Kurşunlu	3.6	5	0.4	-0.7	5	1.4	-3
Çaprazçay	0.2	9	0.2	-0.2	9	0.5	-0.2
CN1-sl-01	960.2	5	0.1	-0.1	5	0.2	-0.2
CN1-sl-02	954.2	5	0.1	-0.1	5	0.2	-0.2
CN1-sl-03	862.6	5	0.1	-0.1	5	0.2	-0.2
CN1-sl-04	782	5	0.1	-0.1	5	0.2	-0.2
CN1-sl-05	716.4	5	0.1	-0.1	5	0.3	-0.2
CN1-sl-06	645	5	0.1	-0.1	5	0.3	-0.3
CN1-sl-07	617.6	5	0.1	-0.1	5	0.4	-0.3
CN1-sl-08	483	5	0.1	-0.1	5	0.4	-0.3
CN1-sl-09	339.3	5	0.2	-0.1	5	0.4	-0.3
CN1-sl-10	223.5	5	0.1	-0.1	5	0.4	-0.4
CN1-sl-11	89.7	5	0.2	-0.2	5	0.6	-0.4
CN1-sl-12	79.3	5	0.2	-0.1	5	0.7	-0.4
CN1-sl-13	66	5	0.3	-0.1	5	0.8	-0.5
CN1-sl-14	55.7	5	0.3	-0.2	5	0.9	-0.7
CN1-sl-15	353.4	5	0.1	-0.1	5	0.3	-0.3

Table 6.8 (continued). The summary sheet of the simulation results of submarine landslide tsunami at CN1.

CN1-sl-16	490	5	0.1	-0.1	5	0.3	-0.3
CN1-sl-17	613.3	5	0.1	-0.1	5	0.4	-0.3
CN1-sl-18	439.2	5	0.1	-0.1	5	0.5	-0.3
CN1-sl-19	597.9	5	0.1	-0.1	5	0.4	-0.3
CN1-sl-20	571.6	5	0.1	-0.1	5	0.4	-0.3

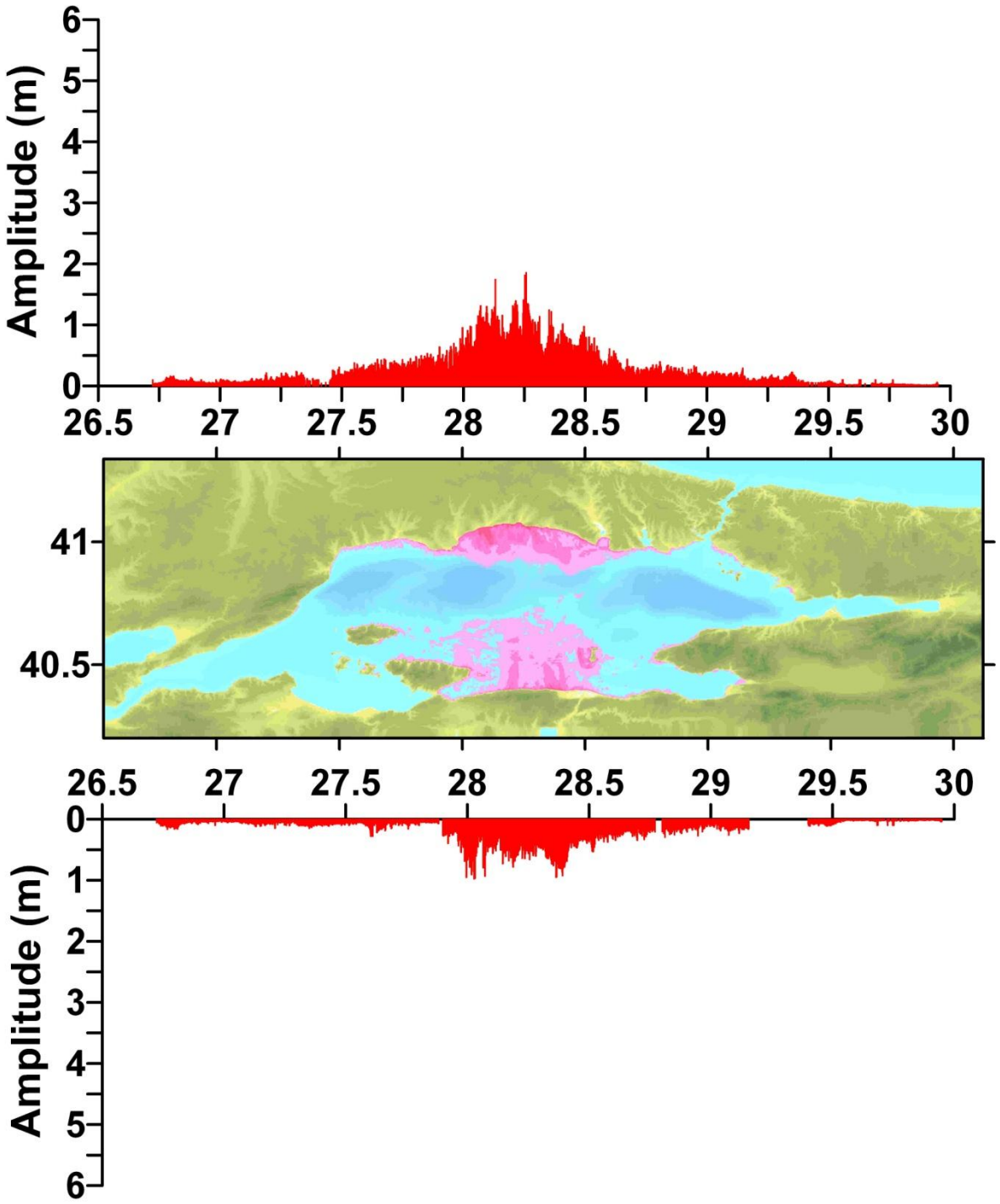

Figure 6.52. Maximum water level distributions (m) along North and South coasts of Marmara computed by the 120 minutes simulations due to the 10 m thickness of submarine landslide at CN1.

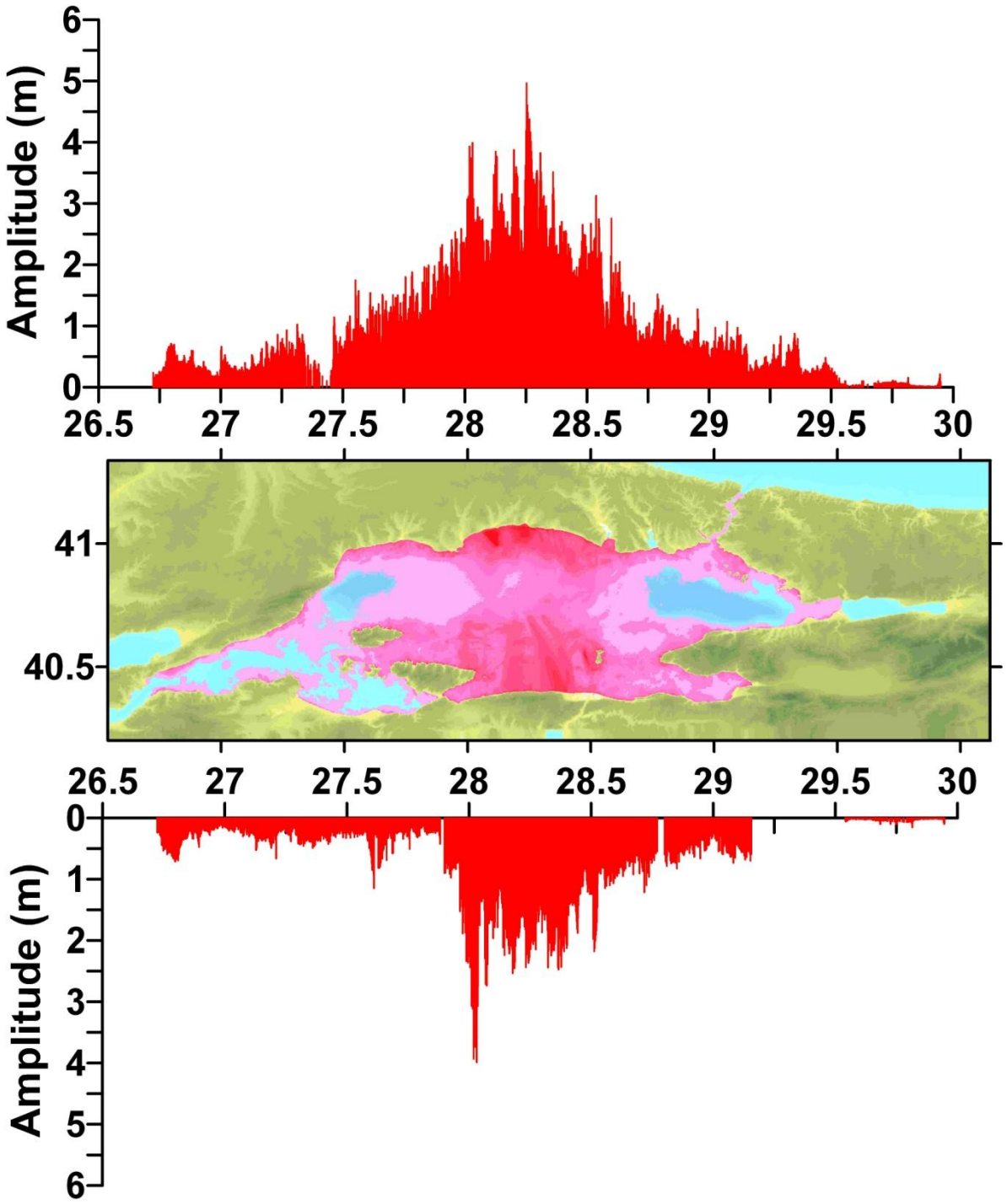

Figure 6.53. Maximum water level distributions (m) along North and South coasts of Marmara computed by the 120 minutes simulations due to the 50 m thickness of submarine landslide at CN1.

6.5. Tsunami Due to Submarine Landslide Occurrence at Offshore of Küçükçekmece1

In the Küçükçekmece1 case, an underwater landslide scenario is assumed to occur at offshore Küçükçekmece around the 28.59ºE and 40.95ºN coordinates. The study domain used in modeling of Küçükçekmece1 submarine landslide is showed in Figure 6.54.

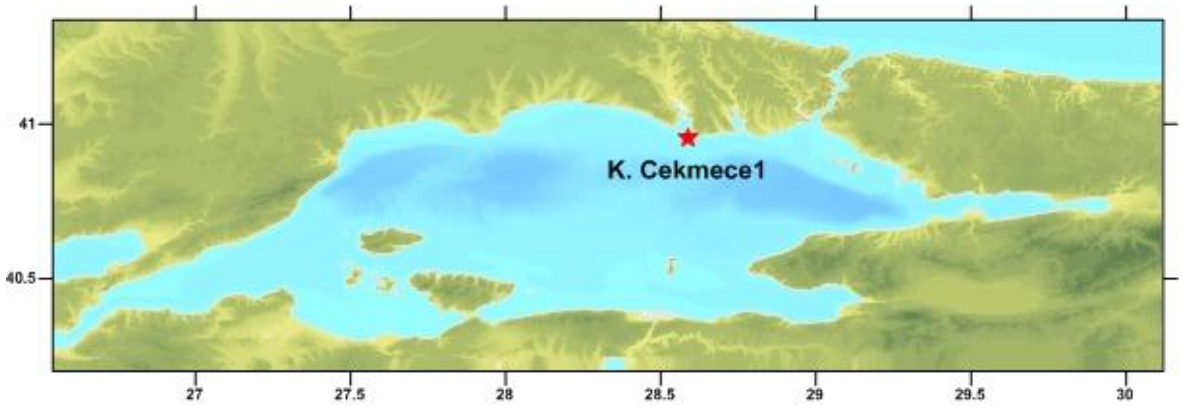

Figure 6.54. Landslide point at the study domain used in modeling of Küçükçekmece1.

Figure 6.55, 6.56 and 6.57 show relation between submarine landslide velocity and time. For 5 m, 10 m and 50 m sediment thicknesses, sl-06 gauge point is at the center of the landslide. It is seen from Figure 6.55 that landslide velocity for 5 m sediment thickness is approximately 4.75 m/sec. It is seen from Figure 6.56 and 6.57 that velocity increases for 10 m and 50 m sediment thicknesses. For 10 m, the landslide velocity is 7 m/sec at the sl-06 gauge point. In addition, it is 23 m/sec for 50 m sediment thickness.

Along the coast of the Sea of Marmara, 30 gauge points are selected which are indicated in Figure 6.58 and the coordinates and depths of these points are given in Table 6.9. Moreover, 15 gauge points are selected which are perpendicular direction to landslide axis and around the landslide area.

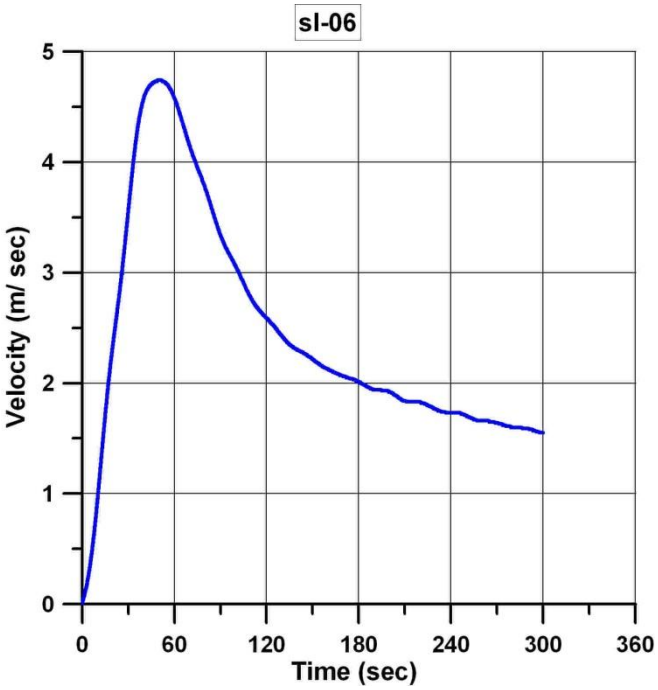

Figure 6.55. Time change of submarine landslide velocity at the center of the slide area (sl-06) due to slide of 5 m sediment thickness (Küçükçekmece1).

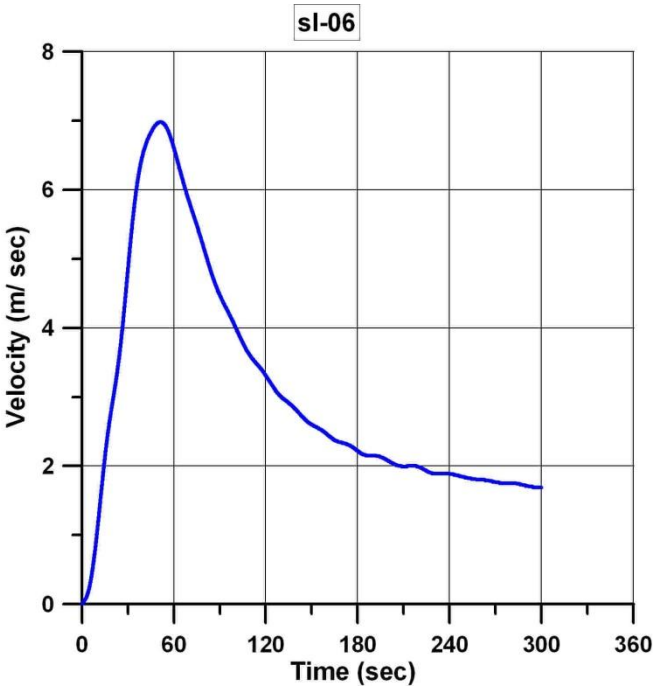

Figure 6.56. Time change of submarine landslide velocity at the center of the slide area (sl-06) due to slide of 10 m sediment thickness (Küçükçekmece1).

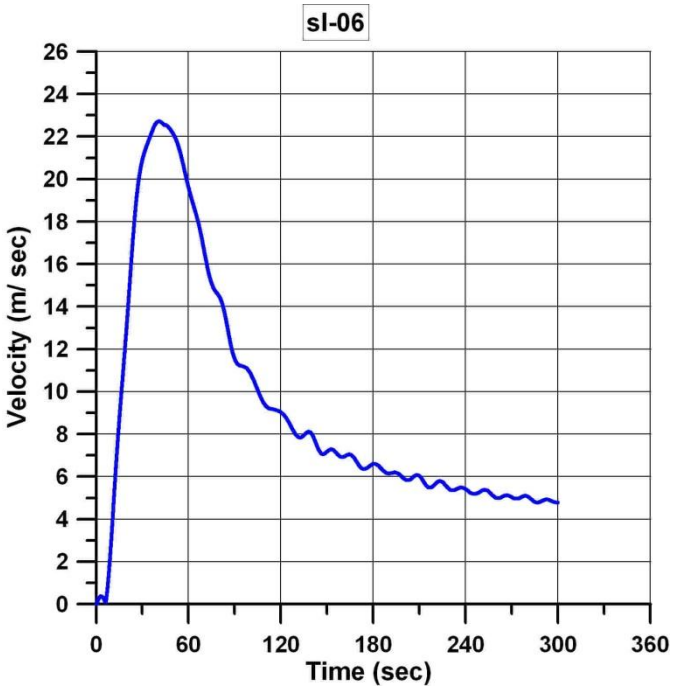

Figure 6.57. Time change of submarine landslide velocity at the center of the slide area (sl-06) due to slide of 50 m sediment thickness (Küçükçekmece1).

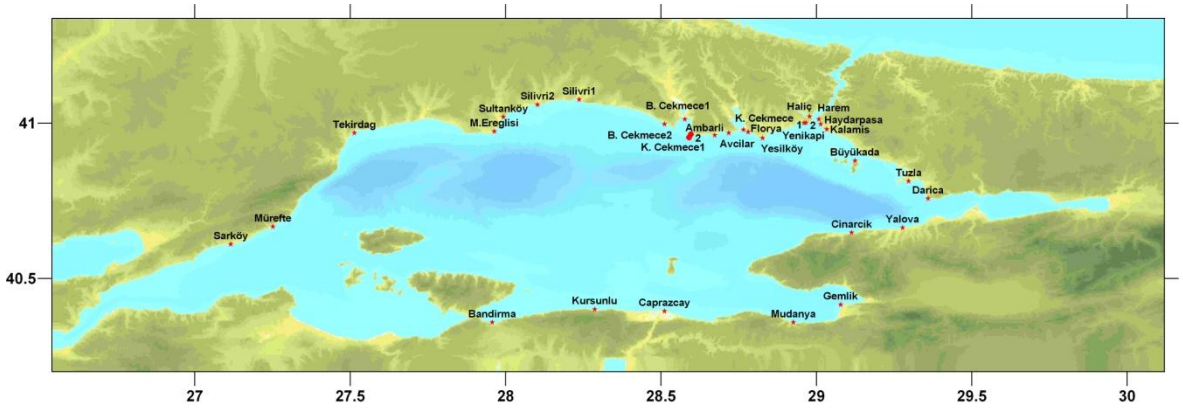

Figure 6.58. The locations of the selected gauge points for the simulations of Küçükçekmece1 submarine landslide.

The water surface elevation for 5 m, 10 m and 50 m sediment thicknesses are indicated in Figure 6.59, 6.60 and 6.61. As it can be seen from the Figure 6.59, for 5 m sediment thicknesses, the water surface elevation is 0.3 m at Büyükçekmece2 (B. Çekmece2) gauge point. As it can be seen from the Figure 6.60 and Figure 6.61, when the sediment thicknesses are 10 m and 50 m, the water surface elevation increases. Thus, the water surface elevations are 0.6 m and 2.4 m at B. Çekmece2 gauge point, respectively. In addition, the most affected areas by the landslide are the south and north coast along the location the slide happens.

According to the simulation results, it can be seen that the tsunami wave reaches Ambarlı in 5 minutes, Büyükçekmece in 6 minutes and Florya in 7 minutes. The depths, arrival times of first waves, maximum and minimum water elevation for the 34 selected gauge points are summarized in Table 6.10 for 5 m,10 m and 50 m sediment thicknesses. According to the results, Büyükçekmece region is affected by the tsunami wave.

The distributions of maximum surface elevation that the waves result in the shoreline along north and south coasts in the Marmara Sea are indicated in Figure 6.62, 6.63 and 6.64. According to Figure 6.62, the maximum positive tsunami amplitudes are 0.95 m at the north shore and 0.23 m at the south coast for 5 m sediment thickness. For 10 m sediment thickness, positive tsunami amplitudes are approximately 1.6 m at the north and 0,6 m at the south coast in Figure 6.63. For 50 m sediment thickness, the maximum positive amplitudes are 3.5 m at the north and 2 m at the south coast in Figure 6.64.

Table 6.9. The coordinates and depths of the selected gauge points for the simulations of Küçükçekmece1 submarine landslide.

Name	X Coordinate	Y Coordinate	Depth (m)
Şarköy	27.1156	40.6099	12.4
Mürefte	27.251	40.6669	7.8
Tekirdağ	27.5130	40.9681	8.5
M. Ereğlisi	27.9638	40.9734	8.3
Sultanköy	27.9926	41.0195	1.9
Silivri1	28.2364	41.0757	5.7
Silivri 2	28.1024	41.0594	3.2
B. Çekmece 1	28.5768	41.0127	9.9
B.Çekmece 2	28.5109	40.9966	9.2
Ambarlı	28.6730	40.9610	16.9
Avcılar	28.7176	40.9681	13.6
K. Çekmece	28.7657	40.9788	5.1
Florya	28.7799	40.9717	7
Yeşilköy	28.8263	40.9521	10
Yenikapı 1	28.9599	41.0002	8.2
Yenikapı 2	28.9662	41.0015	16.5
Haliç	28.9778	41.0216	29.9
Harem	29.008	41.0127	7.5
Haydarpaşa	29.0134	40.9966	9.1
Kalamış	29.0330	40.9806	4.8
Büyükada	29.1239	40.879	10.1
Tuzla	29.2967	40.8131	10.4
Darıca	29.3589	40.757	19.4
Yalova	29.2771	40.6634	1.7
Çınarcık	29.1132	40.6473	3.2
Gemlik	29.0775	40.4156	12.9
Mudanya	28.9261	40.3586	1.5
Bandırma	27.9567	40.3586	1.7
Kurşunlu	28.2865	40.4008	3.6
Çaprazçay	28.5110	40.3946	0.2
K1-sl-01	28.5907	40.9044	145.3
K1-sl-02	28.5907	40.9144	88.7
K1-sl-03	28.5907	40.9244	73.5
K1-sl-04	28.5907	40.9344	62.6
K1-sl-05	28.5907	40.9444	56.5
K1-sl-06 (Center of Landslide)	28.5907	40.9544	46.6
K1-sl-07	28.5907	40.9644	22.3
K1-sl-08	28.5907	40.9744	10.2
K1-sl-09	28.5907	40.9844	14.3
K1-sl-10	28.5907	40.9944	18.3
K1-sl-11	28.5951	40.9579	34
K1-sl-12	28.5791	40.9582	44.3

Table 6.9 (continued). The coordinates and depths of the selected gauge points for the simulations of Küçükçekmece1 submarine landslide.

K1-sl-13	28.5969	40.9489	51.4
K1-sl-14	28.5773	40.9476	55.1
K1-sl-15	28.6103	40.9528	42.5

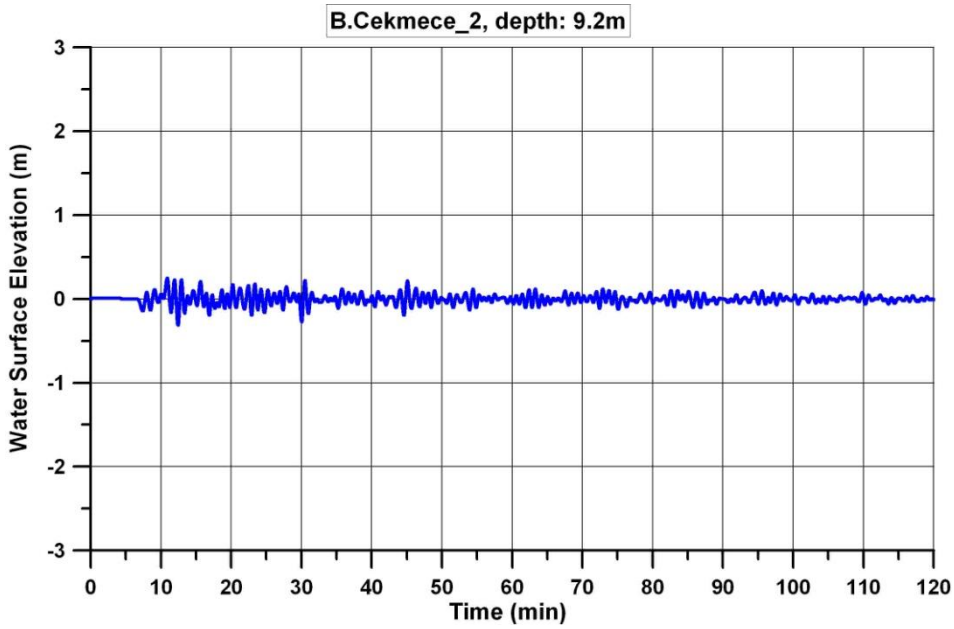

Figure 6.59. The time histories water surface fluctuations computed at selected gauge point (B. Çekmece_2) for the simulation due to landslide of 5 m submarine sediment thickness at offshore of Küçükçekmece1.

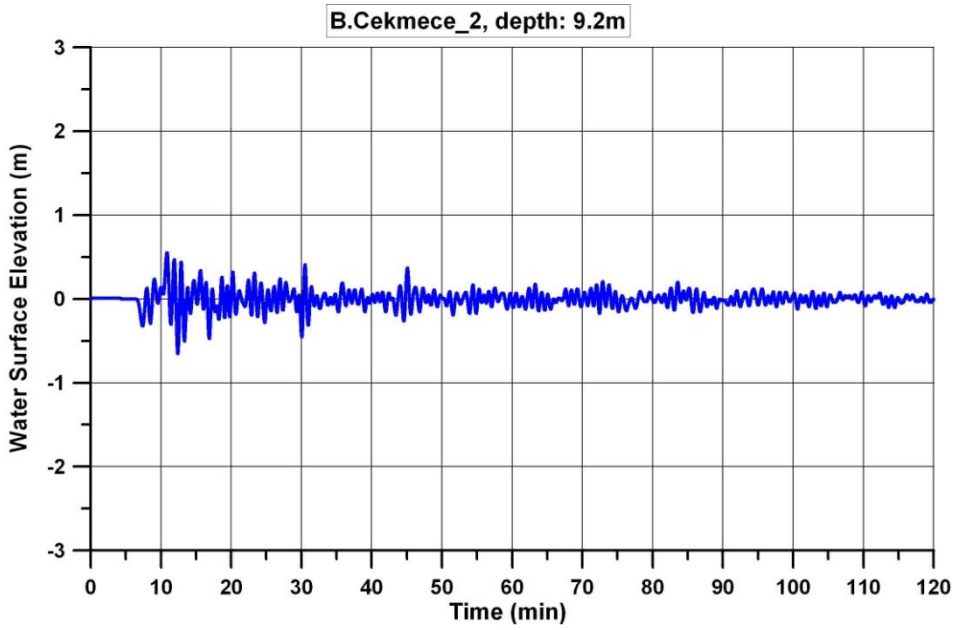

Figure 6.60. The time histories water surface fluctuations computed at selected gauge point (B. Çekmece_2) for the simulation due to landslide of 10 m submarine sediment thickness at offshore of Küçükçekmece1.

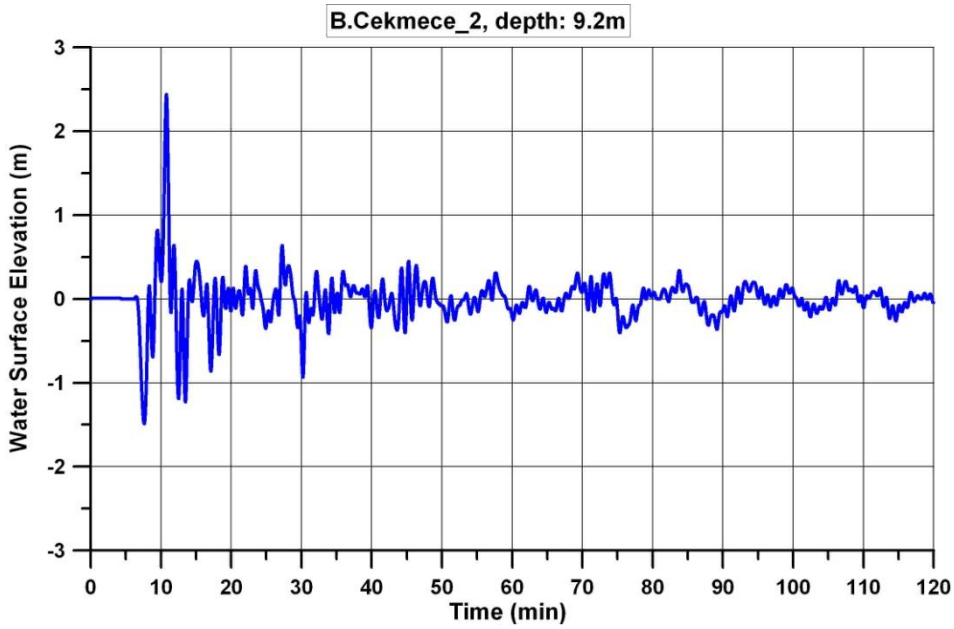

Figure 6.61. The time histories water surface fluctuations computed at selected gauge point (B. Çekmece_2) for the simulation due to landslide of 50 m submarine sediment thickness at offshore of Küçükçekmece1.

Table 6.10. The summary sheet of the simulation results of submarine landslide tsunami at Küçükçekmece1(Amplitude: Amp).

		5M			10M			50M		
Gauge Point	**Depth (m)**	**T_first (min)**	**Amp. (+) (m)**	**Amp. (-) (m)**	**T_first (min)**	**Amp. (+) (m)**	**Amp. (-) (m)**	**T_first (min)**	**Amp. (+) (m)**	**Amp. (-) (m)**
M. Ereğlisi	8.3	12	0.1	-0.1	12	0.1	-0.1	12	0.4	-0.4
Sultanköy	1.9	7	0.1	-0.1	7	0.1	-0.1	7	0.3	-0.6
Silivri 1	5.7	7	0.1	-0.1	7	0.1	-0.2	7	0.5	-0.5
Silivri 2	3.2	8	0.1	-1	8	0.2	-0.2	8	0.4	-0.8
B.Çekmece1	9.9	5	0.3	-0.3	5	0.4	-0.5	5	1	-1.4
B.Çekmece2	9.2	6	0.3	-0.3	6	0.6	-0.7	6	2.4	-1.5
Ambarlı	16.9	5	0.2	-0.3	5	0.4	-0.6	5	1.5	-1.3
Avcılar	13.6	7	0.4	-0.4	7	0.7	-0.7	7	2	-1,6
K. Çekmece	5.1	6	0.2	-0.1	6	0.3	-0.2	6	1	-1.1
Florya	7	6	0.2	-0.2	6	0.4	-0.5	6	1.3	-1.2
Yeşilköy	10	5	0.2	-0.1	5	0.2	-0.2	5	0.5	-0.7
Yenikapı 1	8.2	6	0.1	-0.1	6	0.1	-0.1	6	0.3	-0.3
Yenikapı2	16.5	6	0.1	-0.1	6	0.1	-0.1	6	0.2	-0.2
Harem	7.5	5	0.1	-0.1	5	0.1	-0.1	5	0.2	-0.2
Haydarpaşa	9	5	0.1	-0.1	5	0.1	-0.1	5	0.3	-0.2
Kalamış	4.8	11	0.1	-0.1	11	0.1	-0.1	11	0.5	-0.6
Büyükada	10.1	6	0.04	-0.1	6	0.1	-0.1	6	0.2	-0.2
Mudanya	1.5	13	0.1	-0.04	14	0.1	-0.1	13	0.3	-0.3
Kurşunlu	3.6	5	0.1	0.1	5	0.1	-0.1	5	0.4	-0.7
K1-sl-01	145.3	5	0.1	-0.1	5	0.1	-0.1	5	0.2	-0.2
K1-sl-02	88.7	5	0.1	-0.1	5	0.1	-0.2	5	0.4	-0.3
K1-sl-03	73.5	5	0.1	-0.1	5	0.2	-0.1	5	0.8	-0.4
K1-sl-04	62.6	5	0.1	-0.1	5	0.2	-0.2	5	0.7	-0.4
K1-sl-05	56.5	5	0.2	-0.1	5	0.2	-0.2	5	0.8	-0.5
K1-sl-06	46.6	5	0.2	-0.3	5	0.5	-0.5	5	1.4	-1.3
K1-sl-07	22.3	5	0.3	-0.3	5	0.6	-0.6	5	0.9	-0.5
K1-sl-08	10.2	5	0.2	-0.2	5	0.4	-0.3	5	0.8	-0.6
K1-sl-09	14.3	5	0.2	-0.2	5	0.4	-0.4	5	1	-0.6
K1-sl-10	18.3	5	0.2	-0.2	5	0.4	-0.3	5	1	-0.5
K1-sl-11	34	5	0.3	-0.4	5	0.7	-0.8	5	1.7	-1
K1-sl-12	44.3	5	0.2	-0.1	5	0.3	-0.3	5	0.8	-0.5
K1-sl-13	51.4	5	0.1	-0.1	5	0.2	-0.2	5	1.1	-0.6
K1-sl-14	55.1	5	0.1	-0.1	5	0.3	-0.2	5	1.1	-0.8
K1-sl-15	42.5	5	0.2	-0.1	5	0.3	-0.1	5	1.3	-0.5

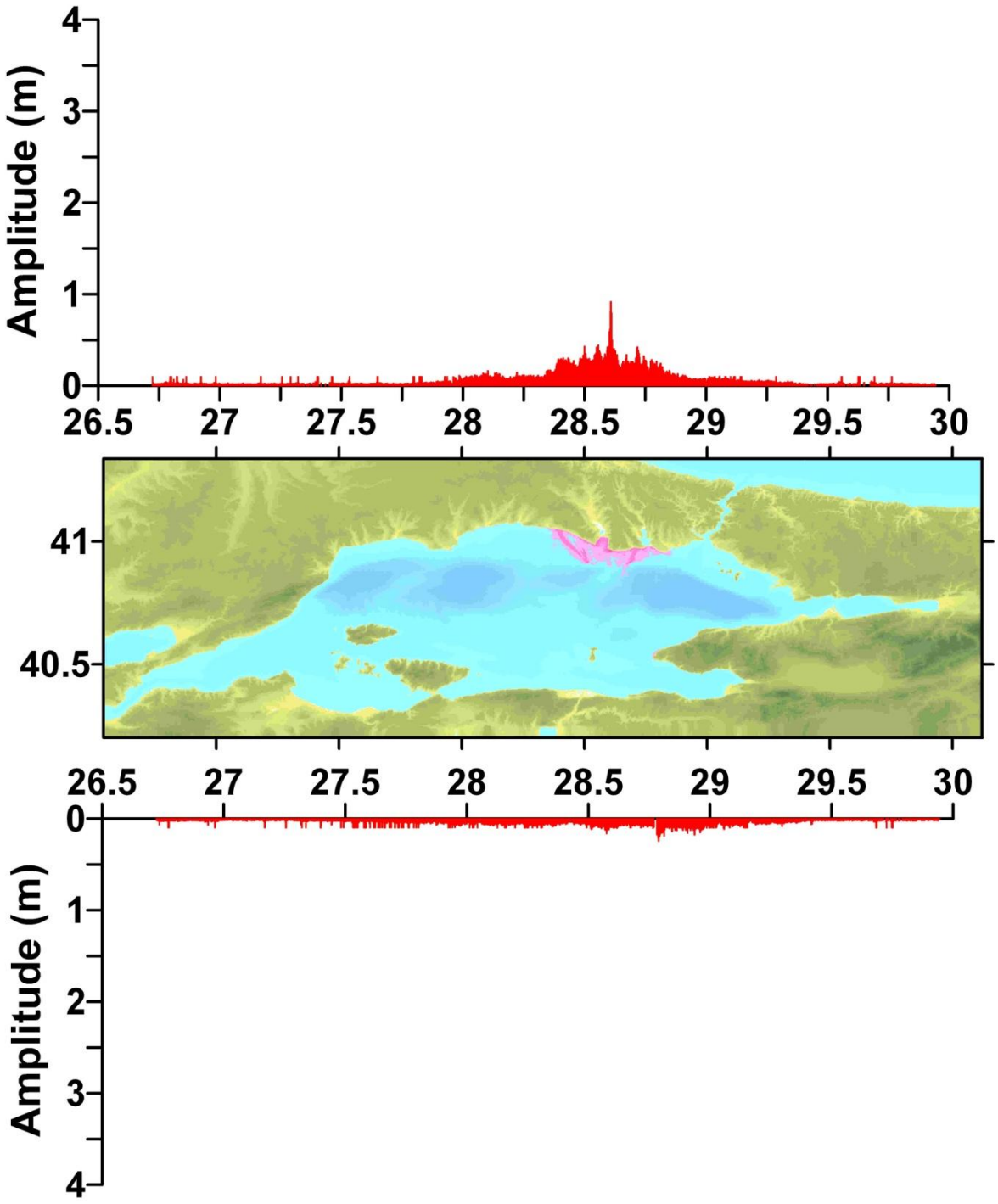

Figure 6.62. Maximum water level distributions (m) along North and South coasts of Marmara computed by the 120 minutes simulations due to the 5 m thickness of submarine landslide at Küçükçekmece1.

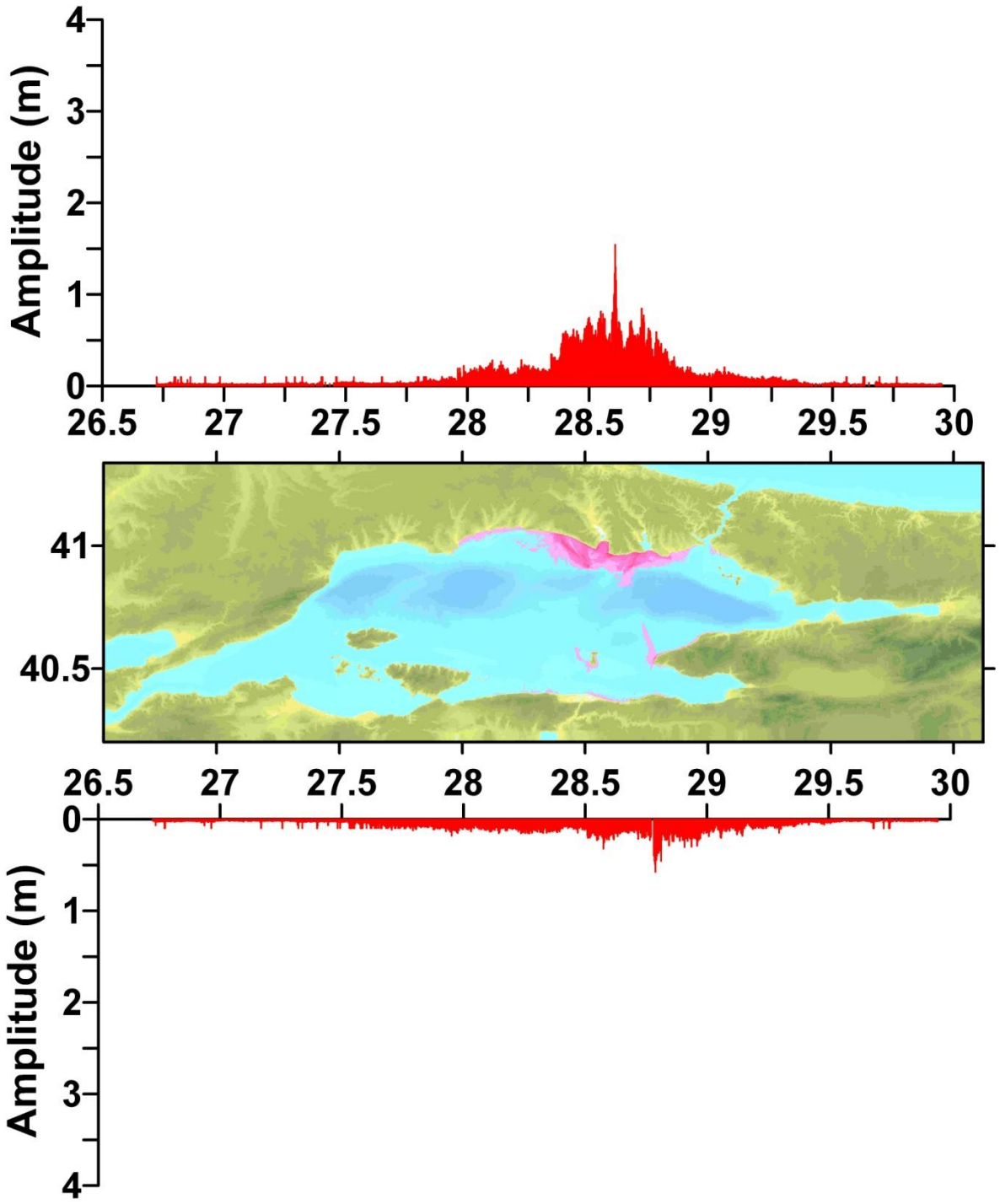

Figure 6.63. Maximum water level distributions (m) along North and South coasts of Marmara computed by the 120 minutes simulations due to the 10 m thickness of submarine landslide at Küçükçekmece1.

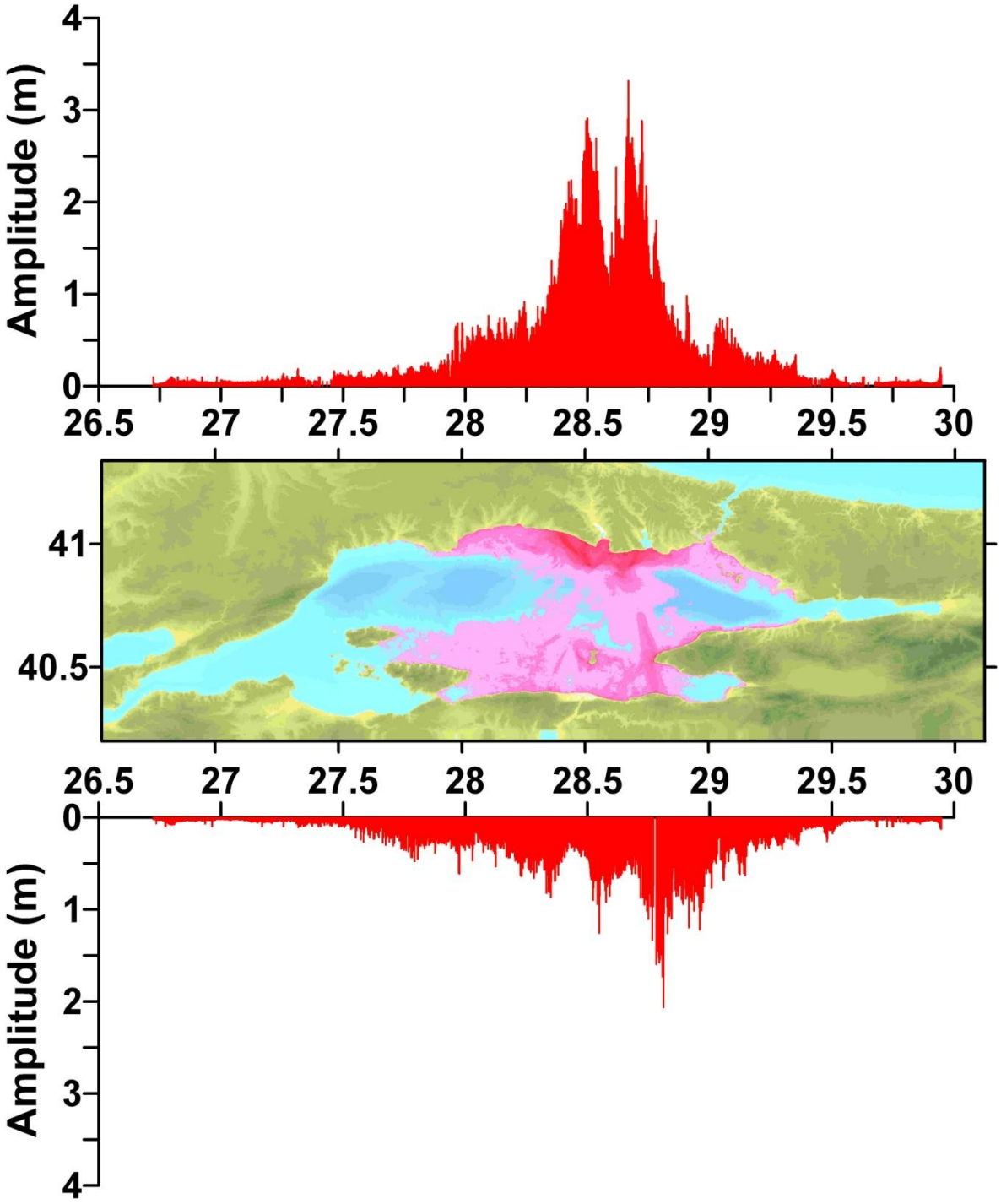

Figure 6.64. Maximum water level distributions (m) along North and South coasts of Marmara computed by the 120 minutes simulations due to the 50 m thickness of submarine landslide at Küçükçekmece1.

6.6. Tsunami Due to Submarine Landslide Occurrence at Offshore of Küçükçekmece2

In the Küçükçekmece2 case, an underwater landslide scenario is assumed to happen at offshore Küçükçekmece around the 28.59ºE and 40.96ºN coordinates. The study domain used in modeling of Küçükçekmece2 submarine landslide is indicated in Figure 6.65.

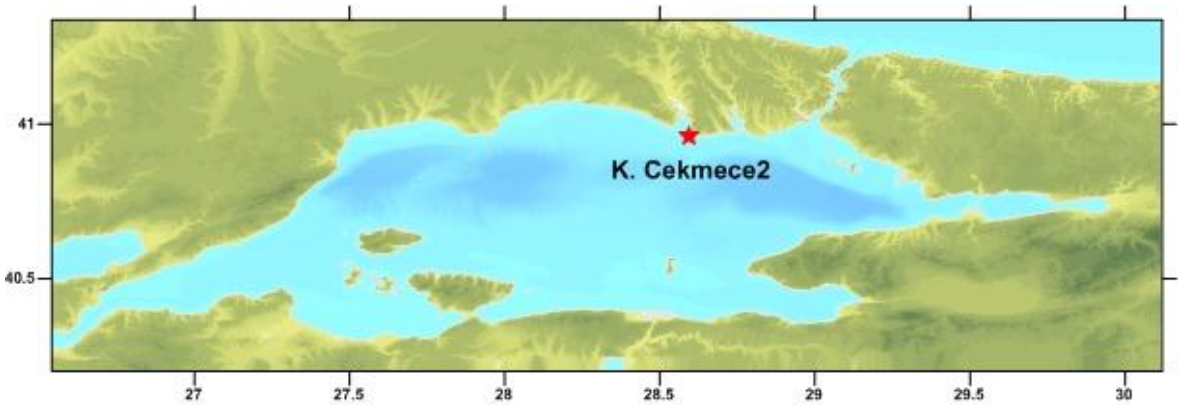

Figure 6.65. Landslide point at the study domain used in modeling of Küçükçekmece2.

Figure 6.66, 6.67 and 6.68 represent relation between submarine landslide velocity and time. sl-04 gauge point is at the center of the landslide. It is seen from Figure 6.66 that landslide velocity is approximately 5.75 m/sec for 5 m sediment thickness at the center of the landslide. As it can be seen from the Figure 6.67, it is 8 m/sec for 10 m thickness. In Figure 6.68, landslide velocity is 28.50 m/sec for 50 m sediment thickness. If the sediment thickness increases, the landslide velocity will increase.

Along the coast of the Sea of Marmara, 30 gauge points are selected which are indicated in Figure 6.69 and the coordinates and depths of these points are given in Table 6.11. In addition, 9 gauge points are selected which are perpendicular direction to landslide axis and around the landslide area.

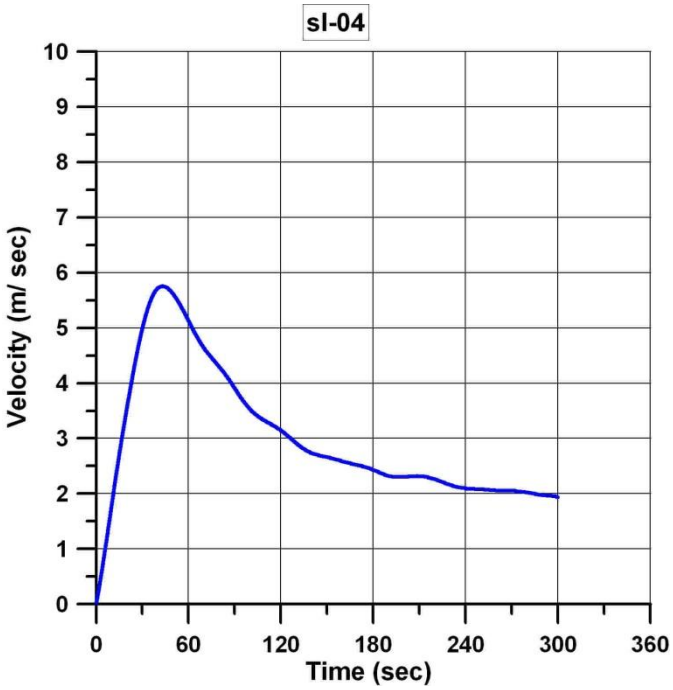

Figure 6.66. Time change of submarine landslide velocity at the center of the slide area (sl-04) due to slide of 5 m sediment thickness (Küçükçekmece2).

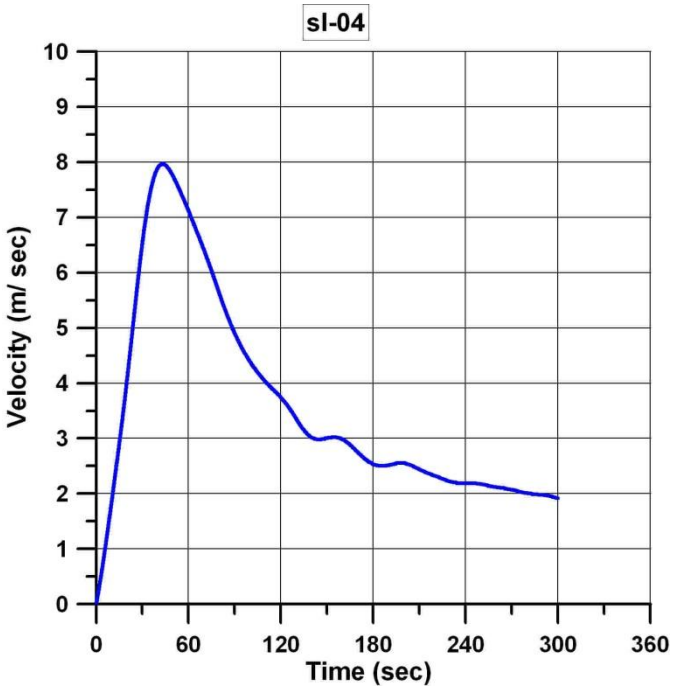

Figure 6.67. Time change of submarine landslide velocity at the center of the slide area (sl-04) due to slide of 10 m sediment thickness (Küçükçekmece2).

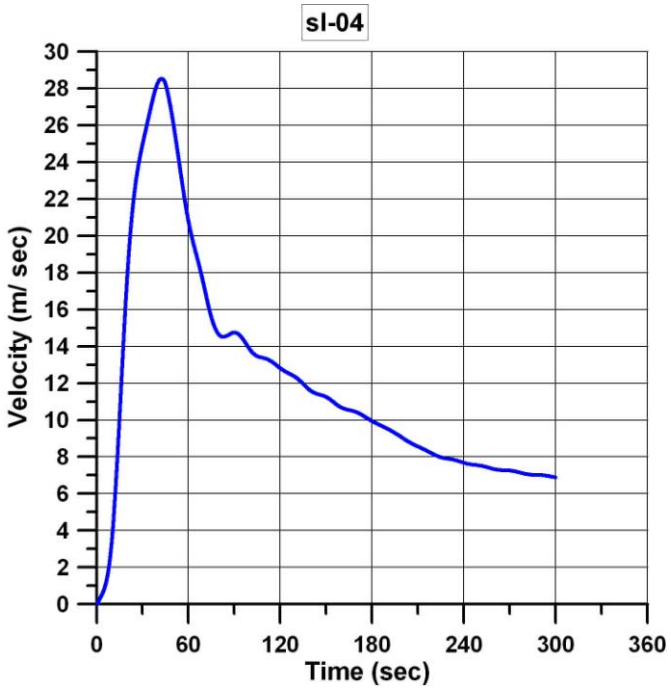

Figure 6.68. Time change of submarine landslide velocity at the center of the slide area (sl-04) due to slide of 50 m sediment thickness (Küçükçekmece2).

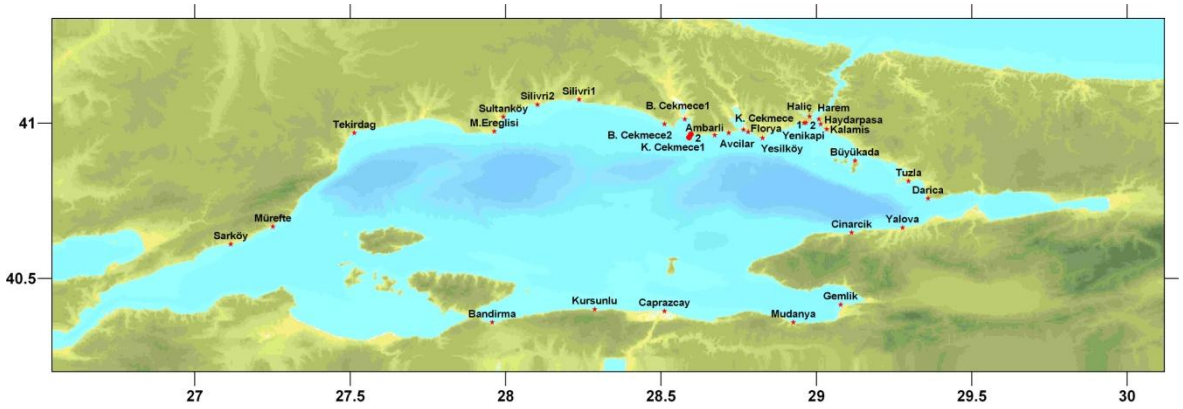

Figure 6.69. The locations of the selected gauge points for the simulations of Küçükçekmece2 submarine landslide.

The water surface elevation for 5 m, 10 m and 50 m sediment thicknesses are showed in Figure 6.70, 6.71 and 6.72. As it can be seen from the Figure 6.70, for 5 m sediment thickness, the water surface elevation is 0.2 m at Büyükçekmece. When the sediment thicknesses are 10 m and 50 m, the water surface elevation increases. Thus, the water surface elevations are 0.5 m and 2.3 m at Büyükçekmece, respectively.

According to the simulation results, it can be seen that the tsunami wave reaches Ambarlı in 5 minutes, Büyükçekmece and Avcılar in 7 minutes. Büyükçekmece and Ambarlı are in danger. The depths, arrival times of first waves, maximum and minimum water elevation for the 24 selected gauge points are summarized in Table 6.9 for 5 m, 10 m and 50 m sediment thicknesses.

The distributions of maximum surface elevation that the waves result in the shoreline along north and south coasts in the Marmara Sea are displayed in Figure 6.73, 6.74 and 6.75. According to Figure 6.76, the maximum positive tsunami amplitudes are approximately 0.75 m at the north shore and 0.15 m at the south coast for 5 m sediment thickness. For 10 m sediment thickness, positive tsunami amplitudes are 1.35 m at the north and 0.6 m at the south coast. For 50 m sediment thickness, they are 3.75 m at the north and 1.8 m at the south coast.

Table 6.11. The coordinates and depths of the selected gauge points for the simulations of Küçükçekmece2 submarine landslide.

Name	X Coordinate	Y Coordinate	Depth (m)
Şarköy	27.1156	40.6099	12.4
Mürefte	27.2510	40.6669	7.8
Tekirdağ	27.5130	40.9681	8.5
M. Ereğlisi	27.9638	40.9734	8.3
Sultanköy	27.9926	41.0195	1.9
Silivri1	28.2364	41.0757	5.7
Silivri2	28.1024	41.0594	3.2
B. Çekmece 1	28.5768	41.0127	9.9
B.Çekmece 2	28.5109	40.9966	9.2
Ambarlı	28.6730	40.9610	16.9
Avcılar	28.7176	40.9681	13.6
K. Çekmece	28.7657	40.9788	5.1
Florya	28.7799	40.9717	7
Yeşilköy	28.8263	40.9521	10
Yenikapı 1	28.9599	41.0002	8.2
Yenikapı 2	28.9662	41.0015	16.5
Haliç	28.9778	41.0216	29.9
Harem	29.0080	41.0127	7.5
Haydarpaşa	29.0134	40.9966	9.1
Kalamış	29.0330	40.9806	4.8
Büyükada	29.1239	40.8790	10.1
Tuzla	29.2967	40.8131	10.4
Darıca	29.3589	40.7570	19.4
Yalova	29.2771	40.6634	1.7
Çınarcık	29.1132	40.6473	3.2
Gemlik	29.0775	40.4156	12.9
Mudanya	28.9261	40.3586	1.5
Bandırma	27.9567	40.3586	1.7
Kurşunlu	28.2865	40.4008	3.6
Çaprazçay	28.5110	40.3946	0.2
K2-sl-01	28.5964	40.9335	63.8
K2-sl-02	28.5964	40.9435	56.1
K2-sl-03	28.5964	40.9535	46
K2-sl-04 (Center of Landslide)	28.5964	40.9635	16.7
K2-sl-05	28.5923	40.9651	19.2
K2-sl-06	28.5904	40.9614	30.3
K2-sl-07	28.6057	40.9595	18.3
K2-sl-08	28.5969	40.960	26.9
K2-sl-09	28.5899	40.9582	39.6

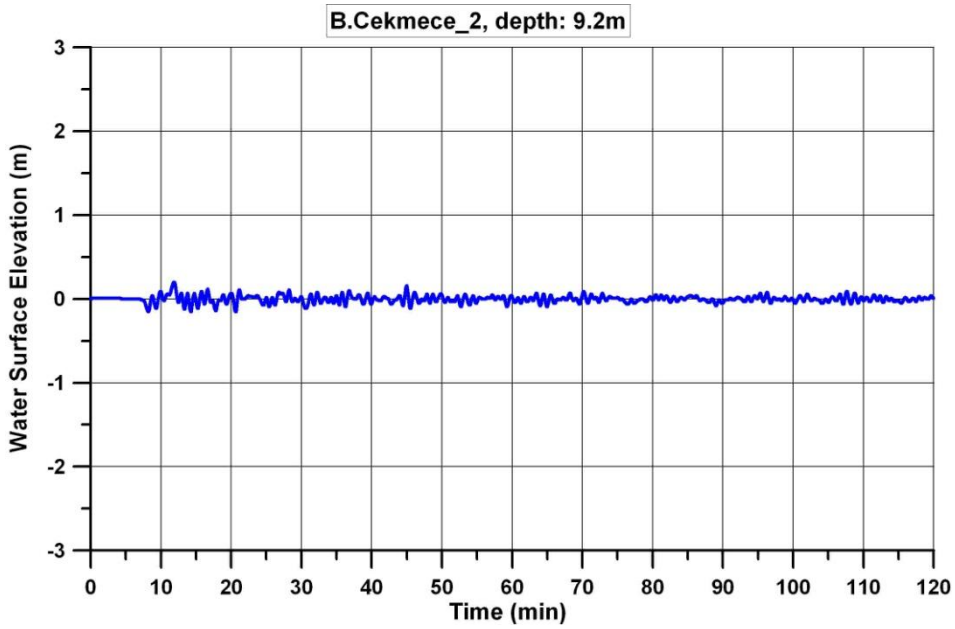

Figure 6.70. The time histories water surface fluctuations computed at selected gauge point (B. Çekmece_2) for the simulation due to landslide of 5 m submarine sediment thickness at offshore of Küçükçekmece2.

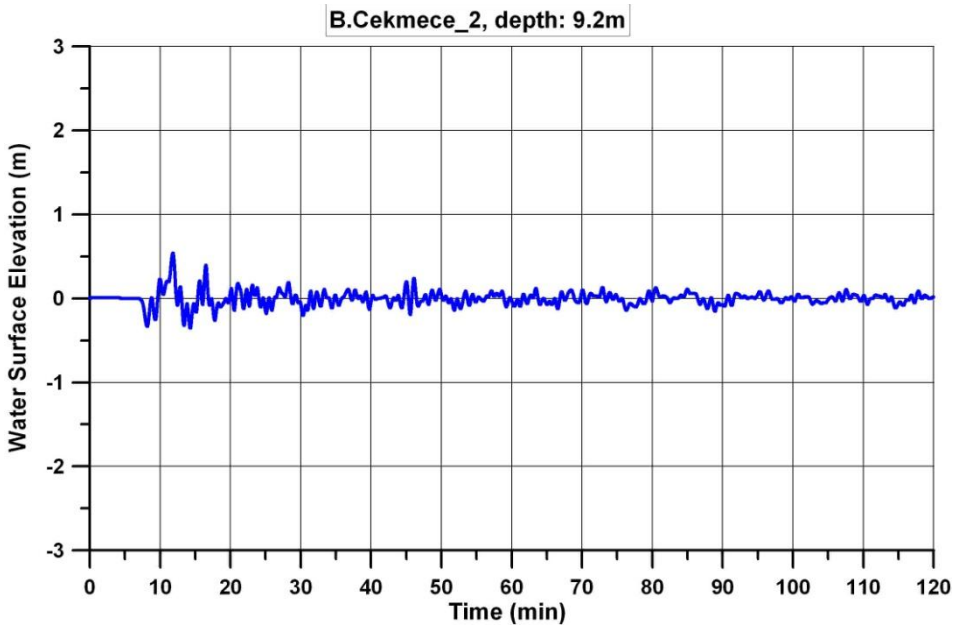

Figure 6.71. The time histories water surface fluctuations computed at selected gauge point (B. Çekmece_2) for the simulation due to landslide of 10 m submarine sediment thickness at offshore of Küçükçekmece2.

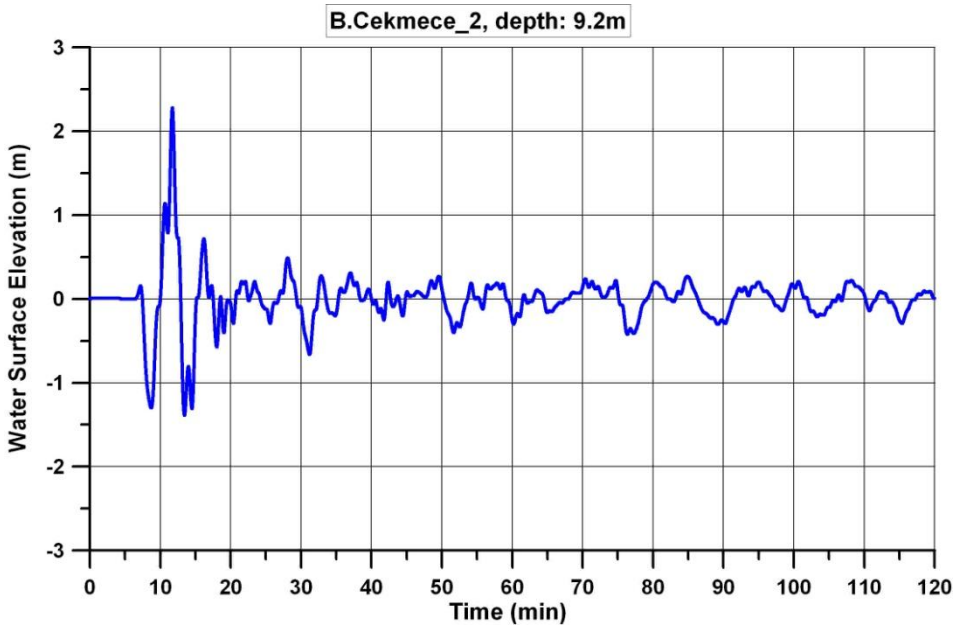

Figure 6.72. The time histories water surface fluctuations computed at selected gauge Point (B. Çekmece_2) for the simulation due to landslide of 50 m submarine sediment thickness at offshore of Küçükçekmece2.

Table 6.12. The summary sheet of the simulation results of submarine landslide tsunami at Küçükçekmece2 (Amlitude: Amp).

		5M			10M			50M		
Gauge Point	**Depth (m)**	**T_first (min)**	**Amp. (+) (m)**	**Amp. (-) (m)**	**T_first (min)**	**Amp. (+) (m)**	**Amp. (-) (m)**	**T_first (min)**	**Amp. (+) (m)**	**Amp. (-) (m)**
M.Ereğlisi	8.3	12	0.1	-0.1	12	0.1	-0.1	12	0.5	-0.6
Sultanköy	1.9	7	0.1	-0.1	7	0.1	-0.2	7	0.6	-0.7
Silivri 1	5.7	7	0.1	-0.1	7	0.2	-0.2	7	0.6	-0.6
Silivri 2	3.2	8	0.1	-0.1	8	0.2	-0.2	8	0.7	-1.2
B.Çekmece1	9.9	5	0.3	-0.3	5	0.4	-0.5	5	1.3	-1
B.Çekmece2	9.2	7	0.2	-0.2	7	0.5	-0.4	6	2.3	-1.4
Ambarlı	16.9	5	0.1	-0.2	5	0.4	-0.4	5	1.7	-1
Avcılar	13.6	7	0.2	-0.2	7	0.3	-0.3	7	1.3	-1.4
K. Çekmece	5.1	6	0.1	-0.1	6	0.2	-0.3	6	0.8	-1.2
Florya	7	6	0.2	-0.1	6	0.3	-0.3	6	0.8	-1
Yeşilköy	10	5	0.1	-0.1	5	0.2	-0.1	5	0.3	-0.4
Yenikapı 1	8.2	6	0.1	-0.04	6	0.1	-0.1	6	0.2	-0.2
Kalamış	4.8	11	0.1	-0.1	11	0.1	-0.1	11	0.5	-0.5
Mudanya	1.5	13	0.1	-0.04	13	0.1	-0.1	13	0.3	-0.3
Kurşunlu	3.6	5	0.1	-0.1	5	0.1	-0.1	5	0.6	-0.7
K2-sl-01	63.8	5	0.1	-0.1	5	0.2	-0.2	5	0.5	-0.2
K2-sl-02	56.1	5	0.1	-0.1	5	0.2	-0.1	5	0.5	-0.3
K2-sl-03	46	5	0.2	-0.1	5	0.2	-0.2	5	0.5	-0.4
K2-sl-04	16.7	5	0.3	-0.3	5	0.3	-0.2	5	0.5	-0.6
K2-sl-05	19.2	5	0.3	-0.2	5	0.2	-0.2	5	0.4	-0.6
K2-sl-06	30.3	5	0.2	-0.1	5	0.2	-0.2	5	0.4	-0.5
K2-sl-07	18.3	5	0.2	-0.2	5	0.4	-0.4	5	0.7	-0.4
K2-sl-08	26.9	5	0.2	-0.3	5	0.2	-0.2	5	0.4	-0.5
K2-sl-09	39.6	5	0.2	-0.2	5	0.2	-0.2	5	0.4	-0.5

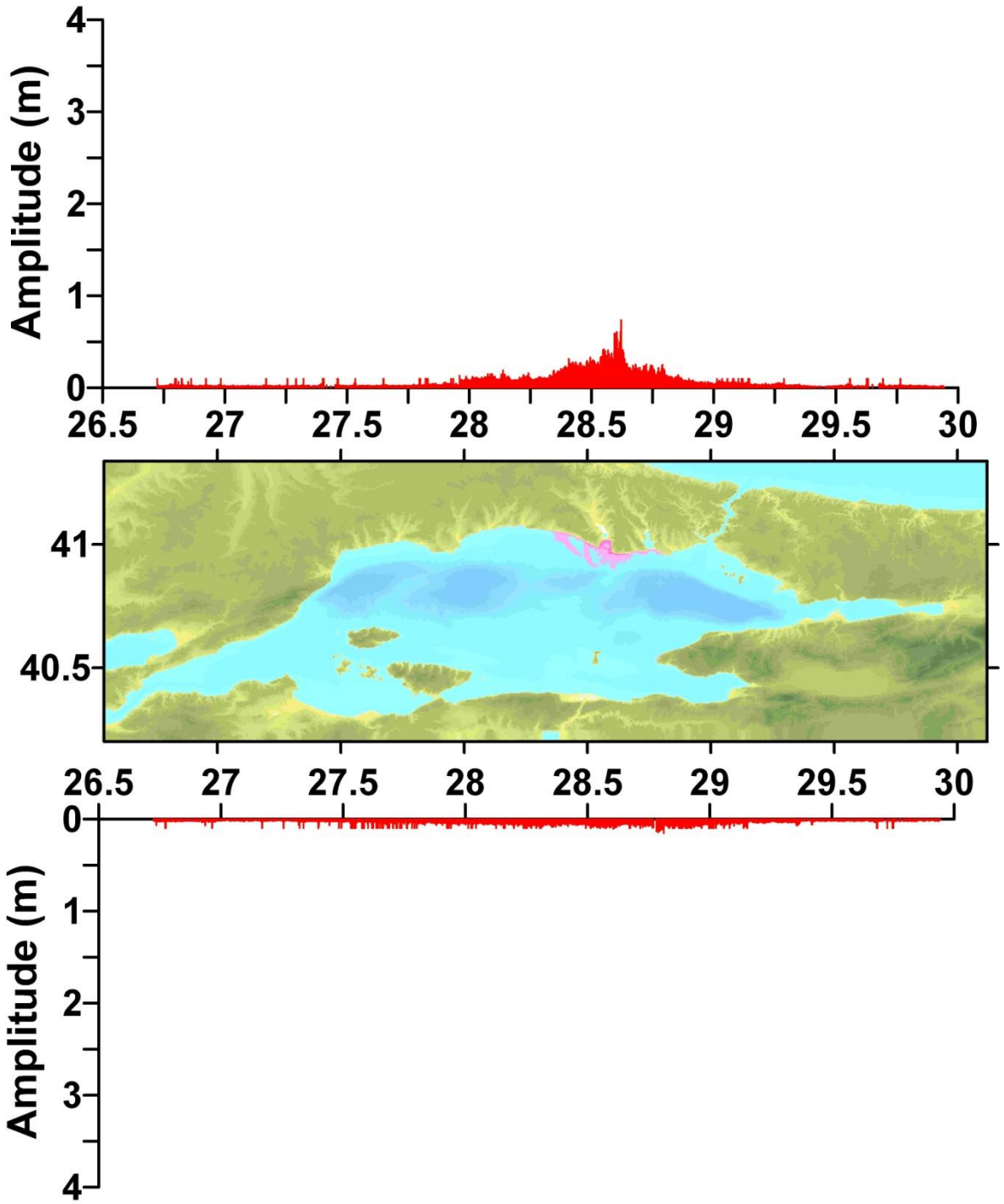

Figure 6.73. Maximum water level distributions (m) along North and South coasts of Marmara computed by the 120 minutes simulations due to the 5 m thickness of submarine landslide at Küçükçekmece2.

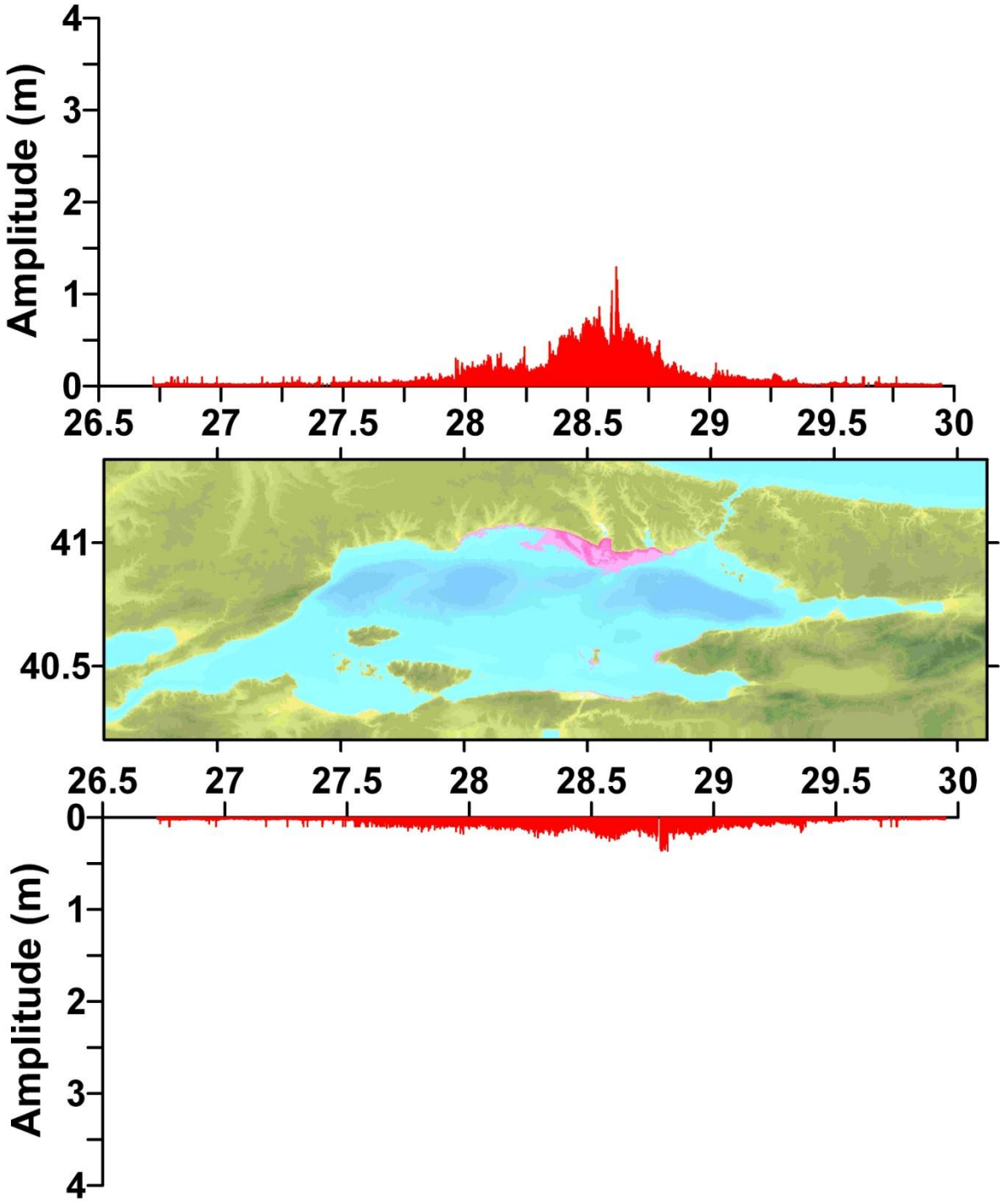

Figure 6.74. Maximum water level distributions (m) along North and South coasts of Marmara computed by the 120 minutes simulations due to the 10 m thickness of submarine landslide at Küçükçekmece2.

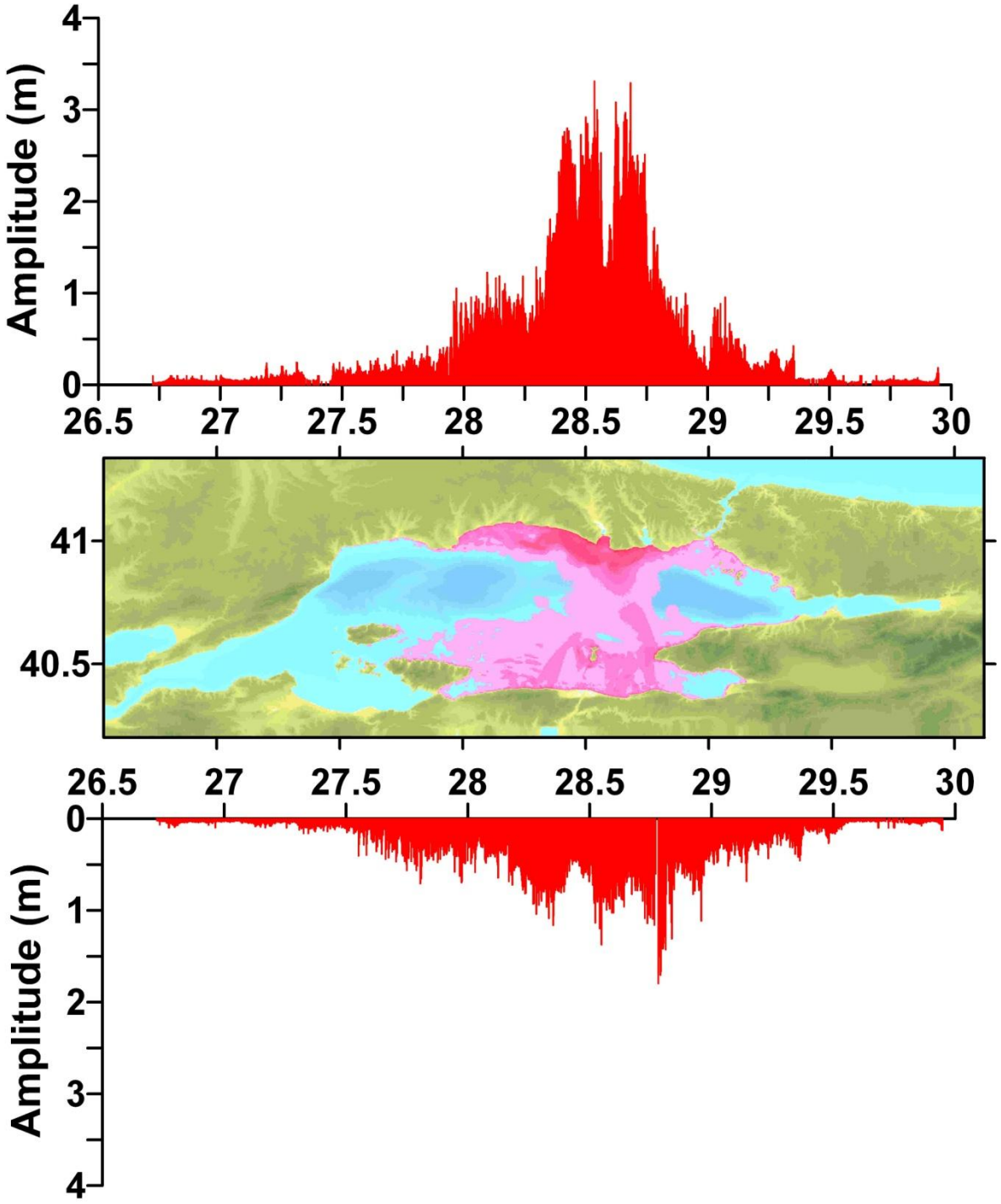

Figure 6.75. Maximum water level distributions (m) along North and South coasts of Marmara computed by the 120 minutes simulations due to the 50 m thickness of submarine landslide at Küçükçekmece2.

7. CONCLUSIONS

In this thesis, tsunamis generated by submarine landslides in the Marmara Sea are investigated. The main purpose of this study is to analyze effects of the submarine landslides generated tsunamis.

Some tsunami and landslide simulations have been generated at different points. Based on these studies, and together with additional studies, we performed landslide modelings at some points of the Marmara Sea. In this study, we used Marmara-150m bathymetry data. Ganos, Küçükçekmece, CN1 (central portion in Central Basin) and Yenikapı points in the Marmara Sea are selected as case studies. Sediment thicknesses are set as 10 m-50 m for Ganos, whereas for CN1 and Küçükçekmece, they are set as 5 m, 10 m and 50 m. Sediment thicknesses are 5 m, 10 m, 30 m, 60 m and 120 m in Yenikapı. It should be noted here that slide material is considered as mud in this study. It should also be noted that the landslide thicknesses selected in this study are determined by using the information from different studies on submarine landslides (Yalçıner *et al.*, 2005). According to these studies, the thickness of landslide sediment are in the range up to 100 m. Therefore, the thickness range in this study is used in the similar range.

TWO-LAYER model is used to model the generation of the tsunamigenic landslides and the model is applied to possible landslide points. With the help of TWO-LAYER code, velocity of the landslide is investigated. The Figures show us velocity is reduced from the landslide center to the boundary of the sliding (rupture) surface. Furhermore, the velocity of the landslide increases while the sediment thickness is increased. In addition, it is observed that there is a linear relation between thickness and velocity in Yenikapı case. The propagation and coastal amplification of the landslide generated tsunamis in the Sea of Marmara are studied using the tsunami simulation and visualization code NAMI-DANCE. During 120 minutes simulations, we investigated the maximum water elevations in the study domains, the time histories at selected gauge points, arrival times of the first and maximum waves. In addition, they are interpreted via the Figures.

In Yenikapı case, according to the simulation results, the tsunami waves for Yenikapı reaches Yeşilköy, Ambarlı, Avcılar and Florya in 5 minutes.In addition, The

maximum water elevations are 2.95 m for northern coast of Marmara Sea and 2.75 m for southern coasts. In Ganos points, according to the simulation results, it is observed that the tsunami waves reaches Aksaz and Hoşköy in 5 minutes, Mürefte and Eriklice in 6 minutes, Tekirdağ in 7 minutes, and Gelibolu in 5 and 12 minutes. For Ganos1 point, the maximum water elevations are 7 m for northern coast of Marmara Sea and 4 m for southern coasts. They are 3.9 m and 3.4 m at the Ganos2 point, respectively. For CN1 point, it is observed that the tsunami waves reaches Kurşunlu in 5 minutes, Sultanköy and Marmara Ereğlisi in 6 minutes, Büyükçekmece in 7 minutes, and Silivri in 8 minutes. The maximum water elevation is 5.1 m in the northern coast of Marmara Sea. For southern coast of Marmara, it is 4 m. In Küçükçekmece1 point, The simulated arrival time of tsunami waves are 5 minutes to Ambarlı, 6 minutes to Florya and B. Çekmece_2 and 7 minutes to Avcılar. The maximum water elevations are 3,5 m and 2 m in the northern coast and in the southern coast of Marmara Sea, respectively. It is seen that the tsunami wave reaches Ambarlı in 5 minutes and, Avcılar and B. Çekmece_2 in 7 minutes. The maximum water elevations are 3.75 m for northern coast of Marmara Sea and 1.8 m for southern coasts. Consequently, the effects of the tsunami waves may change depending on the velocity of the slide, the thickness of the sediment and source. Tsunami generated submarine landslides may pose a threat for the Marmara coasts. When the maximum amplitudes values of the tsunami waves are more than 2 m, very intense currents and extensive damage to property can take place at coasts. If experience in Japan (Shuto and Imamura, 2000) is an important indicator, then when the runup values exceed 2.5 m, there can be loss of life and general loss of property (Yalçıner *et al.,* 2002).

Moreover, during the excavations for the Marmaray Project at Yenikapı, The Port of Theodosius was explored. 34 shipwrecks were found in the area (Perinçek D., 2010). The sedimentary sequence discovered at archaeological excavations in Theodosius Harbour includes the records of sea level (Algan *et al.,* 2009). In addition, in the marine part of the sedimentary sequence, a high-energy deposits has interpreted as being of tsunami (Bony *et al.,* 2011).

Numerous earthquakes and tsunami have occurred in the Marmara throughout history. The coasts of the Marmara Sea have been affected by 30 tsunami events during the past 2000 years. In addition, a numerical model of tsunami propagation in the Marmara

estimates approximately maximum nearshore tsunami heights of 6 m (Yalçıner *et al.*, 2002 and Bony *et al.*, 2011) for seismic tsunami sources.

There are uncertainties in occurrence of submarine landslides and associated tsunamis in the Sea of Marmara. The landslide traces detected by marine surveys at some locations warn that there were the potential of landslide generated tsunamis in the Marmara Sea. Therefore, the evaluation of submarine landslide tsunamis and estimation of their possible effects in the Sea of Marmara will help to provide useful information to the operational systems of tsunami warning system in Turkey and to disaster managers and decision makers. This aim could be achieved by tsunami numerical modeling. This study has been performed to develop necessary data, information and knowledge about the possible landslide tsunamis for the Tsunami Warning System in Boğaziçi University Kandilli Observatory and Earthquake Research Institute.

REFERENCES

Algan, O., M. N. Özdoğan, I. Yılmaz, E. Sarı, E. K. Elmas, D. Ongan, O. B.,Yeşiladalı, Y. Yılmaz and I. Karamut, 2009, ‘‘A Short Note on the Geo-archeological Significance of the Ancient Theodosius Harbour (İstanbul, Turkey)’’, *Quaternary Research,* 72, 457-461.

Altınok, Y. and S. Ersoy, 2000, ‘‘Tsunamis Observed on and Near the Turkish Coast’’, *Nat. Hazards,* 21, 185–205.

Alpar, B. and C. Yaltırak, 2000, ‘‘Tectonic Setting of the Eastern Marmara Sea’’, *Proceedings of the NATO Advanced Research Seminar, Integration of Earth Sciences Research on the 1999 Turkish and Greek Earthquakes,* İstanbul, Turkey, 14–16 May 2000, 9–10.

Alpar, B., A. C. Yalçıner, F. Imamura and C. E. Synolakis, 2001, ‘‘Determination of Probable Underwater Failures and Modeling of Tsunami Propagation in the Sea of Marmara’’, in *Proceedings of the International Tsunami Symposium ITS (Session 4),* pp. 535–544., August 4–7, Seattle.

Bernardi, E. N., H. O. Mofjeldi, V. Titovi, C. E. Synolakis and F. I. Gonzalezi, 2006, ‘‘Tsunami: Scientific Frontiers, Mitigation, Forecasting and Policy Implications’’, 1987–2007.

Bony, G., N. Marriner, C. Morhange, D. Kaniewski and D. Perinçek, 2011, ‘‘A High-Energy Deposit in the Byzantine Harbor of Yenikapı’’, İstanbul (Turkey), *Quaternary International,* 266, 117-130.

Booth, J. S., D. W. O. Leary, P. Popenoe and W. W. Danforth, 1993, ‘‘U. S. Atlantic Continental Slope Landslides: Their Distribution, General Attributes, and

Amplifications, in Submarine Landslides'', 2002, 80225. *U.S. dept. Of Interior, Denver, Co*, pp. 14–22.

Brune, A. Y., S. Babeyko, Ladage and S. V. Sobolev , 2010, ''Landslide Tsunami Hazard in the Indonesian Sunda Arcs'', *Nat. Hazards Earth Syst. Sci.,* 10, 589–604.

Çağatay, M.N., N. Görür, O. Algan, C. Eastoe, A. Tchapalyga, D. Ongan, T. Kuhn and I. Kuşcu, 2000, ''Last Glacial-Holocene Palaeoceanography of the Sea of Marmara: Timing of the Last Connections with the Mediterranean and the Black Sea'', *Marine Geology,* 167, 191–206.

Fine, I.V., A. B. Rabinovich, R. E. Thomson and E. A. Kulikov, 2003, ''Numerical Modeling of Tsunami Generation by Submarine and Subaerial Landslides'', *Submarine Landslides and Tsunamis,* 69-88.

Fine, I. V., A. B. Rabinovich, B. D. Bornhold, R. E. Thomson and E. A. Kulikov, 2004, ''The Grand Banks Landslide Generated Tsunami of November 18, 1929: Preliminary Analysis and Numerical Modeling'', *Marine Geology,* 215 (2005) 45-57.

Fryer G.J., P. Watts and L. F. Pratson, 2004, ''Source of the Great Tsunami of 1 April 1946: A Landslide in the Upper Aleutian Forearc'', *Marine Geology,* 203 201-218.

Grilli, S. T., J. Skourup and I. A. Svendsen, 1989, ''An Efficient Boundary Element Method for Nonlinear Water Waves'', *Engrg. Analysis Boundary Elements,* 6(2), 97-107.

Grilli, S. T. and R. Subramanya, 1996, ''Numerical Modeling of Wave Breaking Induced by Fixed or Moving Boundaries'', *Comp. Mech.,* 17, 374-391.

Grilli, S. T. and P. Watts, 2005, ‘‘Tsunami Generation by Submarine Mass Failure I: Modelling, Experimental Validation, and Sensitivity Analyses’’, *Journal of Waterway, Port, Coastal, and Ocean Engineering © ASCE November/December,* 283-297.

Gusiakov, V. K., 2003, ‘‘Identification of Slide-Generated Tsunamis in the Historical Catalogues’’.

Gutenberg, B., 1939, ‘‘Tsunami and Earthquakes’’, *Bulletin of the Seismological Society of America*, 29 (4), 517-526.

Hampton, A., J. L. Homa, 1996, *“Submarine Landslides”*.

Harbitz, C.B., F. Lovholt, G. Pedersen and D. G. Masson, 2006, ‘‘Mechanisms of Tsunami Generation by Submarine Landslides: a Short Review’’, *Norwegian Journal of Geology,* Vol. 86, pp. 255-264.

Hayır, A., B. Seseoğulları, I. Kılınç, A. Ertürk, H. K. Cığızoğlu, M. S. Kabdaslı, O. Yağcı and K. Day, 2008, ‘‘Scenarios of Tsunami Amplitudes in the North Eastern Coast of Sea of Marmara Generated by Submarine Mass Failure’’, *Coastal Engineering*, 55, 333-356.

Imamura, F. and M. A. Imteaz, 1995, ‘‘Long Waves in Two Layer, Governing Equations and Numerical Model’’, *Journal of Science Tsunami Hazards”,* Vol.13 No.1, pp. 3-24.

İnsel, I., 2009, *The Effects of the Material Density and Dimensions of the Landslide on the Generated Tsunami*, M.S. Thesis, Middle East Eechnical University, Department of Civil Engineering, Ocean Engineering Research Center, Ankara, Turkey.

Lee, H., H. Ryan, R. E. Kayen, P. J. Haeussler, P. Dartnell and M. A. Hampton, 2006, ‘‘Varieties of Submarine Failure Morphologies of Seismically-Induced Landslides in Alaskan Fjords’’, *Norwegian Journal of Geology*, Vol. 86, pp. 221-230.

Locat, J. and H. J. Lee, 2002, ‘‘Submarine Landslides: Advences and Challenges’’, *Canadian Geotechnical Journal”,* 39, 193–212.

Lopez-Venegas, A.M., U. S. Ten Brink and E. L. Geist, 2008, ‘‘Submarine Landslide as the Source for the October 11, 1918 Mona Passage Tsunami: Observations and Modeling’’, *Marine Geology,* 254, 35-46.

Lynett, P. and P. L. F. Liu, 2003, ‘‘Submarine Landslide Generated Waves Modeled Using Depth-Integrated Equations’’, *Submarine Landslides and Tsunamis,* 51-58.

Masson, D.G., C. B. Harbitz, R. B. Wynn, G. Pedersen and F. Lovholt, 2006, ‘‘Submarine Landslides: Processes, Triggers and Hazard Prediction’’, *Phil. Trans. R. Society A,* 364, 2009-2039.

Minoura, K., 2005, ‘‘A Tsunami Generated by a Possible Submarine Slide: Evidence for Slope Failure Triggered by the North Anatolian Fault Movement’’, *Natural Hazards,* (2005) 36: 297-306.

Murty, T.S., 1977, ‘‘Seismic Sea Waves, Tsunamis’’, Marine Environmental Data Service Branch, Fisheries and Marine Service, Ottawa, Canada.

Murty, T.S., 2003, ‘‘Tsunami Wave Height Dependence on Landslide Volume’’, *Pure appl. Geophys,* 160, 2147-2153.

Okal, E.A. and C. E. Synolakis, 2003, ‘‘A Theoretical Comparison of Tsunamis from Dislocations and Landslides’’, *Pure and Applied Geophysics,* 160, 2177-2188.

Okal, E.A., C. E. Synolakis, B. Uslu, N. Kalligeris and E. Voukouvalas, 2009, ‘‘The 1956 Earthquake and Tsunami in Amorgos, Greece’’, *Geophys. J. Int*, 178, 1533–1554.

OYO and IMM, 2007, *Project Report on Simulation and Vulnerability Analysis of Tsunamis Affecting the İstanbul Coasts*, Prepared by OYO Int. co. (Japan) for İstanbul Metropolitan Municipality (IMM).

Özbay, I., 2000, *Two Layer Numerical Model for Tsunami Generation and Propagation*, M.S. Thesis, Middle East Technical University, Department of Civil Engineering, Ocean Engineering Research Center, Ankara, Turkey.

Özer, C. and A. C. Yalçıner, 2011, ‘‘Sensitivity Study of Hydrodynamic Parameters During Numerical Simulations of Tsunami Inundation’’, Pure and Applied Geophysics, *Netherlands.* Vol.168 N.11, pp. 2083-2095.

Özeren, S., M. N. Çağatay, N. Postacıoğlu, C. Şengör, N. Görür and K. Eris, 2010, ‘‘Mathematical Modelling of Potential Tsunami Associated with a Late Glacial Submarine Landslide in the Sea of Marmara’’, *Geo–Mar Lett*, 523–539.

Pelinovsky, E. and A. Poplavsky, 1996, ‘‘Simplified Model of Tsunami Generation by Submarine Landslides’’, *Phys. Chem. Earth*, Vol.21, No. 12, pp. 13-17.

Perinçek, D., 2010, ‘‘The Geoarcheology of the Yenikapı Excavation Site in the last 8000 years and Geological Traces of Naturel Disasters (İstanbul-Turkey)’’, *Mineral Res. Expl. Bull.*, 141, 69-92.

Richardson, S. R., 2002, *Numerical Simulation of Impulsive Wave Overtopping Events Resulting from Landslides*, Ph.D. Thesis, the Manchester Metropolitan University.

Shuto, N., C. Goto and F. Imamura, 1990, ‘‘Numerical Simulation as a Means of Warning for Near Field Tsunamis’’, *Coastal Engineering in Japan*, V. 33, No:2, pp:173-193.

Shuto, N. and F. Imamura, F., 2000, ‘‘An Idea of the Sanriku Network for Tsunami Prediction and Forecasting in the Area Most Frequently Damaged in the World’’, Presentation at Hazard 2000, *8th Conference on Mitigation of Natural and Man Made Hazards,* 22-26 May, 2000, Tokushima, Japan.

Shuto, N., 2003, ‘‘Tsunamis of Seismic Origin, Science, Disaster and Mitigation’’.

Synolakis, C. E., 2002, “The Slump Origin of the 1998 Papua New Guinea Tsunami”, *Proc. R. Soc. London, Ser. A,* 458, 763–790.

Tappin, D. R., P. Watts and S. T. Grilli, 2008, ‘‘The Papua New Guinea Tsunami of 17 July 1998: Anatomy of a Catastrophic Event’’, *Nat. Hazards Earth Syst. Sci.,* 8, 243–266.

Tinti, S., A. Manucci, G. Pagnoni, A. Armigliato and F. Zaniboni, 2005, ‘‘The 30 December 2002 Landslide-Induced Tsunamis in Stromboli: Sequence of the Events Reconstructed from the Eyewitness Accounts’’, *Natural Hazards and Earth System Sciences,* 5, 763–775.

Trifunac, M. D. and M. I. Todorovska, 2001, ‘‘Evolution of Accelerographs, Data Processing, Strong Motion Arrays and Amplitude and Spatial Resolution in Recording Strong Earthquake Motion’’, *Soil Dyn. Earthq. Eng.,* 21(6), 537– 555.

Trifunac, M. D. and M. I. Todorovska, 2002, ‘‘A Note on Differences in Tsunami Source Parameters for Submarine Slides and Earthquakes’’, *Soil Dynamics and Earthquake*

Engineering, 22 (2), 143–155.

Varnes, D. J., 1978, ‘‘Slope movement types and processes’’, in R. L. Schuster and R. J. Krizek, (Editors), *Landslides Analysis and Control*, Transportation Research Board Special Report 176, National Academy Of Sciences, Washington, 11-33.

Watts, P., F. Imamura and S. Grilli, 2000, ‘‘Comparing Model Simulations of Three Benchmark Tsunami Generation Cases’’, *Science of Tsunami Hazards,* vol.18, No.2, pp.107-123.

Yalçıner, A. C., I. Özbay and F. Imamura, 2001, ‘‘A Comparison of Tsunami Set-Up With Relation to the Dimensions of Underwater Landslide’’, *NATO Underwater Ground Failures on Tsunami Generation, Modeling, Risk and Mitigation,* Ed: Ahmet C. Yalçıner, May 23-26, 2001, istanbul, Turkey, pp: 60-65.

Yalçıner, A. C., B. Alpar, I. Özbay, Y. Altınok and F. Imamura, 2001, ‘‘Tsunami Generation and Coastal Amplification in the Sea of Marmara’’, *NATO Underwater Ground Failures on Tsunami Generation, Modeling, Risk and Mitigation,* Ed: Ahmet C. Yalçıner, May 23-26, 2001, Istanbul, Turkey, pp: 138-144.

Yalçıner, A. C., C. E. Synolakis, B. Alpar, J. C. Borrero, Y. Altınok, F. Imamura, S. Tinti, Ş. Ersoy, U. Kuran, S. Pamukçu and U. Kanoğlu, 2001c, ‘‘Field Surveys and Modeling of the 1999 İzmit Tsunami’’, Paper Presented at International Tsunami Symposium 2001, Int. Union of Geodesy and Geophys., Seattle, Wash.

Yalçıner, A.C., B. Alpar, Y. Altınok, I. Özbay and F. Imamura, 2002, ‘‘Tsunamis in the Sea of Marmara, Historical Documents for the Past, Models for the Future’’, *Marine Geology,* 190 445-463.

Yalçıner, A. C., E. Pelinovsky, T. G. Talipova, A. A. Kurkin, A. C. Kozelkov and A. Zaytsev, 2002b, “Tsunamis in the Black Sea: Comparison of the Historical,

Instrumental and Numerical Data", *J. Geophys.Research,* 2004, Vol. 109, No. C12, C12023 10.1029/2003JC002113.

Yalçıner, A. C., H. Karakuş, C. Özer and G. Özyurt, 2005, *Short Courses on Understanding the Generation, Propagation, Near and Far-Field Impacts of Tsunamis and Planning Strategies to Prepare for Future Events*, Course notes, METU Civil Eng. Dept. Ocean Eng. Res. Center.

Yalçıner, A. C., E. Pelinovsky, A. Zaytsev, A. Kurkın, C. Özer and H. Karakuş, 2006, Nami Dance Manual, METU, Civil Engineering Department, Ocean Engineering Research Center, Ankara, Turkey.

Yalçıner, A. C., C. E. Synolakis, M. Gonzales and U. Kanoğlu, 2007, Joint Workshop on Improvements of Tsunami Models, Inundation Map and Test Sites of EU Transfer Project, June 11-14, Fethiye, Turkey.

Yalçıner, A. C., E. Pelinovsky, A. Zaytsev, A. Kurkin, C. Özer and H. Karakuş, 2007a, "Modeling and Visualization of Tsunamis: Mediterranean Examples, from, Tsunami and Nonlinear Waves" (Ed: Anjan Kundu), *Springer,* 2007, 2731-2839.

Yalçıner, A. C., C. E. Synolakis, M. Gonzales and U. Kanoğlu, 2007b, Joint Workshop on Improvements of Tsunami Models, Inundation Map and Test Sites of EU Transfer Project, June 11-14, Fethiye, Turkey.

Yalçıner, A. C., C. Özer, H. Karakuş, A. Zaytsev and I. Güler, 2010, "Evaluation of Coastal Risk at Selected Sites Against Eastern Mediterranean Tsunamis", *Proceedings of 32nd International Conference on Coastal Engineering (ICCE 2010), Shanghai, China,* June 30– July 5, 2010, http://journals.tdl.org/ICCE/issue/current/showToc.

Yalçıner, A. C., C. Özer, A. Zaytsev, A. Suppasri, E. Mass, N. Kaligeris, Ö. Necmioğlu, C. Synolakis, F. Imamura and N. M. Özel (2011a), ‘‘Field Survey and Modeling of 2011 Great East Japan Tsunami’’, General Assembly of American Geophysical Union. USA.

Yalçıner, A. C., C. Özer and A. Zaytsev, 2011b, ‘‘Amplifications of Nearshore Tsunami Parameters during Tohoku Kanto Tsunami’’, XXV General Assembly of Int. Union of Geology and Geophysics, Melbourne Australia.

Yaltırak, C., B. Alpar, M. Sakınç and H. Yüce, 2000, ‘‘Origin of the Strait of Çanakkale (Dardanelles): Regional Tectonics and the Mediterranean-Marmara Incursion’’, *Marine Geology,* 164, 139–156.

Yılmaz, Y., E. Gökasan and A. Y. Erbay, 2010, ‘‘Morphotectonic Development of the Marmara Region’’, *Tectonophysics,* 488 (2010) 51–70.

Yolsal, S., T. Taymaz and A. C. Yalçıner, 2007, ‘‘Understanding Tsunamis, Potential Source Regions and Tsunami-Rrone Mechanisms in the Eastern Mediterranean’’, *Geological Society* , 291: 201-230.

Zahibo, N., E. Pelinovsky, A. C. Yalçıner, A. Kurkin, A. Kozelkov and A. Zaytsev, 2003a, ‘‘The 1867 Virgin Island Tsunami: Observations and Modeling’’, *Oceanologica Acta*, Vol. 26, N. 5-6, pp. 609-621.

Zahibo, N., E. Pelinovsky, A. Kurkin and A. Kozelkov, 2003b, “Estimation of Far-Field Tsunami Potential for the Caribbean Coast Based on Numerical Simulation”, *Science Tsunami Hazards,* 2003, Vol. 21, N. 4, p. 202 -222.

Zitter, T. A. C., C. Grall, P. Henry, M. S. Özeren, M. N. Çağatay, C. Şengör, A. M. P. Gasperini, B. Mercier de Lepinay and L. Geli, 2012, ‘‘Distribution, Morphology and Triggers of Submarine Mass Wasting in the Sea of Marmara’’, *Marine Geology*, 329-351, 58-74.

Zaytsev, A., H. Karakuş, A. C. Yalçıner, A. Chernov, E. Pelinovsky, A. Kurkin, C. Özer, D. I. Dilmen, I. İnsel and G. Özyurt, 2008, ‘‘Tsunamis in Eastern Mediterranean, Histories, Possibilities and Realities’’, COPEDEC VII. Dubai. Paper No:Z-01.

Zaytsev, A., A. C. Yalçıner and E. Pelinovsky, 2011, ‘‘The Forecast of the Tsunami Waves Heights at the Russian Black Sea Coast’’, Transactions of Nizhny Novgorod State Technical University, 2011, Russia. Vol.86, pp. 35-43.

Nami Dance Manual, 2010, METU, Civil Engineering Department, Ocean Engineering Research Center, Ankara, Turkey.

TRANSFER 2009, http://www.transferproject.eu/ Reviewed on 05/27/2011.

USGS, 2004, *U.S. Department of the Interior, U.S. Geological Survey*, http://landslides.usgs.gov.